ANL-GenIV-059

Evaluation of High Temperature Gas-Cooled Reactor Physics Experiments as VHTR Benchmark Problems

prepared by
Nuclear Engineering Division
Argonne National Laboratory

Argonne National Laboratory is managed by
The University of Chicago for the U. S. Department of Energy

About Argonne National Laboratory

Argonne is managed by The University of Chicago for the U.S. Department of Energy under contract W-31-109-Eng-38. The Laboratory's main facility is outside Chicago, at 9700 South Cass Avenue, Argonne, Illinois 60439. For information about Argonne and its pioneering science and technology programs, see www.anl.gov.

Availability of This Report

This report is available, at no cost, at http://www.osti.gov/bridge. It is also available on paper to U.S. Department of Energy and its contractors, for a processing fee, from:

U.S. Department of Energy
Office of Scientific and Technical Information
P.O. Box 62
Oak Ridge, TN 37831-0062
phone (865) 576-8401
fax (865) 576-5728
reports@adonis.osti.gov

Disclaimer

This report was prepared as an account of work sponsored by an agency of the United States Government. Neither the United States Government nor any agency thereof, nor The University of Chicago, nor any of their employees or officers, makes any warranty, express or implied, or assumes any legal liability or responsibility for the accuracy, completeness, or usefulness of any information, apparatus, product, or process disclosed, or represents that its use would not infringe privately owned rights. Reference herein to any specific commercial product, process, or service by trade name, trademark, manufacturer, or otherwise, does not necessarily constitute or imply its endorsement, recommendation, or favoring by the United States Government or any agency thereof. The views and opinions of document authors expressed herein do not necessarily state or reflect those of the United States Government or any agency thereof, Argonne National Laboratory, or The University of Chicago.

ANL-GenIV-059

Evaluation of High Temperature Gas-Cooled Reactor Physics Experiments as VHTR Benchmark Problems

by
T.A. Taiwo, T.K. Kim, W.S. Yang, and H.S. Khalil
Nuclear Engineering Division, Argonne National Laboratory

W.K. Terry, J. Blair Briggs, and D.W. Nigg
Idaho National Laboratory

September 15, 2005

Argonne National Laboratory is managed by
The University of Chicago for the U.S. Department of Energy

ANL-GenIV-059

Evaluation of High Temperature Gas-Cooled Reactor Physics Experiments as VHTR Benchmark Problems

T. A. Taiwo, T. K. Kim, W. S. Yang, and H. S. Khalil

Nuclear Engineering Division
9700 South Cass Avenue
Argonne National Laboratory
Argonne, IL 60439

W. K. Terry, J. Blair Briggs, and D. W. Nigg

P. O. Box 1625
Idaho National Laboratory
Idaho Falls, ID 83415

September 15, 2005

Table of Contents

- EXECUTIVE SUMMARY 1
- ACKNOWLEDGMENTS 7
- REFERENCES 8
- EVALUATION OF THE COMPACT NUCLEAR POWER SOURCE (CNPS) CRITICAL EXPERIMENTS
- EVALUATION OF THE HIGH TEMPERATURE ENGINEERING TEST REACTOR (HTTR) START-UP EXPERIMENTS
- EVALUATION OF THE INITIAL CRITICAL CONFIGURATION OF THE HTR-10 PEBBLE-BED REACTOR

EXECUTIVE SUMMARY

Background

The Very High Temperature Reactor (VHTR) is a leading candidate for the Next Generation Nuclear Plant (NGNP) because of its high temperature and passive safety design, and its potential for efficient electricity and hydrogen generation. The physics characteristics of this system is quite different from that of operating light-water-cooled reactors (LWRs) because of the use of (1) an annular core design, (2) solid graphite moderator, (3) higher enrichment of the uranium fuel, and (4) TRISO fuel particles. Consequently, a suite of core physics models and analysis tools different from those utilized for analyzing the LWRs are required for accurately representing the physics of the VHTR. These models have typically been based on Monte Carlo codes and associated libraries, or the deterministic code systems (lattice physics and whole-core analysis codes) that can accurately represent the core physics impacts of the coated fuel particles (CFPs), neutron streaming along channels (prismatic block-type) or at core top (pebble-type), and inner reflector-core interface in the annular VHTR core design. These models and analysis tools must be verified and validated to ensure their accuracy, quantify their prediction uncertainties and support their use in VHTR design, safety confirmation and licensing.

The verification and validation (V&V) of the code packages is typically done in two ways. The first, *verification*, is the assurance that the code actually performs as designed, i.e., it solves accurately the equations that represent the physical phenomena occurring in the systems. This step is typically accomplished by model and software inspection, and by comparing code solutions to analytical solutions for simple problems, or to solutions from previously verified and validated codes, or to solutions from higher fidelity codes. The second step of *validation* gives the assurance that the models employed can provide physically valid representations of the system characteristics and can be used to derive core parameters. This step is usually accomplished by comparing calculated results to experimental measurements or results of models that have already been validated against relevant measurements.

To implement and qualify the neutronics analysis tools for the NGNP/VHTR, the Gen IV program includes the following activities:

- Nuclear data assessment by uncertainty and target accuracy studies.
- Survey of existing data and development of benchmark database for VHTR code validation and qualification.
- Assessment and development of analysis tools for lattice and whole-core physics calculations.

In FY 2004, ANL and INL examined information on several past and present experimental and prototypical facilities based on HTGR concepts that could potentially be used for the V&V basis of codes employed in the design and analysis of the VHTR cores. A preliminary assessment of the applicability of the existing test data for benchmarking the pebble-bed and prismatic block-type cores was performed as part of that effort. The experiments assessed included [1]

- Pebble-bed type cores: ASTRA, AVR, CESAR II, GROG, HTR-10, HTR-PROTEUS, KAHTER, SAR, and THTR, and
- Prismatic block-type cores: CNPS, DRAGON, Fort St. Vrain, GGA HTGR criticals, HITREX-1, HTLTR, HTTR, MARIUS-IV, Peach Bottom HTGR, Peach Bottom Criticals, SHE, NESTOR/HECTOR, and VHTRC.

The FY 2004 preliminary evaluation revealed that the VHTR systems under development in the Gen IV program differ in significant ways from previous high-temperature reactors (e.g., thorium utilization, highly enriched fuel, BISO versus TRISO fuel, thermal efficiency, operating temperatures, etc). These differences limit the applicability and direct usefulness of some of the existing experimental data for NGNP core designs. Furthermore, it was acknowledged that for data produced on commercial basis or by foreign governments, availability of the data might be quite limited. An effort was made to identify experimental tests of the highest priority, recover the data for those cases, and then develop standard problems (benchmarks) that are of sufficient quality for use in the licensing of the VHTR analysis codes. A set of criteria was employed to judge the relevance of the different tests. These included, purpose of the previous experiment, geometry of core, fuel forms, core materials, physics parameters measured, measurement state,

availability of design and uncertainty data, and applicability of data to V&V. Based on these criteria, the experiments judged to be of the highest priorities are:

- ASTRA, AVR, HTR-10, HTR-PROTEUS for the pebble-bed cores and
- HTTR, VHTRC, and CNPS for the prismatic block-type cores.

Some attributes of these facilities and experimental tests are summarized in Table 1.

Table 1. High Priority Experiments of Potential Interest to VHTR Systems. [1]

Facility	Geometry	Size	Fuel type	Asymptotic state or zero-power startup	Availability of data	Priority
Pebble-Bed Reactor Type						
ASTRA	Annular, but not azimuthally symmetric	Small	As desired	Zero-power startup	Existing facility – data can be obtained	High
AVR	Cylindrical	Short; radial extent appropriate	Various; some low-enrichment TRISO	Both	Uncertain	High
HTR-10	Cylindrical	Small	Low-enriched TRISO	Both	Existing facility – data can be obtained	High
HTR-PROTEUS	Cylindrical	Small	LEU pebble-bed fuel	Zero-power	PSI and IAEA would need to be contacted	High
Prismatic-Block Reactor Type						
HTTR	Cylindrical/ Annular	Small	LEU	Both	Existing facility – data can be obtained	High
VHTRC	Hexagonal	Small	LEU	Zero	JAERI data	High
CNPS	Cylindrical	Small	LEU	Zero	LANL data	High

In FY 2005, three of these cases have been further analyzed for purposes of creating a set of standard benchmark problems that could be used for validating codes and nuclear data; INL evaluated the available HTR-10 data, while ANL evaluated the CNPS and HTTR data. The results of these evaluations have been documented in laboratory reports and they have been collated into this single report.

Summary

ANL conducted a technical evaluation of the CNPS and HTTR measurements; this included sensitivity studies to understand discrepancies in data or impact of modeling assumptions on the results. Due to insufficient data (particularly the uncertainties to be associated with the design data) these efforts did not progress to the stage of defining a standard benchmark following the structure that has been recently defined by the International Reactor Physics Experiments Preservation (IRPhEP) sub-group of the OECD/NEA. It is noted, however, that the models developed could be used for specifying numerical benchmarks based on the experiments. On the other hand INL concentrated on developing a standard benchmark for the HTR-10.

The conclusions from the ANL and INL evaluation activities are:

- CNPS: An evaluation of the Compact Nuclear Power Source (CNPS) experiments conducted at the Los Alamos National Laboratory (LANL) in the late 1980s has been done using information available in the open literature. The Monte Carlo results that were obtained for critical test configurations have been quite good with k_{eff} values within 0.5% of the critical value of unity. The material worths calculated in this study were found fairly close to the measurement values. The lack of information on design data uncertainties and the inconsistency in the design data from different sources make it difficult to quantify the uncertainty in the core integral parameters arising from data uncertainties. The evaluated configurations could however be useful as numerical benchmarks that are based on the currently available information.

- HTTR: An evaluation of the High Temperature Engineering Test Reactor (HTTR) start-up experiments has been performed using the data available in the open literature. Monte Carlo (MCNP) and deterministic models were developed and used for the analysis of the four critical configurations of the HTTR, which were attained along the path to full-core loading. The results obtained show a significant difference (1.8% $\Delta k/k$) between the core criticality calculated by the MCNP code and the experimental measurement; larger differences of about 2.3 – 3.4% $\Delta k/k$ were found

for the deterministic codes. These discrepancies are consistent with those reported during an HTTR experiment evaluation effort previously organized by the IAEA. The magnitudes of these differences are attributed to the incomplete specification of the HTTR core configuration (e.g., impurities and nitrogen in graphite, design data uncertainties, etc), uncertainties in nuclear data, and of approximations inherent in the code solution methods (primarily for the deterministic codes). Due to the incomplete data, it is not possible at this stage to state conclusively the major contributions to the discrepancies. It is recommended that the Gen IV program should continue to engage JAERI (Japan) and other international partners in order to obtain additional VHTR-related core physics experimental data.

- HTR-10: Using the COMBINE and PEBDAN codes for cross section generation and the PEBBED code for whole-core calculation, a baseline value of 1.03257 was calculated for the k_{eff} of the critical HTR-10 core in this evaluation. This baseline value is farther from unity (1.0) than one would expect. The PEBBED code has been validated extensively but its results are dependent on the quality of the cross sections supplied to it. Calculation of cross sections in graphite systems presents problems that need resolution. There are also other sources of uncertainty, such as the shape of the upper surface of the core, for which PEBBED assumes a planar upper core surface. The error introduced by this assumption has not yet been evaluated. A statistical combination of all sources of potential uncertainties in the benchmark result (assumed uncorrelated) yields an overall uncertainty of 0.54% in the k_{eff} of the HTR-10 critical core. This value was obtained by making consistently conservative assumptions on the variability of parameters on which k_{eff} may depend. The parameters that could have the largest effect are the boron densities, the graphite matrix density, the fuel loading, and the pebble diameter. It is unlikely that any of the boron densities and impurity level, on average, are as far from the nominal value as the tolerance range permits. Therefore, the *initial criticality measurement in HTR-10 is judged to be an acceptable benchmark*. However, a number of improvements have been identified during internal review of this evaluation. Many of these improvements will be made prior to formal submittal to the IRPhEP on September 30,

2005. Additional improvements will be made prior to the IRPhEP Meeting in November as a result of continued internal review as well as IRPhEP external review. Furthermore, contact with key individuals at Tsinghua University in China has been reestablished with the hope of more complete information to follow in the coming months.

Based on the findings of this study, the need for new integral measurements cannot be ruled out. Cost effective approaches for creating high quality measurements will be pursued by ANL and INL in collaboration with other local and international organizations.

ACKNOWLEDGMENTS

This joint ANL and INL work on the evaluation of high-temperature physics experiments was supported by the U.S. Department of Energy, Office of Nuclear Energy, Science and Technology (Design and evaluation Methods element of the Generation IV Program).

The following people contributed to either the evaluation or review of the experimental tests reported in this work: Soon-Sam Kim (INL), Sang-Ji Kim (ANL, a visiting scientist from KAERI (ROK)), Frank Szakaly (ANL, a 2004 summer intern from the Texas A&M University), and Mark Paulson (ANL, a 2005 summer intern from the University of Wisconsin, Madison). Their efforts are greatly appreciated.

REFERENCES

1. W. K. Terry, J. K. Jewell, J. Blair Briggs (INEEL), and T. A. Taiwo, W. S. Park, H. S. Khalil (ANL), "Preliminary Assessment of Existing Experimental Data for Validation of Reactor Physics Codes and Data for NGNP Design and Analysis," Gen IV Report, Argonne National Laboratory, September 15, 2004.

Evaluation of the Compact Nuclear Power Source (CNPS) Critical Experiments

T. A. Taiwo, W. S. Yang, S. J. Kim, T. K. Kim, and Mark Paulson

Nuclear Engineering Division
9700 South Cass Avenue
Argonne National Laboratory
Argonne, IL 60439

September 14, 2005

Table of Contents

Page

Abstract 1

1.0 INTRODUCTION 3

2.0 GENERAL CNPS REACTOR AND EXPERIMENT DESCRIPTIONS 5

2.1 CNPS Critical Configurations 5

2.2 Core Configurations and Experiments 9

2.3 Comparison of CNPS Data from Various Sources 14

3.0 MCNP MODELING OF CNPS 17

3.1 Introduction 17

3.2 Input Information 17

3.3 Impact of Number of Neutron Histories 18

3.4 Impact of Discrepancies in CNPS Design Data on Solutions 19

3.5 Control Rod Thimble Configuration 20

3.6 Control and Material Worths 22

3.7 Shim Differential Worth 23

4.0 RELEVANCE OF CNPS TO VHTR 26

4.1 Double Heterogeneity Effect 26

4.2 Neutron Spectrum 27

5.0 CONCLUSIONS 29

ACKNOWLEDGEMENT 30

REFERENCES 31

APPENDICES A-D 32

List of Tables

Page

Table 1. CNPS Critical Core Configurations 9

Table 2. MCNP Neutron History Effect on CNPS First Core Eigenvalue (k_{eff}) 19

Table 3. CNPS Core Eigenvalues using Values from Various Sources 20

Table 4. CNPS Configuration Sensitivities to Control Thimble Data 21

Table 5. Comparison of CNPS Design Element Worths 22

Table 6. Eigenvalues of CNPS with Different Coated Fuel Particle Models 27

List of Figures

Page

Figure 1. Planar View of the CNPS core.....6

Figure 2. Vertical Cross Section of the CNPS Core.....7

Figure 3. First Critical Core Configuration.....10

Figure 4. 202 Fuel Channel Configuration.....11

Figure 5. 380 Fuel Channel Configuration.....12

Figure 6. Full Critical Core Loading Configuration.....13

Figure 7. Shim Integral Worths.....24

Figure 8. Shim Differential Worths.....25

Figure 9. Neutron Spectra for the CNPS and Block-Type VHTR.....27

Abstract

An evaluation of the Compact Nuclear Power Source (CNPS) experiments conducted at the Los Alamos National Laboratory (LANL) in the late 1980s has been done using information available in the open literature. The Monte Carlo results that were obtained for critical test configurations have been quite good with k_{eff} *values within 0.5% of the critical value of unity. The material worths calculated in this study were found fairly close to the measurement values. The lack of information on design data uncertainties and the inconsistency in the design data from different sources make it difficult to quantify the uncertainty in the core integral parameters arising from data uncertainties. The evaluated configurations could however be useful as numerical benchmarks that are based on the currently available information.*

1. INTRODUCTION

The Compact Nuclear Power Source (CNPS) [1] was a small reactor system designed to provide power at sites where fuel costs and logistics make fossil-fuel-powered systems less attractive. In the 1980s, it was proposed that the system be used to provide power for the short-range radar sites in the upgrade of the North Warning System. [1] The CNPS design used TRISO fuel particles and could produce 20 KWe continuously for 20 years without refueling and be walk-away safe; the core had an inherently large negative temperature reactivity coefficient and relied on the stability of the TRISO fuel particle at the highest temperature achievable following a maximum credible accident. Due to the size and weight constraints, the CNPS was criticality limited and its ability to remain critical for the life of the core had to be verified, hence the original plans to conduct physics experiments at the Los Alamos National Laboratory (LANL). The CNPS project was cancelled after the fuel and graphite blocks had been delivered to LANL. A reduced critical experiments program was however undertaken to obtain integral data.

The available open information on physics experiments for the Compact Nuclear Power Source (CNPS) has been reviewed. The features of the CNPS make these experiments of interest to the Next Generation Nuclear Plant/Very High Temperature Reactor (NGNP/VHTR). The core used low-enriched (19.9%) uranium graphite fuel in TRISO form, with a C/U-235 atomic ratio of 3000 (i.e., C/U ~ 600). The heterogeneous uranium graphite core was reflected using graphite. The core physics experiments for the CNPS included measurements of reactivity worths relative to void, of graphite, BeO, depleted fuel, and polyethylene in 20 replacement holes. The worth of the safety rod was also determined using the rod-drop method. Other measurements included material and central control rod worths, shim differential worth, and limited temperature reactivity coefficient measurements using electrical radiant heaters. Measurement of the activation rate of ^{235}U in heat pipe channels was also performed.

Using the available data for the CNPS critical experiments has not been straightforward, as one could expect for an experiment that was conducted 20 years ago by another institution. Making the task difficult is the unavailability of the personnel that conducted the experiments at LANL. There are, however, a few publications by the same authors on the CNPS experiments that list design specifications, geometry and material composition, and experimental results.

However, amongst the literature on the CNPS critical experiments, there are discrepancies on geometrical dimensions and material compositions. In order to generate a set of benchmark problems, the approach that has been taken is to evaluate the range of design data that are available in open literature. Using engineering judgment, the best set of data was used to derive a reference dataset. Then data deviations from this set were used in sensitivity studies performed to judge the impact of these uncertainties in design data on the results. Additionally, only Monte Carlo models have been used in this study. A NGNP/VHTR code package would use deterministic tools, particularly to expedite tradeoff and design studies, and hence it would be quite important to verify and validate these tools for use in NGNP analysis.

In Section 2, a description of the CNPS reactor is provided. A collection of the data used in this study is also given along with discussions on the differences between the data sources. The MCNP model used in this study is documented in Section 3. The results of the sensitivity studies and MCNP calculations are summarized in Section 4. Conclusions from the work are presented in Section 5.

2. GENERAL CNPS REACTOR AND EXPERIMENT DESCRIPTIONS

The primary sources of data on the CNPS are Refs. 1 to 5, with most of the data obtained from Ref. 1. There is however no or limited information on data uncertainties. In Section 2.1 a description of the CNPS core is provided. Information on the configuration and experiments are provided in Section 2.2. The discrepancies that were found in the references are discussed in Section 2.3.

2.1 CNPS Critical Configurations

The CNPS was designed to use a heterogeneous uranium graphite cylindrical core, depicted schematically in Figures 1 (planar view) and 2 (vertical view). The core height is 113 cm and the diameter is 120 cm. The core is reflected both radially and axially with graphite. The thicknesses of the graphite reflectors were 39 cm (average) and 24 cm at the core top and bottom, respectively, and 20 cm radially. An average reflector thickness is provided for the top reflector, because a flat top is not used; the smallest thickness is 25 cm at the periphery, and largest thickness is 45 cm at the core center. [1] In the experimental setup, there is a 0.4 cm radial gap between the core and radial reflector (not visible in Figure 1). This gap, which would not have been in the actual reactor planned for deployment, was used as clearance for the movement of the core into the reflector and was necessary for the operation of the vertical critical assembly machine used at LANL. [1] The core and bottom reflector were supported by a 6 cm thick aluminum plate attached to a hydraulic ram. [1]

The active core consisted of 9 graphite segments (blocks), with penetrations (channels) for fuel pellets, control rods and heat pipes. There was a central cylindrical sector called the *inner* core and eight curved-trapezoidal *outer* core sectors. The core contained 492 fuel channels, 5 control rod channels, and 12 heat pipe channels. An extra 20 channels were also available near the core center. These extra channels were provided in the event that additional fuel was required to make the core critical by the addition of beryllium rods. (The radial locations of the 20 extra holes are provided in Appendix A.) Each fuel channel or extra channel had a diameter of 1.285 cm. The control channels had a diameter of 3.494 cm and penetrated the upper reflector. The heat pipe channels had a diameter of 6.185 cm and penetrated the upper reflector (completely) and bottom reflector (by 3.175 cm). [1] The requirement of ensuring a minimum web thickness

between any two free surfaces made it difficult to maintain a constant fuel element pitch. To minimize this problem, the CNPS was designed with a 45 degree azimuthal symmetry. The coordinates of the channels (centers) in a 45 degree core sector were obtained from Ref. 1 and are summarized in Appendix A.

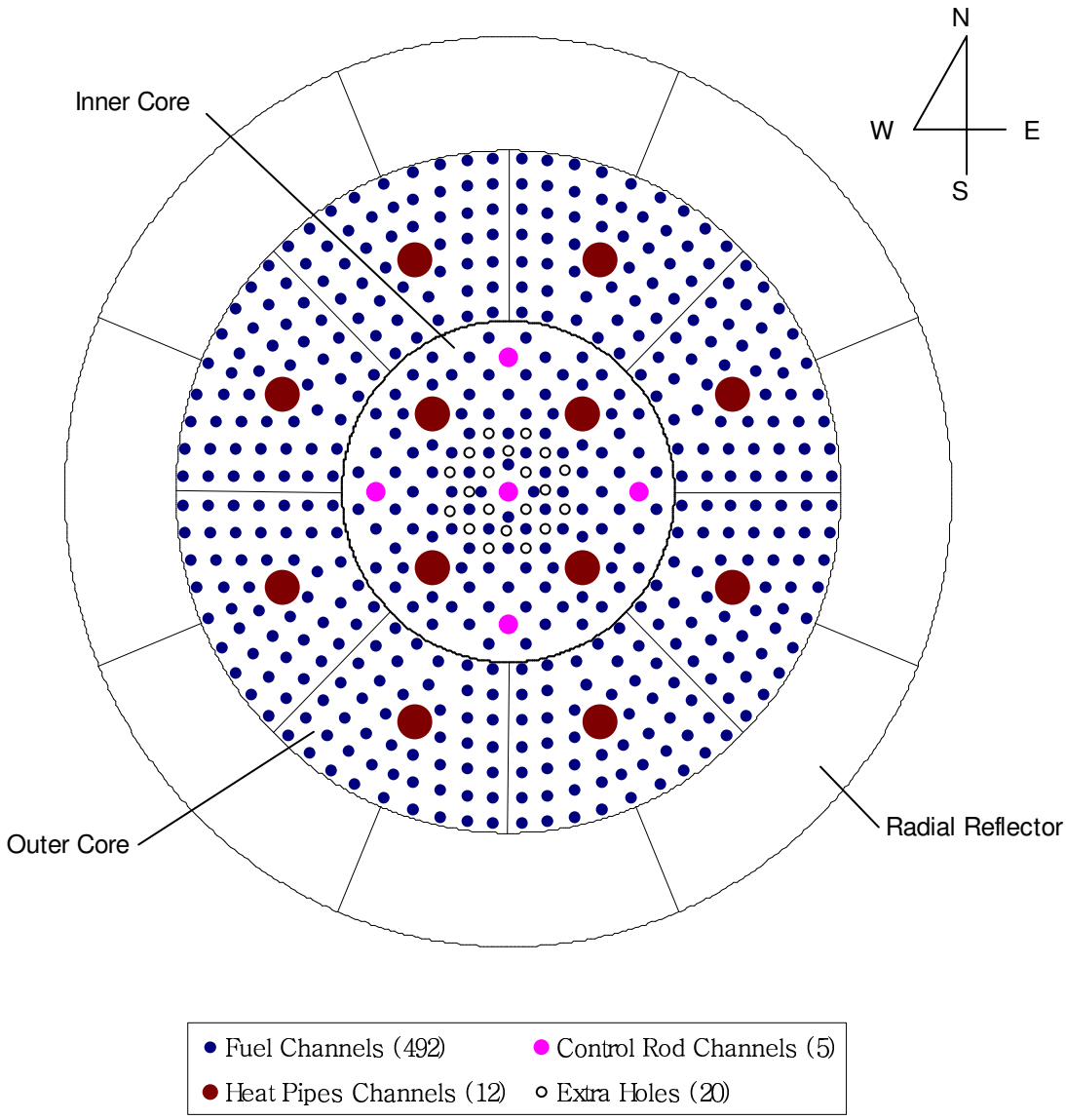

Figure 1. Planar View of the CNPS Core.

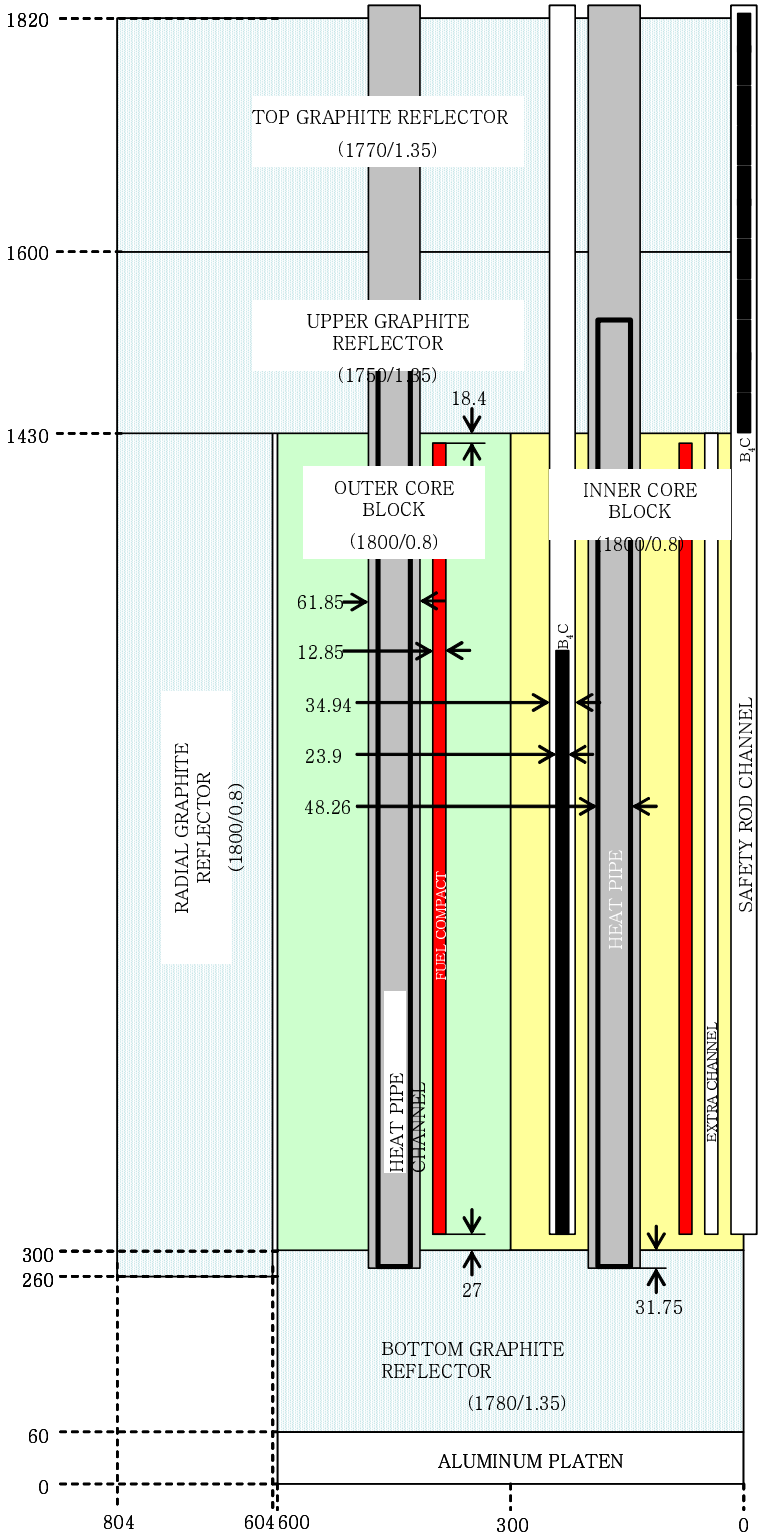

Figure 2. Vertical Cross Section of the CNPS Core. (The dimensions shown are in mm.)

As aforementioned, the reactor was fueled with rodded compacts of TRISO fuel particles in a graphite material. This is similar to the fuel type that is being considered for the NGNP/VHTR. Information on the coated fuel particles (CFPs) and the compact composition are presented in Appendix B. Each fuel channel contained 22 fuel compacts. The equivalent boron impurity content in the compact was 5.2 ppm. The *active* core height was 108.46 cm, which is less than the height of the core block (113 cm). The active core zone ranged from 2.7 cm above the bottom of the graphite core blocks. [1]

To simulate the heat pipes that would have been present if the CNPS was put into operation, two materials were tested. In separate configurations, pipes of type 316 stainless steel (4.826 cm o.d., 0.368 cm wall thickness, and 123.7 cm long) and zirconium (4.826 cm o.d., 0.264 cm wall thickness, and 119.9 cm long) were fully inserted into the heat pipe channels. Although stainless steel is a stronger neutron absorber than the zirconium, it was being considered strongly for the demonstration reactor because testing of the zirconium indicated that there might be long-term problems with the wall integrity. [2] It was realized that the use of stainless steel would place additional uncertainty on the ability of the reactor to operate at power for 20 years without refueling.

The mockup for the CNPS control rods consisted of B_4C cylindrical pellets 2.39 cm in diameter and 5.013 cm in length containing 7.44g of ^{10}B at 19.75 at.% boron. These pellets were stacked in a control rod channel from the bottom of the active core up to various heights depending on the particular CNPS configuration. The CNPS critical experiment also used 22 cylinders of enriched B_4C, each containing 20.7 g of ^{10}B at 54.88 at.% boron for various CNPS configurations. [1] Additionally, the other control design element, called a shim rod, is a thin walled aluminum tube 163.3 cm long with an inner diameter of 1.257 cm, packed with natural B_4C at a density of 0.89 g/cm. This shim rod is inserted in the south control rod channel from the top of the CNPS reactor into an otherwise empty control channel. During the CNPS critical experiment, the central control rod was used as a safety rod. [1]

2.2 Core Configurations and Experiments

Critical state measurements were conducted under the CNPS experimental program. Four of the simple critical loadings were described in Ref. 1 and these are summarized in Table 1. They included cores with loadings of 184 to 492 fuel channels, the latter being the fully-loaded core, and different axial positions of the shim rod. To simulate the heat pipe, both zirconium and stainless steel were utilized.

Table 1. CNPS Critical Core Configurations. [1]

Fueled Channels	Simulated Heat Pipes	B_4C Pellets	Shim Rod Position Above Active Core (cm)
184	0	0	105.3
202	11 zirconium	0	36.6
380	12 SS-316	21 in N*	72.4
492	12 SS-316	13 each W,N,E*	60.4

* Control rod channel position in Fig. 1; N – North, W – West, E – East.

First Critical Core

The first critical core was obtained when 184 fuel channels were loaded as shown in Figure 3. [1] In this configuration, the 20 replacement (extra) channels were filled with graphite rods, the shim and safety rods were out to their limits (105.3 cm and 112.5 cm above the bottom of the active core, respectively), and all the other control and heat pipe channels were empty. [1] The loading (radially) were from the core center all the way out to include the second ring in the outer core, but with the exclusion of the four channels. Due to its clean nature, most of the core physics experiments were performed with this core configuration. These included:

- The worths of graphite, BeO, depleted fuel, and polyethylene relative to void, were measured in the 20 replacement holes. [1]

- The safety rod worth was measured using the rod-drop method in which neutron detectors monitor count rates before a fast pneumatic insertion (drop) of the rod and either during the drop or after the drop. Measurements were taken using internal and external core detectors. [1]

- Shim differential worth measurements were obtained with about 180 to 200 filled channels and the 20 extra channels loaded with miscellaneous materials. [1]

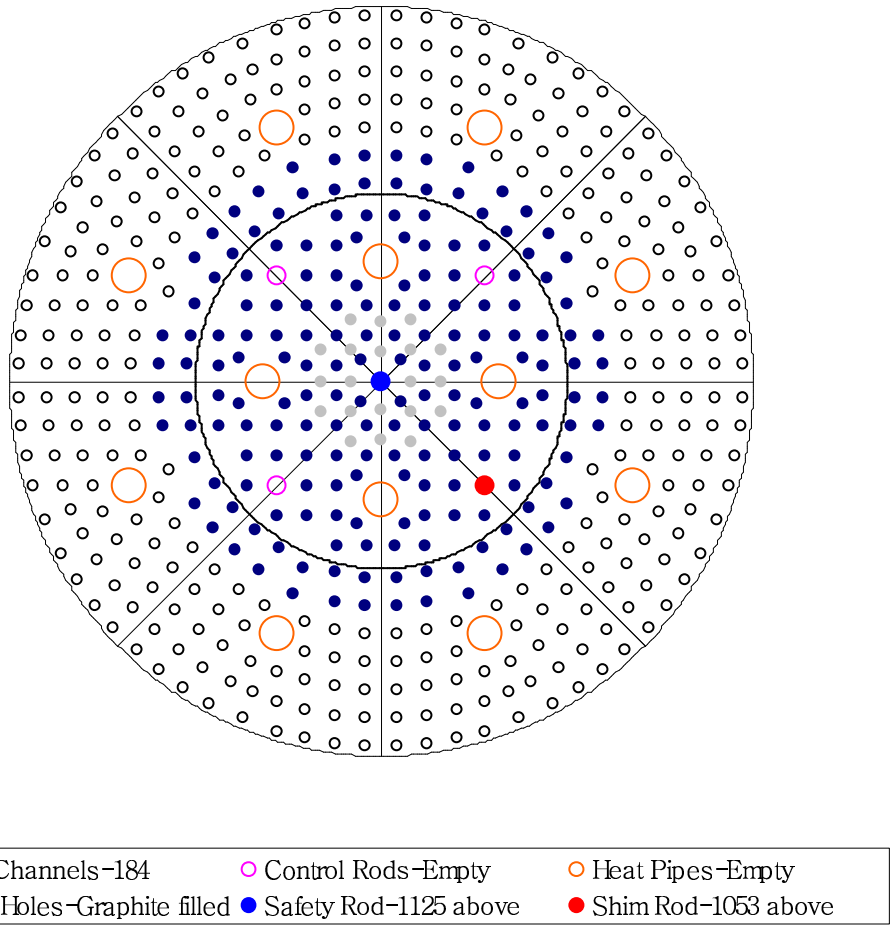

Figure 3. First Critical Core Configuration.

Other Configurations

The three other configurations were obtained in stages. These included various loadings of zirconium and stainless steel tubes used to mock up the heat pipe walls, and various arrangements of mock up control rod configurations. As in the first core, the last three cores had graphite rods in the 20 replacement channels (i.e., extra hole locations).

The second core was obtained by the addition of 11 zirconium heat pipes, which necessitated the increase in the core loading to 202 fuel channels. This loading extends from the core center to the second ring in the outer core and additional 14 channels in the third ring as shown in Figure 4. The empty heat pipe location was approximately the south-east (SE) position in the outer core. [1]

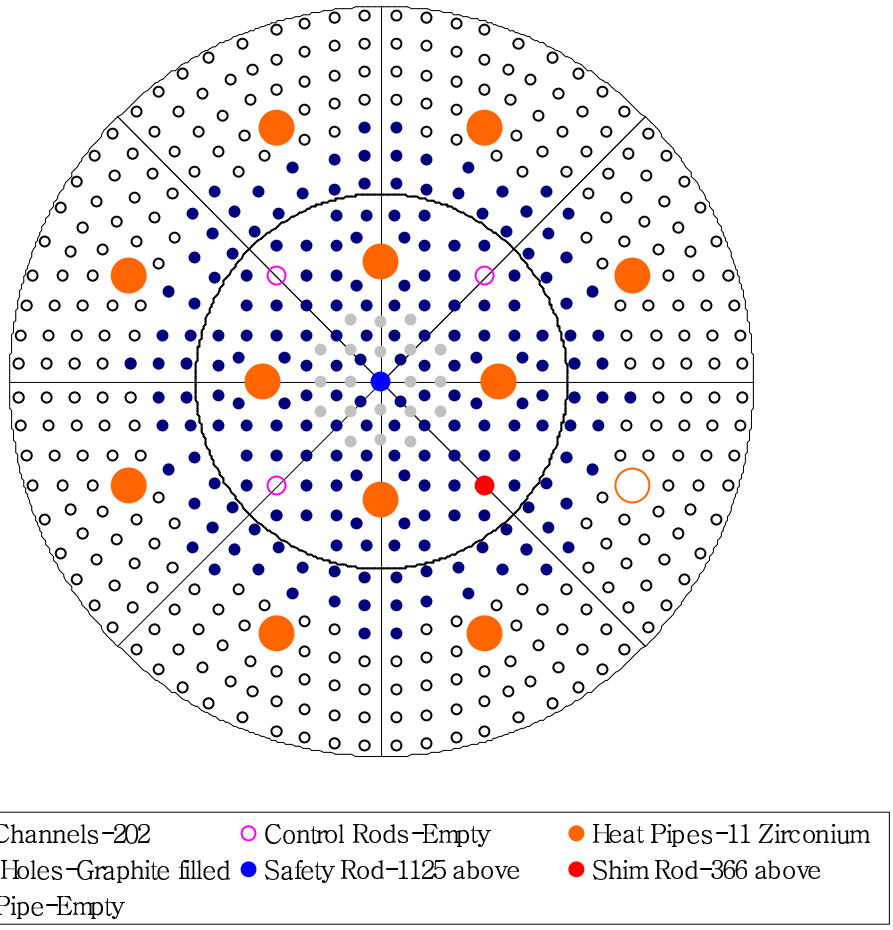

Figure 4. 202 Fuel Channel Configuration.

A relatively larger loading (380 channels) were required for the third core, because of the use of both 12 stainless steel simulated heat pipes and the loading of a stack of 21 natural B_4C pellets to represent a fully inserted CNPS control rod. [1] This loading extends from the core

center to the fifth ring in the outer core plus 32 channels in the sixth ring as shown in Figure 5. [1]

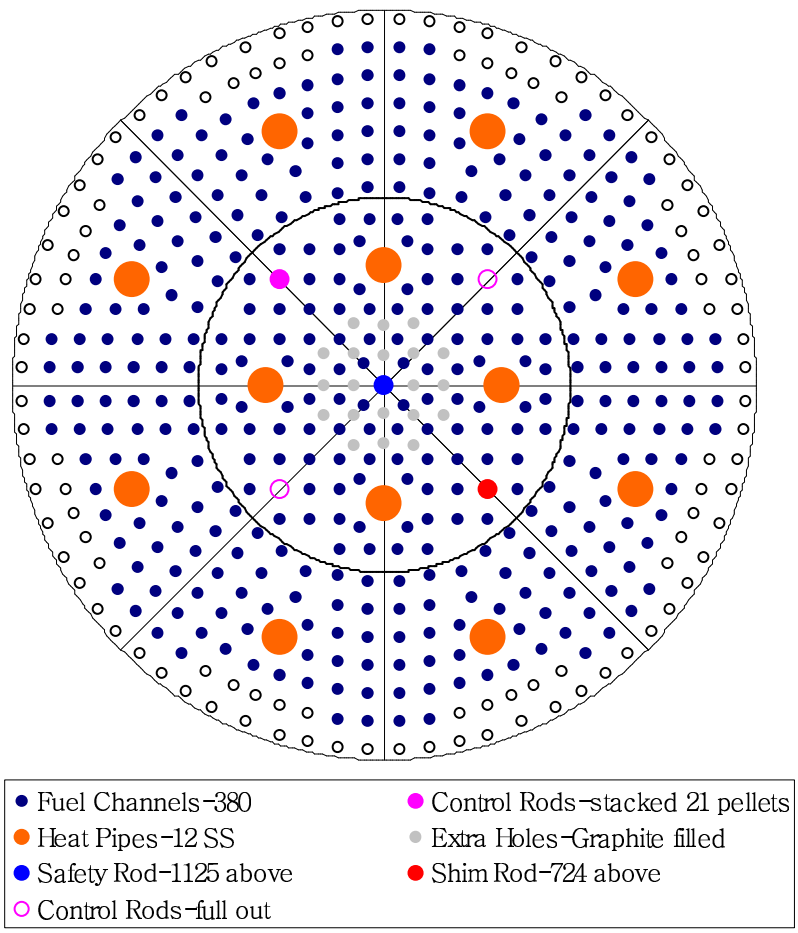

Figure 5. 380 Fuel Channel Configuration.

The full critical core loading (492 channels) was achieved with a combination of 12 stainless steel rods and the equivalent of 3 partially inserted (location in the core bottom) CNPS control rods as shown in Figure 6. Worth measurements were performed with this core configuration. [1] These include:

- Shim differential worth measurements by varying the number of B_4C cylinders in the outer control channels.

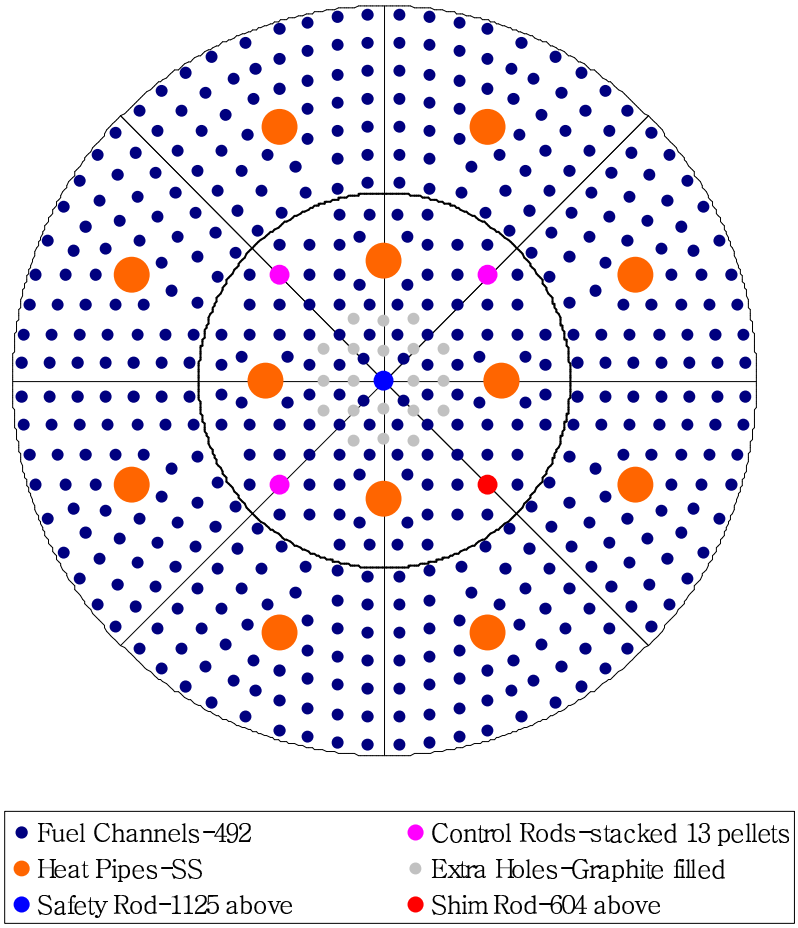

Figure 6. Full Critical Core Loading Configuration.

- Materials worths and central control rod worth measurements. The worth of the 54.88 at.% enriched B_4C rod was also measured.

- Temperature reactivity coefficient over a small range above the ambient room temperature (to less than 353 K) to confirm the negative temperature reactivity coefficient. This was done using electrical radiant heaters (calrods) placed near the radial surface of the exposed core. The calrods and the core were enclosed radially by an aluminum foil shroud to increase the efficiency of the heating process. Eighteen thermocouples were used to sample the temperature distributions in the core (none in the radial reflector). [1]

- Activity of foils placed in the outer surface of the heat pipes to confirm a uniform heat load to the stainless steel heat pipes (i.e., all pipes were designed to remove the same heat load).

2.3 Comparison of CNPS Data from Various Sources

Fuel Packing Fraction in Graphite Matrix

The initial Monte Carlo (MCNP) model developed for this study used a fuel packing fraction of 0.399. This value is based on the information provided in Table II of Ref.1, which gave a value for the "Packing fraction (by volume)". With this value of the packing fraction, the ^{235}U loading in a filled fuel channel was estimated to be 20.79 g. However, another paper by the same authors reported, without including detailed geometry and composition data, that a filled fuel channel contained 29.25 g of ^{235}U. [3] In order to resolve this inconsistency, Monte Carlo simulation of a CNPS core was performed using the detailed data in Ref. 1. The CNPS configuration containing 184 fueled channels was analyzed using the MCNP code with mostly ENDF/B-VI Release 6 library. For simplicity, homogenized fuel compacts were used rather than modeling fuel particles explicitly. The core eigenvalue determined with five million neutron histories was 0.9655 ±0.0004. This result suggested that the detailed information in Ref. 1 includes unidentified errors, since the grain heterogeneity effect of the CNPS fuel reported by the GA Technology is only 200 to 300 pcm. There was therefore a need to confirm or find additional source of data from those contained in Ref. 1.

Following evaluation of additional data (Refs. 2-4), it was found that the value in Ref. 1 is open to misinterpretation because of the apparent misuse of the word *packing fraction*. Apparently the value in Ref. 1 referred to the packing fraction (volume fraction) of the graphite matrix in the compact. With a fuel packing fraction of 0.601 (instead of 0.399) and a 1.245 cm diameter fuel compact with $UC_{0.3}O_{1.7}$ kernels, the uranium mass per fuel channel reported in Ref. 3 (29.25 g) was obtained. A re-analysis of the CNPS critical core configuration gave a k_{eff} value closer to unity. The information on the fuel compact was found in an LANL memorandum "Experimental Plan No. 215 – Delayed Critical Operation of CNPS Mock-up Assemblies," [5] (see discussion below).

The process of determining a correct core packing fraction for the CFP in the graphite matrix led to the finding of discrepancies between the data in the open literature for the CNPS design. These additional discrepancies were not as significant as that in the fuel packing fraction. Our solution to this issue is to collect a reference set of data, from which sensitivity calculations could be performed.

Resolution of Other Discrepancies

There are three reports in which data on the CNPS critical experiment are provided, including core configuration and experimental results; these are Ref. 1, 2 and 3. Additionally, a report on the neutronic design studies for a small, long-lived nuclear heat source (Ref. 4), a pre-analysis to the CNPS design, provides information on the TRISO fuel used in the CNPS. However, the information in Ref. 4, essentially corroborated those in Refs. 1 and 2.

The only other available literature on the CNPS is a packet of documents received at ANL from LANL, with the assistance of J. B. Briggs (INL). This packet included several LANL memoranda, a CNPS critical experiment plan, a draft report on the CNPS quality assurance program, and timetables for the CNPS project as well as budget summaries. The only pertinent information for the CNPS core is found under the title, "Experimental Plan No. 215 – Delayed Critical Operation of CNPS Mock-Up Assemblies, Q2-86-WP-67, January 23, 1986." [5] This experimental plan includes fuel compact diameter and a reference design core layout for the CNPS that includes a control rod thimble. In no other CNPS literature is there reference to control rod thimbles. The reference design core layout lists control rod thimble outer diameter of 3.0 cm and thickness of 0.1 cm but no material information. It is reasonable to assume that there was some control rod thimble during the CNPS critical experiment and this is discussed further in the MCNP modeling section of this report (Section 3.5).

A complete comparison of the CNPS configuration values given in the first three references (designated Reports 1, 2 and 3) is shown in Appendix C. The shim position for various CNPS configuration differs in all three reports. The values for graphite densities and uranium enrichment of the fuel are not consistent between Reports 1 and 2. Report 3 generally agrees with Report 1 for those material and dimensional values that are listed. However,

Report 3 gives the least amount of information of which the only difference is the below active core material thickness. The differences among the three reports are small enough that they could be attributed to round-off or human error in reporting. The significance of the CNPS literature differences is determined by MCNP modeling of each case for intra-comparison. The final set of data taken as *reference* in this study is summarized in Appendix B.

3. MCNP MODELING OF CNPS

3.1 Introduction

The complexity of the CNPS core design dictated the use of a code that could accurately represent the intricate geometrical arrangements in the core, for the purpose of creating a reference solution against which more efficient model could be compared. For this reason, the Monte Carlo code, MCNP, was selected for the reference model. MCNP provides a continuous energy capability that also allows detailed representation of the specified geometry. One disadvantage of the method is the enormous computer resources (computational time) required to obtain satisfactory solution with decent accuracy. It is planned in subsequent work to develop more efficient deterministic models for the core modeling. All the full-core results presented in this section were done with the MCNP code.

As a starting point, an MCNP input deck was created for the CNPS configuration with 184 fueled channels, representing these channels and other constituents such as the core graphite moderator, all 20 extra channels filled with graphite moderator, all graphite reflectors, full Al support plate, void heat pipe channels, void empty fuel channels, and void control rod channels. The calculated final eigenvalue given by this initial CNPS configuration is 1.00314 ± 0.00042. This value is reasonable and was expected to decrease as the various CNPS design elements are added to the MCNP model.

3.2 Input Information

The material compositions were initially taken from Ref. 1, being the most complete and most recently published. Using the material composition information, number densities and atom percents for input into the MCNP deck were calculated in a spreadsheet. The resulting "reference" data can be found in Appendix B. When creating the material cards in MCNP, constituent elements were separated to include the most isotope cross sections available. For graphite, $S(\alpha,\beta)$ data at 300 K were used to account for the thermal neutron scattering by the solid graphite moderator.

While the physical geometry of the CNPS configurations was modeled as accurately as possible there were a few assumptions made to simplify the MCNP input deck and speed up run time. The gap between the fuel compacts and fuel channel necessary for the physical loading of fuel was not modeled. Complete information was not provided in the references for this gap; none of the CNPS references listed a different fuel compact and fuel channel diameter. According to the fuel compact diameter found in the LANL memorandum "Experimental Plan No. 215," [5] the gap could have been 0.2 cm. This assumption is likely to cause a small over-prediction of core eigenvalues (since the gap could be a pathway for neutron streaming). Another assumption that was made is the Al cladding wall thickness of the shim rod. Although a thickness of 0.254 cm was assumed, Al has low cross sections for neutron interactions, making the relative significance of the cladding thickness extremely small.

The last significant assumption made was the spatial homogenization of the fuel rods in the MCNP input materials. This means that fuel grain heterogeneity was ignored, smearing the elemental contents of the TRISO fuel evenly throughout the fuel compact using volume weighting. Reference 1, quoting a General Atomics Technologies source, indicated the reactivity effect of the grain shielding to be on the order of 200 to 300 pcm. An evaluation of this effect was later made in this study (see Section 4).

3.3 Impact of Number of Neutron Histories

To ensure that the core k_{eff} values that were obtained are of reasonable accuracy, a first study focused on the impact of the number of neutron histories on the value of this core integral parameter. The total number of MCNP neutron histories is the product of the nominal source size per cycles and the number of k_{eff} cycle values. Additionally, the number of skipped k_{eff} cycles affects the final k_{eff} value. The input information of the neutron history is located under the *kcode* data card of the MCNP input structure. The final number of neutron histories to be employed is determined from a trade-off between run time and solution accuracy. Results have been obtained for different number of neutron histories and are summarized in Table 2.

For the same CNPS configuration, varying the neutron history options (in the range evaluated) did not change the final eigenvalue more than the solution uncertainty, but did

increase the run time substantially. This is because the uncertainty of the MCNP solution is proportional to the inverse square root of histories run. It was determined that using five million neutron histories is enough to give sufficient accuracy in the k_{eff} to the third decimal place. For all other MCNP simulations in this work, a neutron history of five million was used.

Table 2. MCNP Neutron History Effect on CNPS First Core Eigenvalue (k_{eff}).

Critical Configuration		MCNP Calculated Value k_{eff}	Neutron History Options			Approx. run time (hr)
Fueled Channels	Shim Rod Position Above Active Core (cm)		Nom. Source Size Per Cycle	# of Skipped Cycles	# of k_{eff} cycle values stored	
184	105.3	1.00148 ± 0.00030	10000	5	1000	6
184	105.3	1.00156 ± 0.00043	10000	10	500	3
184	105.3	1.00147 ± 0.00045	10000	50	500	3
184	105.3	1.00157 ± 0.00042	10000	5	500	3
184	105.3	1.00166 ± 0.00018	50000	5	500	15
184	106.0	1.00128 ± 0.00043	10000	5	500	3
184	106.0	1.00166 ± 0.00018	50000	5	500	15

3.4 Impact of Discrepancies in CNPS Design Data on Solutions

The impact of discrepancies in the material composition and geometry design data (from References 1 to 3) on the core k_{eff} has been determined for "five" CNPS configurations: a simple no-shim 184-fueled channel case, and the four critical configurations. Results are summarized in Table 3 for the first two only. The results for the other cases have not been included in the table because they are still being verified. However, the observed trends are quite similar. The core k_{eff} values (eigenvalues) obtained using data from each of References 1 to 3 (designated as Reports 1 to 3) are presented. Note that Report 3 did not list enough information to make a full MCNP model. The values listed in Report 1 match those from Report 3 best and were used to fill in the missing information for the MCNP model of Report 3.

As expected the small difference (0.3 cm) in the starting axial position of the active core in Report 3 did not change the eigenvalue because of the thick bottom reflector. The eigenvalue of Report 3 model is statistically identical to that of Report 1 model.

The differences in results between Reports 1 and 2 are at most of the order of 100 pcm. Report 2 lists a slightly lower uranium enrichment and inner pyrolytic carbon layer density, which would have little overall effect in this MCNP model. Additionally, Report 2 lists a higher graphite moderator density and lower graphite reflector density compared to Report 1. The shim positions of Report 2 are on average further in the core than from Report 1. This particular variation of graphite densities and shim rod position causes an increase in neutron absorption in the shim and changes the moderator-to-fuel ratio, resulting in a lower k_{eff}.

Table 3. CNPS Core Eigenvalues using Values from Various Sources [1,2,3].

CNPS configuration as given in →	k_{eff} of MCNP Model		
	Report 1	Report 2	Report 3
184 Fueled Channels NO Shim	1.00314 ± 0.00042	1.00290 ± 0.00043	1.00310 ± 0.00043
184 Fueled Configuration	1.00148 ± 0.00042	1.00037 ± 0.00042	-

3.5 Control Rod Thimble Configuration

As previously mentioned, the control rod thimble thickness was presented as 0.1 cm in a reference design but no material information was provided. To determine the effect of these control rod thimble on the CNPS core eigenvalues they were added to the MCNP model. The control rod thimbles were modeled using both SS-316 and Zr-2.5Nb, common thimble materials. It was observed that in the same CNPS report that mentioned the control rod thimble, other core dimensions, such as heat pipe radius, did not match values given in other CNPS reports. In order to compare eigenvalues and determine sensitivities of the control rod thimble, CNPS configurations using both of these materials at varying thicknesses were modeled. Table 4 is a summary of the results for the 184-fueled channel configuration and also lists the corresponding

literature and the no thimble configuration eigenvalues. Similar calculations have been done for the other configurations. The results for these are still undergoing verification, but trends are similar to that for the 184-fuel channel configuration.

As expected stainless steel has a greater effect on the core eigenvalues than the zirconium alloy; stainless steel has a higher neutron absorption cross section than zirconium alloy. For all stainless steel control rod thimble configurations the core eigenvalue is below 1.0. The CNPS configurations using zirconium alloy, except for the case with a 0.2 cm thimble thickness, result in core eigenvalue slightly greater than 1.0. Also of note is the fact that the maximum difference in k_{eff} for the zirconium alloy cases over the thickness range of 0.05 to 0.2 cm is of the order of 100 pcm, while a much larger difference (~2000 pcm) is observed for the stainless steel cases over the same variation in the thickness.

The addition of stainless steel or zirconium alloy control rod thimbles to the MCNP model of the CNPS did not result in exactly matching the core eigenvalues presented in the references for the CNPS experiment (also shown in Table 4). This does not mean that the current model is wrong however. The eigenvalues from this study (either the no thimble or zirconium alloy thimble cases) are quite close to those reported in the CNPS references and to experimental measurement (C/E about 0 to 0.5%).

Table 4. CNPS Configuration Sensitivities to Control Thimble Data.

Fueled Channels	Simulated Heat Pipes	B_4C Pellets	Shim Rod Position above Active Core (mm)	Thimble Material	Thimble Thickness (mm)	k_{eff}	error ±	Literature k_{eff}	Without Thimble k_{eff}
184	0	0	1053	SS-316	0.25	0.99685	0.00041	0.993±0.003	1.00148
					0.5	0.99174	0.00040		
					1	0.98404	0.00043		
					1.5	0.97720	0.00041		
					2	0.97092	0.00042		
184	0	0	1053	Zr-2.5Nb	0.5	1.00105	0.00042	0.993+0.003	1.00148
					1	1.00046	0.00041		
					1.5	1.00052	0.00043		
					2	0.99972	0.00043		

3.6 Control and Material Worths

The CNPS reports used as reference for this work provided values of various design element worths measured and calculated at the time using MCNP and in some cases deterministic models. This detailed information allows for the comparison between our current MCNP results and the CNPS study results. The CNPS design elements for which worth measurements were performed and that were modeled are: central rod worth in dollars of natural and enriched B_4C for 184 and 492 fueled channels, stainless steel and zirconium alloy heat pipe worth in cents per kilogram separated into inner and outer core blocks for 184 fueled channels, and the worth in cents per kilogram of the 20-hole experimental channels filled with fuel and graphite. The modeling results and literature information are presented for comparison in Table 5 for the 184-fueled channel configuration. The worth is calculated relative to the voided state in the extra channels and the MCNP results used to calculate worth are shown in Appendix D.

The values reported in Table 5 are in either dollar or cent of reactivity. The conversion to these units was done in this work assuming a delayed neutron fraction (beta) value of 0.00737.

Table 5. Comparison of CNPS Design Element Worths.

	Literature Values		Current MCNP Calc.
	MCNP [1]	Experiment [1]	
Central Rod Worth ($), Natural B_4C			
184 fueled channel	8.2 ± 0.7	7.6 ± 0.3	9.03 ± 0.08
Replacement Worth (¢/kg) of 20 extra holes, 184 fueled channels			
Fuel	10.8	11.4 ± 0.4	9.51 ± 0.08
Graphite	3.3 ± 5.4	10.7 ± 0.6	12.20 ± 0.08

The current MCNP modeling for the central rod over-predicted the worth. Conversely, for the other CNPS design elements, the current MCNP model either under-predicted or over-predicted the worths. In general the MCNP modeling results presented in Ref. 1 were closer to experiment values. It is however noted that those earlier MCNP calculations used a much smaller number of neutron histories (50,000) [1] to reduce significantly the computational time. As a result, these earlier MCNP results show much higher uncertainties in the results. Overall, our

current MCNP results are close to measurement values, though only in the case of the 20-hole replacement with graphite worth experiment is the results better than those presented in Ref. 1.

These results do not reveal any overall single bias in the MCNP benchmark modeling. Rather, it is likely that the uncertainty in the exact heat pipe material composition and modeling simplifications of geometry and fuel slightly skew the result obtained with our current model. The number of neutron histories used for the calculations might also be a source of error.

3.7 Shim Differential Worth

The shim differential rod worths for the CNPS "clean" core and fully-loaded core configurations were measured by the experimental team. The measurement results, in cents per centimeter, are presented graphically in Ref. 1. However, it was not described how these plots were generated. The numerical data used to generate the plots were not provided either, so only general information can be obtained from the graph; e.g., the shape of the shim differential worth curve is close to cosine. Note additionally that the exact configuration of the clean core was not provided in Ref. 1; it also referred to the use of an undefined "miscellaneous material" in the 20 extra channels.

We have however generated shim differential worth for the 184- and 492-fueled channel core configurations. These are referred to in the following paragraphs as the *clean* and *fully-loaded* cores, respectively. The first attempt to generate the shim differential worth curve was done by modeling with MCNP the shim at various positions in the CNPS core and comparing cases with 1.0 cm difference in position. This method did not produce meaningful results because the computational uncertainty of each core eigenvalue was larger than the difference between core eigenvalues corresponding to a 1.0 cm shim position difference.

Alternately, the core k_{eff} obtained from the MCNP calculations were used to generate integral worth data for the two core configurations. These integral worth data were then fitted as a function of the shim position. The plots of the integral worth data and polynomial fits are displayed in Figure 7. The correlation coefficient (R^2) indicates the goodness of the fits.

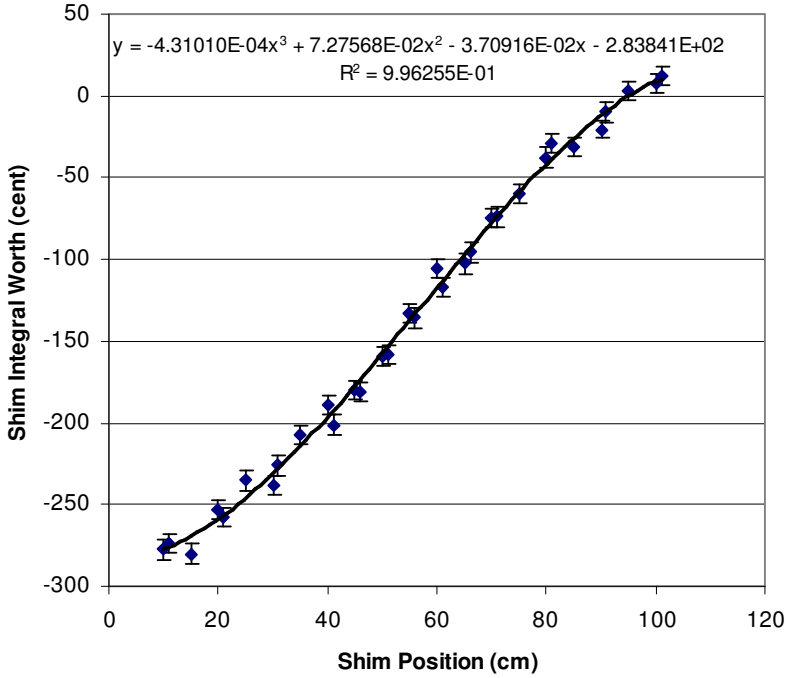

(A)

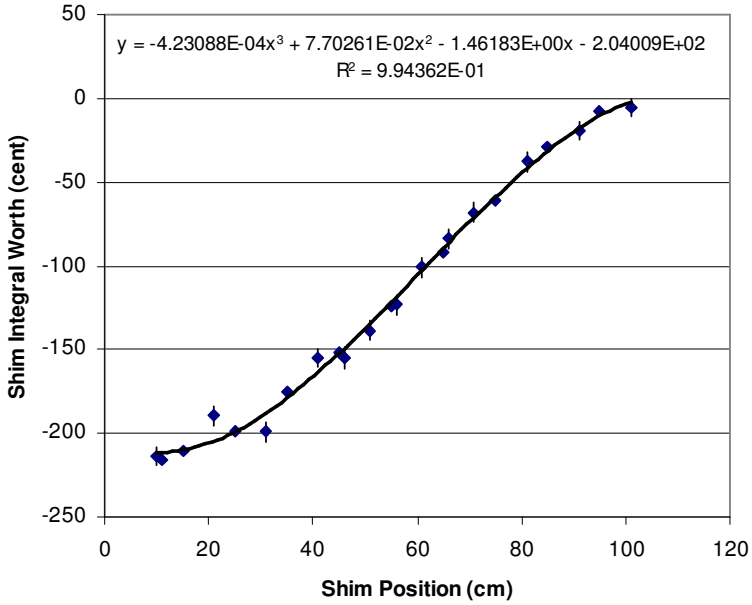

(B)

Figure 7. (A) Shim Integral Worths for 184-Fueled Configuration and (B) Shim Integral Worth for 492-fueld configuration. (Zero position corresponds to the bottom of the active core.)

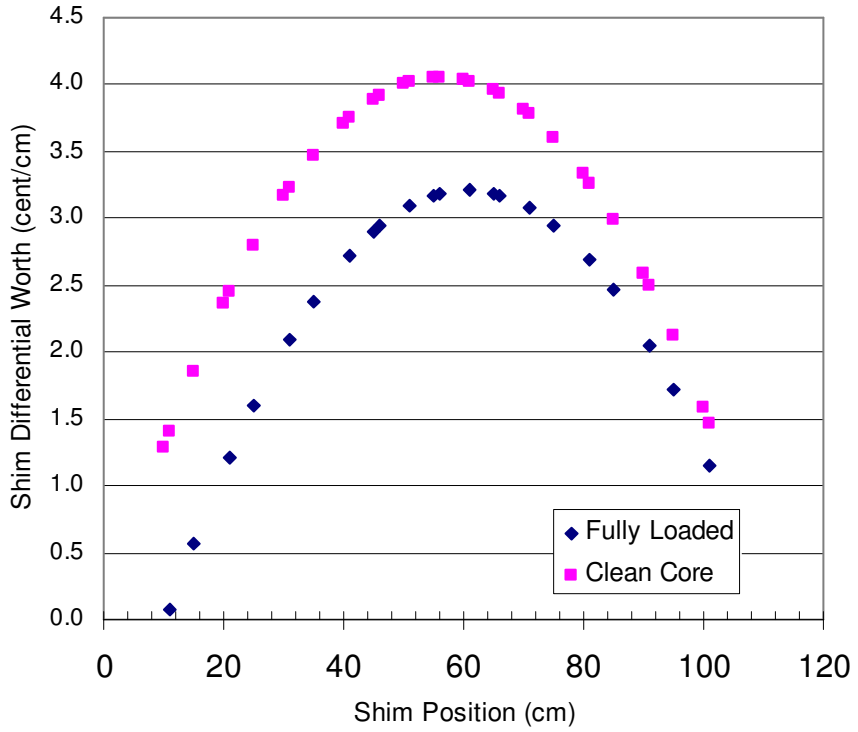

Figure 8. Shim Differential Worths for Clean (184-Fueled) and Full-Loaded (492-Fueled) Core Configurations.

The shim integral curves are then used for determining the shim differential worths by differentiating the curves at points along the core height. The differential worth curves that were obtained are displayed in Figure 8. For both core configurations the maximum shim differential worth agrees with the literature curve, approximately at 3.9 and 3.2¢/cm for the clean and fully-loaded configurations respectively.

The other important trend is the asymmetry exhibited in the differential worth of the fully loaded configuration. The asymmetry is also seen in the shim differential curve presented in Ref. 1 for this case. This is because the fully loaded core is heavily poisoned in the lower half by the B_4C absorber, which tilts the flux upward. [1] Even though calculated values of the shim differential worth do not match the available CNPS literature data, the distinct cosine shape and trends are apparent.

4. RELEVANCE OF CNPS TO VHTR

Some core parameters for the CNPS have been calculated and compared to those for a prismatic block-type VHTR design that were developed in FY 2004. The VHTR used TRISO fuel with a uranium enrichment of 14% U-235. [6] Results of the comparisons are summarized in this section.

4.1 Double Heterogeneity Effect

The fuel packing fraction (coated fuel particle volume fraction in the compact) used for the VHTR design is between 0.20 – 0.25, while that for the CNPS is 0.601. This would suggest different physics behaviors of the cores. A first core parameter that was compared is the double heterogeneity effect of the fuel zone, which provides an indication of the impact of not explicitly treating the self-shielding of the CFPs. This parameter has typically been calculated as the reactivity difference of a calculation using a homogenized compact model and one using an explicit treatment of the CFPs. Calculation of this parameter has been previously done for the VHTR fuel element, and was found to be about 2300 pcm.

The MCNP results reported for the CNPS in Section 3 were performed using a homogenized model in which the coated fuel particles (CFPs) and the graphite matrix were smeared (homogenized) into a single compact composition using volume weighting. This was deemed appropriate for the current study, because the double heterogeneity effect was expected to be small due to the high packing fraction (0.601). A model that explicitly represents the CFPs was subsequently developed and used to evaluate the double heterogeneity effect of the CNPS. The 184 fueled-channel core was selected for the explicit CFP calculations. It was assumed that the shim rod is positioned at 105.3 cm and that the thimble material is Zr-2.5Nb with a thickness of 0.1 cm. The body centered cubic (BCC) regular lattice model was utilized to describe the individual coated fuel particles in the fuel compact. In the BCC model, the “cubic size” was adjusted to conserved the kernel mass. In the Monte Carlo calculations, five-million neutron histories were traced after 50,000 neutron histories were skipped.

Table 6 provides the k_{eff} (eigenvalue) obtained from the MCNP4C calculations. Due to the double heterogeneity effect, the k_{eff} value increases when the coated fuel particles were

explicitly modeled. The double heterogeneity effect of the CNPS is only 174 pcm, compared to the 2300 pcm for the block-type VHTR fuel element. This lower value is due to the much higher CFP packing fraction in the CNPS fuel compact, which tends to minimize the impact of mispredicting the magnitude of the resonance self-shielding.

Table 6. Eigenvalues of CNPS with Different Coated Fuel Particle Models.

Fueled Channels	Shim Position (cm)	Thimble Material	Thimble Thickness (cm)	Coated fuel particle model	k_{eff}
184	105.3	Zr-2.5Nb	0.1	Smeared	1.00046±0.00041
				Explicit	1.00220±0.00044

4.2 Neutron Spectrum

The neutron spectrum of the CNPS core has been compared to that of the VHTR fuel assembly. The spectrum plots are displayed in Figure 9.

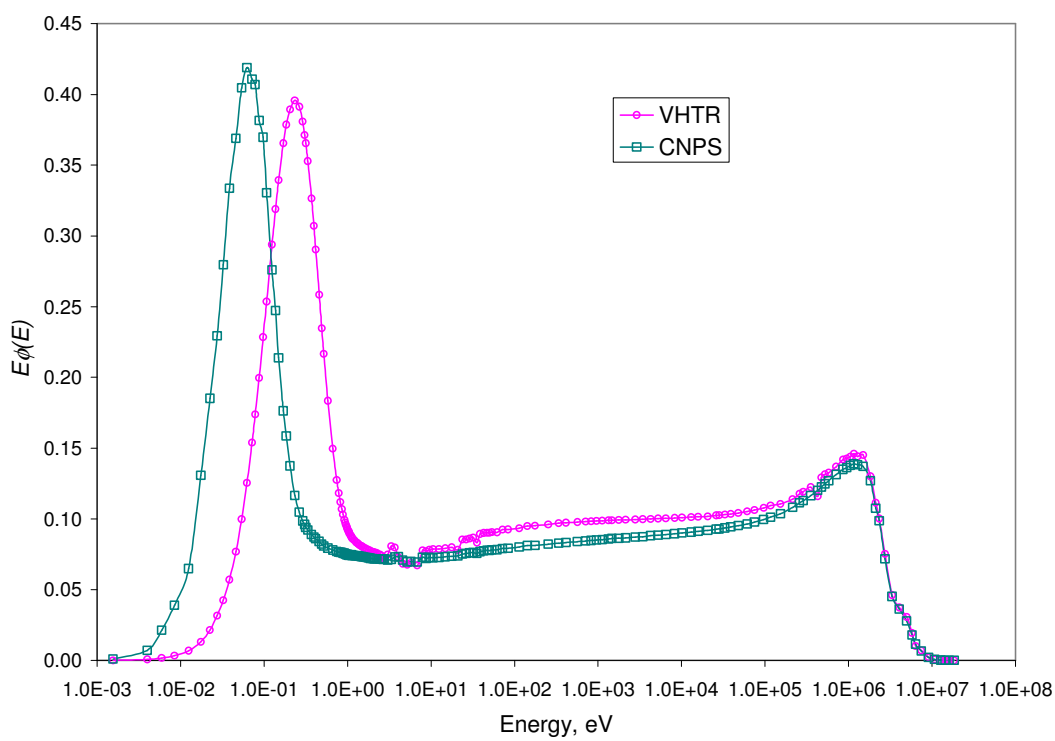

Figure 9. Neutron Spectra for the CNPS and Block-Type VHTR.

The two spectra have quite similar shapes. The thermal fraction of the VHTR spectrum is however lower and its thermal peak is shifted to higher energy, relative to the CNPS spectrum, because the VHTR assembly has a significantly higher fuel-to-moderator ratio than CNPS core and its calculation was performed at operating temperature conditions; the CNPS calculation was for the cold state in which the experimental measurements were performed. These different spectra might result in different reactivity impacts (magnitude) for these resonances, and might account for the lower double heterogeneity effect observed for the CNPS (though the contributions to the double heterogeneity effect have not been evaluated in this study).

5. CONCLUSIONS

An evaluation of the Compact Nuclear Power Source (CNPS) experiments conducted at the Los Alamos National Laboratory (LANL) in the late 1980s was done in this work using information available in the open literature. Even for the limited sources of information, there were inconsistency in specified values that were mostly attributed to numerical round-off and possible human-errors in recording data in the References. The variations in data did not produce large or unexpected differences in core eigenvalues. A major issue was the initial misinterpretation of the value given for the packing fraction of the fuel particles in the fuel compact. Subsequent analysis indicated that the fuel particle packing fraction is about 0.60.

The Monte Carlo (MCNP) results that were obtained for critical test configurations have been quite good with k_{eff} values within 0.5% of the critical value of unity. The material worths calculated in this study were in general close to the measurement values and previous MCNP modeling presented in the CNPS literature. The MCNP calculations have provided useful information on the CNPS design. Sensitivity studies on the shim thimble showed that using zirconium alloy as the thimble material resulted in core k_{eff} value that would be representative of a critical configuration. For this material, the variation of the thimble thickness from 0.05 to 0.2 cm had little impact (of order 100 pcm) on the core k_{eff}.

The lack of information on design data uncertainties and the inconsistency in the design data from different sources make it difficult to quantify the uncertainty in the core integral parameters arising from design data uncertainties. The evaluated configurations could however be useful as numerical benchmarks that are based on the currently available information.

ACKNOWLEDGMENTS

This ANL work was supported by the U.S. Department of Energy, Office of Nuclear Energy, Science and Technology (Generation IV Program) under Contract number W-31-109-Eng-38.

REFERENCES

1. G. E. Hansen and T. G. Palmer, "Compact Nuclear Power Source Critical Experiments and Analysis," *Nucl. Sci. Eng*., **103**, 237 (1989)

2. R. G. Palmer, "Postanalysis of the CNPS Critical Experiments," *Proc. Int'l. Reactor Physics Conference*, Jackson Hole, Wyo., 18 September 1988.

3. G. E. Hansen, J. H. Audas, E. R. Martin, R. A. Pederson, G. D. Spriggs, and R. H. White, "Critical Experiments in Support of the CNPS Programs," *Proc. Int'l. Reactor Physics Conference*, Jackson Hole, Wyo., 18 September 1988.

4. J. W. Durkee Jr. and G. E. Palmer, "Neutronic Design Studies for and Unattended, Low Power Reactor," *Proceeding of the Topical Meeting on Reactor Physics and Safety*, Saratoga Springs, NY, 17-19 September 1986.

5. "Experimental Plan No. 215 – Delayed Critical Operation of CNPS Mock-Up Assemblies, Q2-86-WP-67, January 23, 1986." (LANL document.)

6. T. K. Kim, W. S. Yang, T. A. Taiwo, H. S. Khalil, "Equilibrium Cycle Analysis in Support of Fuel Specification for Next Generation Nuclear Power Plant," *Proc. of ICAPP '05*, Seoul, Korea, May 15-19, 2005.

Appendix A

Table A.1 Fuel, Control Rod, Heat Pipe, and Extra Hole Channel Positions.

Fuel Channel		Fuel Channel		Fuel Channel	
X	Y	X	Y	X	Y
Coordinate of Channels in the 45-deg Core Sector (mm)					
32.33	32.33	534.99	73.41	448.48	209.62
71.63	23.88	580.34	73.41	498.89	206.64
119.37	23.88	119.37	119.37	540.43	223.85
153.59	37.40	167.12	119.37	303.85	267.59
228.40	37.40	214.88	119.37	365.90	262.11
262.62	23.88	300.14	124.32	425.07	253.75
313.91	25.65	341.67	141.53	482.11	243.25
359.06	25.65	386.32	121.16	335.87	299.62
404.06	25.65	433.47	121.16	398.08	294.29
449.36	25.65	479.99	121.16	457.77	286.45
494.38	25.65	526.24	121.16	515.44	276.59
539.39	25.65	572.28	121.16	367.00	331.46
584.49	25.65	214.88	167.12	430.19	326.41
71.63	71.63	268.48	164.68	490.32	319.01
119.37	71.63	465.34	168.91	399.54	363.42
167.12	71.63	512.91	168.91	462.25	358.48
214.88	71.63	560.04	168.91	431.36	395.12
262.62	71.63	239.42	203.84	Control Rods	
306.29	73.41	301.05	197.26	0.00	0.00
352.35	73.41	358.84	187.51	167.12	167.12
398.17	73.41	271.99	235.73	Heat Pipes	
444.06	73.41	333.44	229.65	191.00	0.00
489.57	73.41	392.18	220.85	405.49	167.96
Coordinates of Extra Holes in the 90-deg Sector (mm)					
47.75	0.00	0.00	96.51	95.51	49.60
0.00	47.75	47.75	49.60	47.75	97.40
95.51	0.00				

Appendix B

Table B.1 Description of the Fuel Compact [1,5]

Component	Thickness (mm)	Density (Kg/m^3)	Other
Kernel	0.5065	10620	
C/U ratio			0.3
O/U ratio			1.7
Enrichment (weight)			0.199
Carbon buffer	0.0790	960	
Pyrolytic graphite	0.0330	1900	
Silicon carbide	0.0350	3210	
Pyrolytic graphite	0.0350	1870	
Graphite matrix		700	
Fuel particle packing fraction (by volume)			0.601

Table B.2 Number Densities for Core Materials

	Number Density (Atoms/barn-cm)	Atomic Fractions		Remarks
Fuel Compact	6.13572E-02			
	5.75967E-02			Smeared over fuel channel
		U-235	9.24802E-03	
		U-238	3.67543E-02	
		C	7.87630E-01	inner PyC density = 1.90
		O	7.82039E-02	5.2 ppm boron impurity
		Si	8.81594E-02	
		B-10	8.98535E-07	
		B-11	3.65101E-06	
Core Block	9.02515E-02			density = 1.80 g/cc
		C	9.99999E-01	
		B-10	2.91439E-07	0.8 ppm boron impurity
		B-11	1.18420E-06	
Aluminum Plate	6.02626E-02			
		Al-27	1.00000E+00	
Bottom Reflector	8.92488E-02			density = 1.78 g/cc
		C	9.99998E-01	
		B-10	4.91803E-07	1.35 ppm boron impurity
		B-11	1.99834E-06	
Upper Reflector	8.77446E-02			density = 1.75 g/cc
		C	9.99998E-01	
		B-10	4.91803E-07	1.35 ppm boron impurity

		B-11	1.99834E-06	
Top Reflector	8.87474E-02			density = 1.78 g/cc
		C	9.99998E-01	
		B-10	4.91803E-07	1.35 ppm boron impurity
		B-11	1.99834E-06	
Radial Reflector	9.02515E-02			density = 1.80 g/cc
		C	9.99999E-01	
		B-10	2.91439E-07	0.8 ppm boron impurity
		B-11	1.18420E-06	
Graphite Rod in	9.02515E-02			
Extra Channels	8.47202E-02			Smeared over channel
		C	9.99999E-01	
		B-10	2.91439E-07	0.8 ppm boron impurity
		B-11	1.18420E-06	
B4C Shim	4.84999E-02			B4C density = 0.89 g/cc
		C	2.00000E-01	19.9 a/o B-10
		B-10	1.59200E-01	
		B-11	6.40800E-01	
Natural B4C Pellet	1.25928E-01			B-10 mass = 7.44 g
		C	2.00000E-01	19.75 a/o B-10
		B-10	1.58000E-01	
		B-11	6.42000E-01	
Enriched B4C Pellet	1.26088E-01			B-10 mass = 20.7 g
		C	2.00000E-01	54.88 a/o B-10
		B-10	4.39040E-01	
		B-11	3.60960E-01	
SS316 Heat Pipe	8.67142E-02			density = 7.96 g/cc
		C	3.68085E-03	0.08 w/o
		Mn	2.01180E-02	2 w/o
		Si	1.47573E-02	0.75 w/o
		Cr	1.80678E-01	17 w/o
		Ni	1.12985E-01	12 w/o
		Mo	1.44002E-02	2.5 w/o
		P	8.02873E-04	0.045 w/o
		S	5.17033E-04	0.03 w/o
		N	3.94541E-03	0.1 w/o
		Fe	6.48115E-01	65.495 w/o
Zr Heat Pipe	4.29823E-02			density = 6.511 g/cc

Appendix C

Table C.1 Comparison of Design Specifications from Different Sources

		Reference 1	Reference 2	Reference 3
Fuel Compact				
kernel	diameter (mm)	0.5065	0.5065	NL
	density (kg/m^3)	10620	10620	NL
	C/U ratio	0.274	0.274	NL
	O/U ratio	1.631	1.631	NL
	enrichment (weight)	0.199	0.1989*	0.199
C buffer	thickness (mm)	0.079	0.079	NL
	density (kg/m^3)	960	960	NL
PyC	thickness (mm)	0.033	0.033	NL
	density (kg/m^3)	1900	1870*	NL
SiC	thickness (mm)	0.035	0.035	NL
	density (kg/m^3)	3210	3210	NL
PyC	thickness (mm)	0.035	0.035	NL
	density (kg/m^3)	1870	1870	NL
C matrix	density (kg/m^3)	700	700	NL
Impurity	boron equivalent, ppm	5.2	NL	5.2
Fuel Compact Atomic Ratio				
	O/U	NL	NL	1.7
	Si/U	NL	NL	1.88
	C/U	NL	NL	17.34
Fuel Channel				
	hole diameter (mm)	12.85	12.85	12.85
	height (mm)	1100	1100	1100
	active core height (mm)	1084.6	1084.6	NL
	bottom of active core (mm)	27	27	30*
	fuel compacts	22	22	22
	compact height (mm)	50	50	50
	U235 mass (g)	NL	NL	29.25
Core Dimension				
	height (mm)	1130	1130	1130
	diameter (mm)	1200	1200	1200
Graphite Density (kg/m^3)				
	central core block	1800	1820*	NL
	outer core block	1800	1800	NL
	radial reflector	1800	1800	NL
	bottom reflector	1780	1750*	NL
	upper reflector	1750	1750	NL
	top reflector	1770	1750*	NL

Graphite Impurity (boron equivalent, ppm)			
central core block	0.8	NL	NL
outer core block	0.8	NL	NL
radial reflector	0.8	NL	NL
bottom reflector	1.35	NL	NL
upper reflector	1.35	NL	NL
top reflector	1.35	NL	NL
Shim Rod Position (mm above active core bottom)			
184 fueled channels	1053*	1160*	1130*
202 fueled channels	366*	346*	NL
380 fueled channels	724*	702*	NL
396 fueled channels	NL	NL	502
492 fueled channels	604*	583*	774*
B_4C Control Rod Compacts			
diameter (mm)	23.9	NL	NL
length (mm)	50.13	NL	NL
Natural ^{10}B atomic percent	19.75	NL	NL
Enriched ^{10}B atomic percent	54.88	NL	NL
B_4C Shim Rod			
diameter (mm)	12.57	NL	NL
length (mm)	1633	NL	NL
^{10}B atomic percent	19.9	NL	NL
density (g/cm^3)	0.89	NL	NL

NL-Not Listed
* Difference between references.

References of CNPS Literature

1. G. E. Hansen and T. G. Palmer, "Compact Nuclear Power Source Critical Experiments and Analysis," *Nucl. Sci. Eng.*, **103**, 237 (1989)

2. R. G. Palmer, "Postanalysis of the CNPS Critical Experiments," *Proc. Int'l. Reactor Physics Conference*, Jackson Hole, Wyo., 18 September 1988.

3. G. E. Hansen, J. H. Audas, E. R. Martin, R. A. Pederson, G. D. Spriggs, and R. H. White, "Critical Experiments in Support of the CNPS Programs," *Proc. Int'l. Reactor Physics Conference*, Jackson Hole, Wyo., 18 September 1988

Appendix D

Table D.1 Worth Results

20-Hole	fuel	graphite
	0.6425	0.6425
	108.46	108.46
	140.66	140.66
	1.9	1.8
	267.25	253.18

worths relative to void

	β=	0.00737								
Core Configuration										
	keff			keff						
	without	error ±	ρ	with	error ±	ρ	Δρ	Worth ($)	error ±	
Central Rod										
184-fuled	0.99174	0.00040	-0.00833	0.93033	0.00043	-0.07489	0.06656	9.03102	0.07969	
replacement of 20-hole										
184-fuel										
fuel	0.99746	0.00042	-0.00255	1.00120	0.00040	0.00120	0.00375	0.50815	0.07870	9.50689
graphite	0.99746	0.00042	-0.00255	1.00201	0.00044	0.00201	0.00455	0.61770	0.08253	12.19855

Evaluation of the High Temperature Engineering Test Reactor (HTTR) Start-up Experiments

T. K. Kim, T. A. Taiwo, and Frank Szakaly

Nuclear Engineering Division
9700 South Cass Avenue
Argonne National Laboratory
Argonne, IL 60439

September 12, 2005

Table of Contents

Page

Abstract 1

1. INTRODUCTION 2

2. DESCRIPTION OF HTTR 4

2.1 Overview of HTTR Experiments 4

2.2 Description of HTTR Core Configuration 5

2.3 Fuel Loading Scheme and Fuel Block Designation 7

2.4 Fuel Assembly 8

2.5 Burnable Poison Rods and Control Rods 11

2.6 Replaceable Reflector, Dummy, and Permanent Reflector Blocks 13

3.0 DESCRIPTION OF MATERIALS DATA 14

3.1 Materials Data of Fuel Assembly 14

3.2 Materials Data of Reflector, Control Rods Guide and Dummy Blocks 15

4.0 EXPERIMENTAL MEASUREMENTS 17

5.0 BENCHMARK SPECIFICATION 19

5.1 Description of Model 19

5.2 Materials Data 24

5.3 Temperature and Nitrogen Issue 27

6.0 EVALUATION OF BENCHMARK SPECIFICATION 28

6.1 Reference Monte Carlo Calculations 28

6.1.1 Number of Columns Required for First Criticality 29

6.1.2 Position of Control Rods for Critical Configurations 29

6.1.3 Core Excess Reactivity 30

6.1.4 Comparison to Other Monte Carlo Results 30

Page

6.1.5 Impact of Regular Lattice versus Random CFP Modeling 31
6.1.6 Impact of Nuclear Data Library 32
6.1.7 Impact of Homogeneous versus Heterogeneous Compact Modeling 33
6.1.8 Impact of Impurity on Core Criticality 33
6.2 Whole-Core Deterministic Calculations 34
6.2.1 Descriptions of the DRAGON and DIF3D codes 34
6.2.2 Lattice and Core Modeling 35
6.2.3 Results of Deterministic Calculations 37
7.0 CONCLUSIONS 40
8.0 REFERENCES 41

List of Tables

Page

Table 2.1. Primary Design Parameters of HTTR 5
Table 2.2. Configurations of Fuel Blocks in HTTR Core 11
Table 3.1. Materials Data of Fuel Compacts 14
Table 3.2 Materials Data of Coated Fuel Particles 15
Table 3.3. Materials Data of Fuel Compacts 16
Table 4.1. Measured Data in HTTR Start-up Core 18
Table 5.1. Number Densities of Fuel Compact.....25
Table 5.2. Number Densities of Graphite Block and Control Rods 26
Table 5.3. Number Densities in Replaceable Reflector Blocks 26
Table 5.4. Number Densities of Control Rods Guide Blocks 26
Table 5.5. Number Densities of Dummy Blocks 26
Table 6.1. Comparison of Number of Columns for First Criticality 29
Table 6.2. Control Rods Positions at Critical Conditions.....30
Table 6.3. Eigenvalues of HTTR Core Calculations 30
Table 6.4. Comparison of Monte Carlo Calculations for Full-Core Case 31
Table 6.5. Comparison of k_{eff} Obtained with Different Libraries 32
Table 6.6. Eigenvalues of HTTR Core Calculations 33
Table 6.7. Comparison of HTTR and VHTR Fuel Parameters.....37
Table 6.8. Eigenvalue Comparison for Deterministic HTTR Core Calculations 39

List of Figures

Page

Figure 2.1. Vertical View of HTTR 6
Figure 2.2. Horizontal View of HTTR and Fuel Column Loading Order 7
Figure 2.3. Structure of Fuel Assembly 9
Figure 2.4. Graphite Blocks with 31 and 33 Fuel Holes.....10
Figure 2.5. Fuel Assembly Zones in HTTR Core.....10
Figure 2.6. Axial Heterogeneity of Burnable Poison Rods 12
Figure 2.7. Control Rods Guide Block from 1st to 5th Layers.....12
Figure 5.1. Core Layout for HTTR Benchmark Model 19
Figure 5.2. Horizontal View of Layers 1 and 2 20
Figure 5.3. Horizontal View at 3rd Layer 20
Figure 5.4. Horizontal View at 4th Layer 21
Figure 5.5. Horizontal View at 5th Layer 21
Figure 5.6. Horizontal View at 6th Layer 22
Figure 5.7. Horizontal View at 7th Layer.....22
Figure 5.8. Horizontal View at 8th Layer 23
Figure 5.9. Horizontal View at 9th Layer 23
Figure 6.1. Fuel Compact Models 28
Figure 6.2. An Approximation Model for Generating Cross Sections of Control Rod Guide and Reflector Blocks 36
Figure 6.3. Block Models According to Axial BP Homogenization Approach 37
Figure 6.4. Spectra of HTTR Assemblies.....38

Abstract

An evaluation of the High Temperature Engineering Test Reactor (HTTR) start-up experiments has been performed using the data available in open literature. Monte Carlo (MCNP) and deterministic models were developed and used for the analysis of the four critical configurations of the HTTR, which were attained along the path to full-core loading. The results obtained show a significant difference (1.8% Δk/k) between the core criticality calculated by the MCNP code and the experimental measurement; larger differences of about 2.3 – 3.4 % Δk/k were found for the deterministic codes. These discrepancies are consistent with those reported during an HTTR experiment evaluation effort previously arranged by the IAEA. The magnitudes of these differences are attributed to the incomplete specification of the HTTR core configuration (e.g., impurities and nitrogen in graphite, design data uncertainties, etc), uncertainties in nuclear data, and of approximations inherent in the code solution methods (primarily for the deterministic codes). Due to the incomplete data, it is not possible at this stage to state conclusively the major contributions to the discrepancies.

1. INTRODUCTION

To give assurance that reactor analysts will be using a code capable of generating results that are representative of the system being analyzed, it is imperative that the code be used to model basic experiments or mock-ups of the system. This so-called validation step is important in the licensing of a reactor system. The task is however not straightforward for advanced systems, e.g., the Very High Temperature Reactor (VHTR), for which no experimental or mock-up facilities exists. This problem can be overcome initially by using representative and well documented numerical benchmarks to identify code limitations and needed improvements in code data and methodologies. Additionally, at a latter stage in the system life (e.g., at start-up), data would have to be generated to provide indications of the ability of the codes to represent accurately the system. Another approach that could be used in conjunction with those above would be to find existing representative experiments that could be used to evaluate the code performance for similar systems.

In FY 2004, a set of such existing experimental tests of potential relevance to VHTR (pebble-type and prismatic block-type) were identified by ANL and INL personnel. The experiments were ranked in order of relevance. One of the experiments given a high priority ranking is the High Temperature Engineering Test Reactor (HTTR) start-up test performed at JAERI (Japan) in the late 1990s. [1-3] This facility uses low enriched uranium fuel encased in TRISO fuel layers being considered for the VHTR. Additionally, the moderator and reflectors in the HTTR core are made of materials that are similar to those for the VHTR (graphite). Because of these attractions, the open literature information available on the HTTR start-up tests have been collected and used in an exercise designed to evaluate the performance of some of the Monte Carlo and deterministic tools available at ANL. The limitation in data is due to the fact that at the time of this effort no additional source of data (e.g., more detailed or proprietary data) was available to us. This report summarizes the results of the evaluation.

In Section 2, an overview of the HTTR experiments is presented along with a fairly detailed description of the core configurations and constituents. Material data for the various core constituents are presented in Section 3. Section 4 contains a description of the experimental

measurements and values derived from the measurements. In Section 5, the models that were developed in this study are presented along with the number densities derived from the data provided in Section 3. The results of the evaluations that have been performed are summarized in Section 6. Section 7 contains the conclusions from this study.

2. DESCRIPTION OF HTTR

2.1 Overview of HTTR Experiments

In the late 1980s, the Japan Atomic Energy Commission (JAEC) issued a revised report on the "Long Term Program for Development and Utilization of Nuclear Energy." The report stressed that Japan should proceed to develop more advanced reactor technologies in parallel with the upgrading of existing nuclear reactors. It was recognized in that program plan that though the High Temperature Gas cooled Reactor (HTGR) was not to be incorporated into the existing nuclear power plant systems there were benefits to be derived from its deployment, such as its inherent safety and its utilization for the production of high temperature heat, and should be pursued. [2] The JAEC also concluded that the demand for nuclear heat application (up to ~ 1,000 ^{o}C) is expected to become strong in the early part of the 21st century. Within this program, the committee recommended the construction of a test reactor to test and study advanced HTGRs. The committee's report also stated that the maximum reactor coolant outlet temperature should be 950 ^{o}C, which is the highest temperature attainable considering the current technology level. For irradiation test, a prismatic block type core structure was proposed, with a thermal power rating of 30 MW. Based on these suggestions, the Japan Atomic Energy Research Institute (JAERI) started building the High Temperature Engineering Test Reactor (HTTR) in 1992 and the first criticality was attained with an annular core type on November 10, 1998. [1-4]

The objectives of the HTTR program are to establish and upgrade the technological basis for the Advanced High Temperature Gas-cooled Reactors and to conduct various irradiation tests in support of innovative high-temperature basic research. The HTTR was designed to keep all specific safety features within the graphite blocks. The intermediate heat exchanger is equipped to supply high temperature helium, and the control system is designed to allow operation that simulates anticipated operational occurrences (AOO). The primary design requirement of the HTTR are [2,5] : (1) coated fuel particles shall not fail during normal operation and AOO; to satisfy this requirement, the maximum fuel temperature shall not exceed 1600 ^{o}C for any AOO, (2) the reactor shall be shut-down safely and reliably during operation using the control system;

furthermore, a reserved shutdown system (RSS) which is independent of the control system shall be provided, and (3) the residual heat after shutdown shall be removed safely, etc.

The primary design parameters of the HTTR are provided in Table 2.1. The thermal output of the HTTR is 30 MWt and the coolant outlet temperature is designed to be 850 ^{o}C at the rated operation, but it is allowed to be 950 ^{o}C for high temperature test operating conditions. The design life of permanent structural components in the HTTR plant is 20 years with a load factor of 60% of full power operation. [1,2,4]

Table 2.1. Primary Design Parameters of HTTR [4]

Design parameter	Unit	Value
Thermal power	MWt	30
Coolant outlet temperature	°C	850 (950[a)])
Coolant Inlet temperature	°C	395
Primary coolant pressure	MPa	4
Core structure	-	Graphite
Equivalent core diameter	m	2.3
Effective core height	m	2.9
Average power density	W/cm^3	2.5
Fuel uranium enrichment	wt %	3.4 – 9.9
Cycle length	EFPD	660
Coolant material	-	Helium gas
Flow direction	-	Downward
Reflector thickness (top/radial/bottom)	m	1.16/0.99/1.16
Number of fuel block	-	150
Number of fuel column	-	30
Number of pairs of control rods (in core/reflector)	-	7/9

a) High temperature test condition

2.2 Description of HTTR Core Configuration

Figures 2.1 and 2.2 show the vertical and horizontal cross sections of the HTTR. The core consists of core components and reactor internals. They are arranged in the reactor pressure vessel, which is 13.2 m high and 5.5 m in diameter. The core components are prismatic hexagonal blocks 58 cm high and 36 cm wide across the flats. These include fuel element blocks, control rods guide blocks, replaceable reflector blocks, and irradiation blocks. There is a small gap (2 mm) between the hexagonal graphite blocks. The reactor internals consist of graphite and metallic core support structures and shielding blocks.

The active core, which has a height of 2.9 m and an effective diameter of 2.3 m, consists of 30 fuel columns and 7 control rods guide columns. One column is composed of 9 core components piled up axially. Each fuel column consists of 2 top reflectors, 5 fuel blocks, and 2 bottom reflector blocks. The replaceable reflector region adjacent to the active core consists of 9 control rod columns, 12 replaceable reflector columns, and 3 irradiation columns, which are surrounded by permanent reflector blocks.

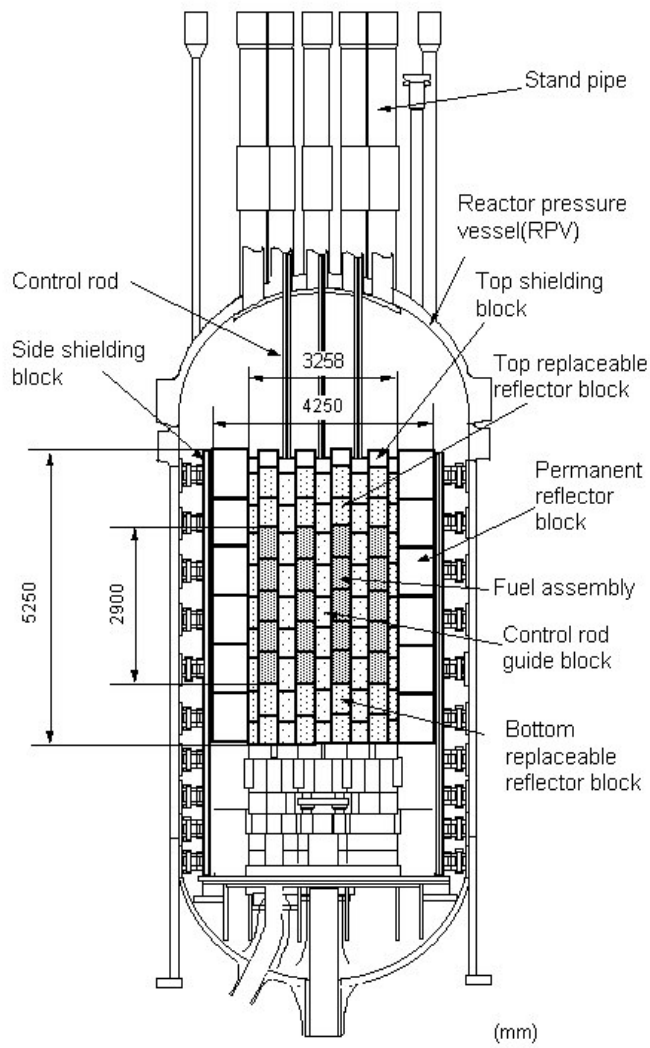

Figure 2.1. Vertical View of HTTR [4]

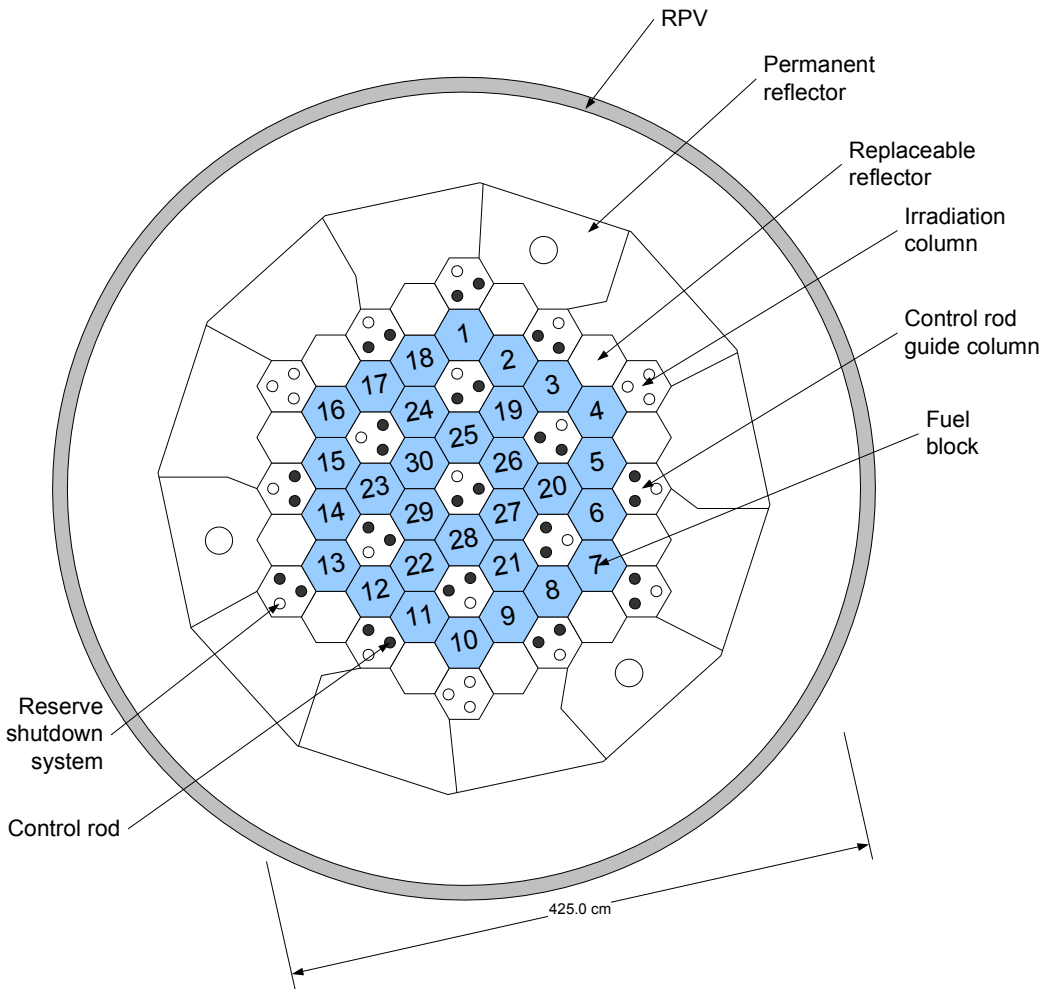

Figure 2.2. Horizontal View of HTTR and Fuel Column Loading Order [4]

2.3 Fuel Loading Scheme and Fuel Block Designation

An annular core is one of the promising core types for the future Very High Temperature Rector (VHTR) because of its high inherent safety characteristics following a loss of coolant accident. The decay heat removal is enhanced by introduction of the annular core because the heat transfer path will be shortened due to the relatively thin active core region. As a result, the fuel temperature in a loss of coolant accident can be maintained at less than the fuel temperature limit of 1600 °C. Thus, an annular core was planned as the approach to the first critical core type of the HTTR. It was anticipated that the experimental data for the annular core would be useful for the validation of computation tools and models for large-scale annular type VHTR cores.

Before fuel loading, the whole fuel region in the core is filled with dummy graphite blocks. The primary coolant system is filled with helium at normal atmospheric pressure and it is not in operation during fuel loading. [4] The core is at room temperature. To implement an annular core, the loading order of the fuel columns into the core was determined as shown in Figure 2.2; the fuels are loaded at first into the outermost rings of the active core and sequentially loaded into the core center. In experiments, the first critical core was obtained with 19 fuel columns [1] and all control rods fully withdrawn from the core. This means that the annular critical core was obtained by loading the fuel columns into the outermost core zone mostly. After the first criticality, subsequent core criticality was maintained by inserting control rods in the core. In the path to a full-core loading, two different annular cores were obtained in this experiment: a *thin annular core* with 18 fuel columns and a *thick annular core* with 24 fuel columns.

In this experiment, the position of a block in the core is distinguished by using the axial layer number and the radial column number. The axial layer numbers are counted from the top to the bottom of the core. For the radial column number, the column rings are alphabetically assigned from the core center, and the fuel blocks in the same ring are counted from the north in clockwise direction. For example, "*4C05*" block means that the block is located at the 4th layer from the top of the core, the 3rd ring from the core center, and the 5th block from the north in clockwise direction.

2.4 Fuel Assembly

Figure 2.3 shows the structure of the fuel assembly. A fuel assembly consists of fuel rods, burnable poison (BP) rods, and a fuel graphite block. The fuel rods are inserted into fuel holes of 4.1 cm diameter. The fuel rod is formed by the graphite sleeve (clad) containing 14 fuel compacts. The outer diameter of the graphite sleeve is 3.4 cm. There is no separate hole for the coolant and the coolant flows between the fuel rods and fuel holes. The fuel compact consists of coated fuel particles (CFPs) and graphite matrix. The form is a hollows cylinder of 1.0 cm inner diameter, 2.6 cm outer diameter, and 3.9 cm in height. Each fuel compact contains about 13000 CFPs embedded in the graphite matrix (the total number of CFPs is dependent on the packing fraction). A CFP consists of a spherical fuel kernel of low enriched UO_2 and the TRISO coating.

From the center of the CFP, the materials of TRISO coating are a low-density porous Pyrolytic Carbon (PyC) buffer layer, a high density PyC layer, a silicon-carbide (SiC) layer, and an outer PyC layer.

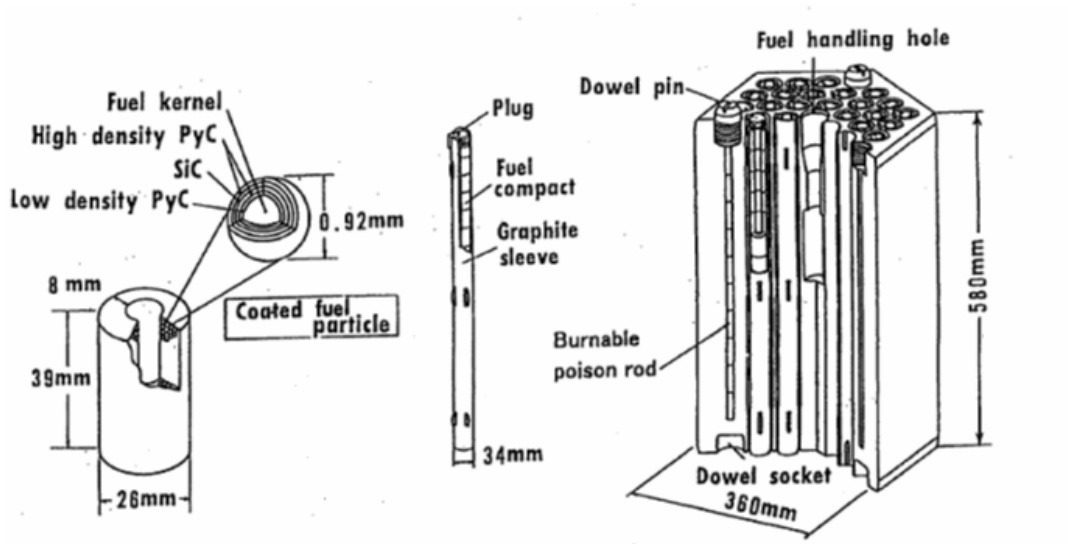

Fuel compact Fuel rod Fuel assembly

Figure 2.3. Structure of Fuel Assembly [4]

The HTTR has two types of fuel graphite blocks having 31 or 33 fuel rods (see Figure 2.4). Both graphite blocks have one fuel-handling hole and three holes for burnable poison (BP) rods; two of these holes are occupied by BPs and the other one is empty. In total, 12 different enriched uranium fuels and two different types of burnable poisons were used in the HTTR core (detailed information about BP are described in Section 2.5). The highest and lowest enrichments are 9.9% and 3.4%, respectively. The active core region is divided into four zones as shown in Figure 2.5 and the configuration of the fuel blocks are provided in Table 2.2. Fuels of higher-enriched uranium are placed in the upper and outer core regions, and fuel graphite blocks having 33 fuel rods are locate in zones 1 and 2. This loading scheme helps to reduce the maximum fuel temperature because a downward coolant flow direction is used in the HTTR.

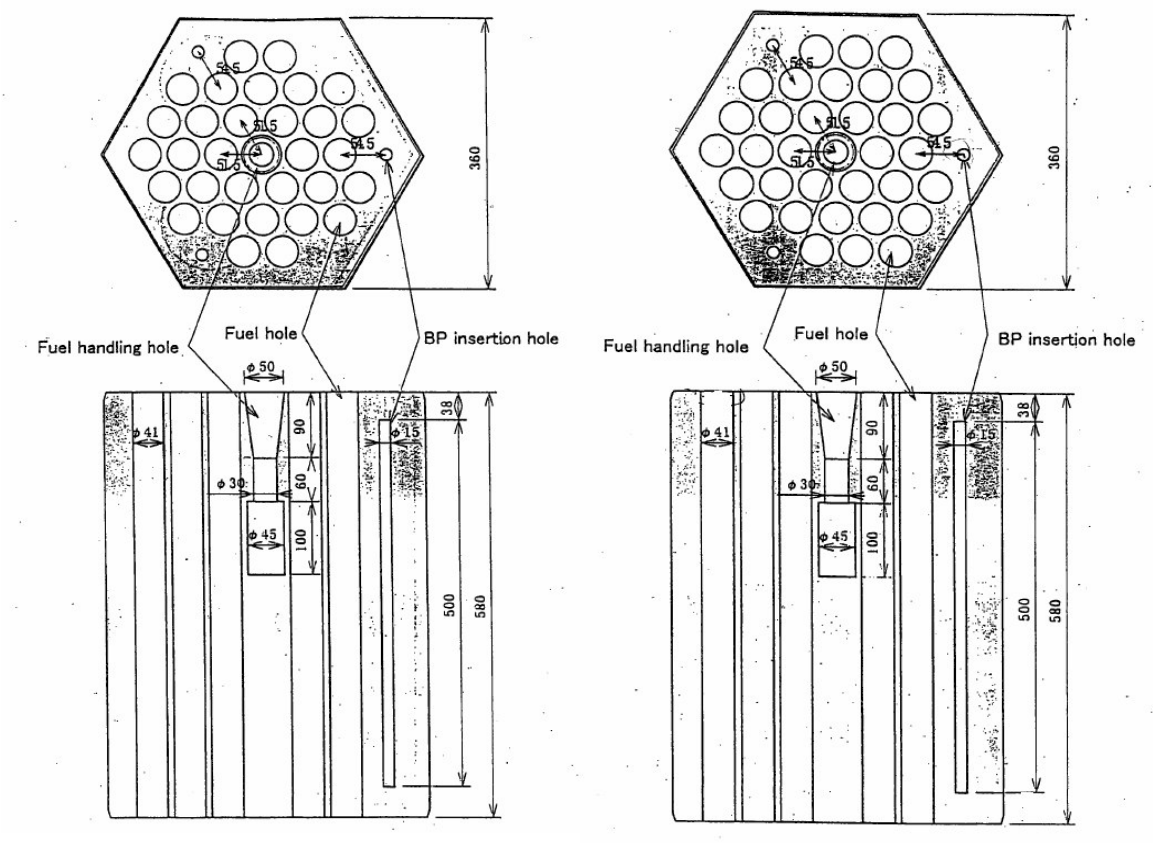

Figure 2.4. Graphite Blocks with 31 (left) and 33 (right) Fuel Holes [4]

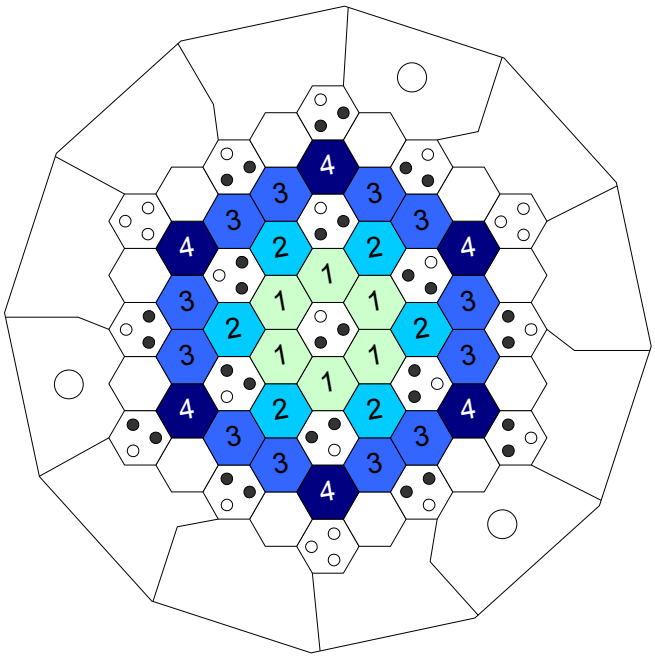

Figure 2.5. Fuel Assembly Zones in HTTR Core [4]

Table 2.2. Configurations of Fuel Blocks in HTTR Core [4]

Axial layer number [a)]	Items	Fuel zone number			
		1	2	3	4
3	Uranium enrichment (%)	6.7	7.9	9.4	9.9
	Number of fuel rods	33	33	31	31
	Burnable poison type	H-1	H-1	H-1	H-1
4	Uranium enrichment (%)	5.2	6.3	7.2	7.9
	Number of fuel rods	33	33	31	31
	Burnable poison type	H-II	H-II	H-II	H-II
5	Uranium enrichment (%)	4.3	5.2	5.9	6.3
	Number of fuel rods	33	33	31	31
	Burnable poison type	H-II	H-II	H-II	H-II
6	Uranium enrichment (%)	3.4	3.9	4.3	4.6
	Number of fuel rods	33	33	31	31
	Burnable poison type	H-1	H-1	H-1	H-1
7	Uranium enrichment (%)	3.4	3.9	4.3	4.6
	Number of fuel rods	33	33	31	31
	Burnable poison type	H-1	H-1	H-1	H-1

a) Axial layer number from the top of the core.

2.5 Burnable Poison Rods and Control Rods

Burnable poison (BP) rods are inserted into two of the three BP holes of the fuel graphite block. The ends of the BP holes are plugged by dowel pins. The BP rods consist of two BP pellets and graphite disks with a diameter of 1.4 cm and height of 50.0 cm. The 20 graphite disks, each of 0.5 cm thickness, are sandwiched between BP pellets (see Figure 2.6). Thus, total axial occupancies of the graphite disk and BP pellets in the BP hole are 10.0 cm and 40.0 cm, respectively. The BP pellet contains boron-carbide (B_4C) and carbon composite. Two types of BP pellets are utilized: H-I contains 2.22 wt.% natural boron and H-II contains 2.74 wt.% of the material.

There are 16 pairs of control rods: 7 in the active core and 9 in the replaceable reflector region. Figure 2.7 shows the control graphite block in the 1st to 5th layers. The control graphite block has three control rods guide holes, each of 12.3 cm diameter, and one fuel-handling hole: two holes are control rod insertion holes and the other hole is reserved for reactor shutdown system in case of an emergency. The control rod consists of 10 axial neutron absorber sections

connected with metallic spine and support ring. Each section contains 5 sintered compacts of B_4C and carbon composite as neutron absorber material in the annular space. The outer diameter of the control rod is 10.5 cm.

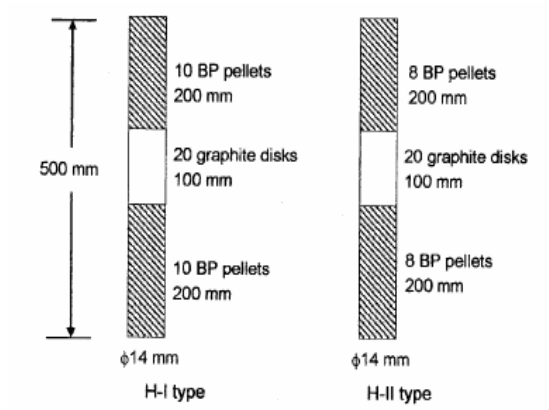

Figure 2.6. Axial Heterogeneity of Burnable Poison Rods [4]

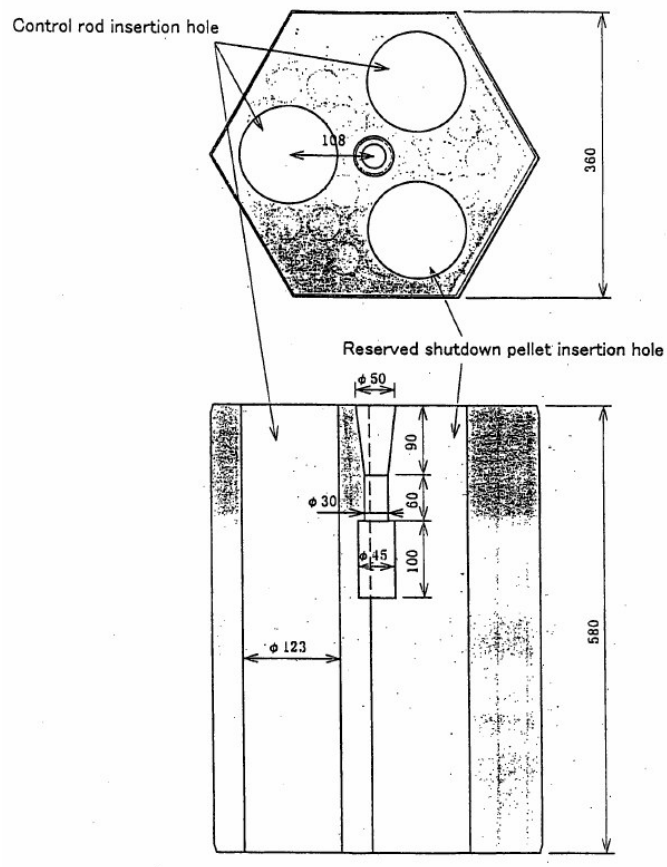

Figure 2.7. Control Rods Guide Block from 1st to 5th Layers [4]

When the control rods are fully withdrawn, the upper limit of control rods is the upper face of the 1st layer of fuel column except for columns E03, E05, E07, E09, E11, and E13. The control rods in these six columns have upper limit at 72.5 cm below from the upper face of the 1st block. [4,5] In operating the reactor, three pairs of control rods in columns E01, E09 and E17 are fully withdrawn; it is noted that these control rods are located in the replaceable reflector region and the naming of the columns was explained in section 2.3.

2.6 Replaceable Reflector, Dummy, and Permanent Reflector Blocks

Top and bottom replaceable reflector blocks are placed above and below the fuel assemblies. Except for the 9th layer reflector block, the number of coolant holes and their positions correspond to the fuel holes in the fuel block. However, the diameter of holes in the top and bottom reflector blocks is smaller than that of the fuel holes in the fuel block (2.3 cm versus 4.1 cm). The most bottom replaceable blocks (i.e., 9th layer) have six large coolant holes of 5.4 cm diameter. The radial replaceable reflector blocks, which surround the active core, have the same external shape to the top and bottom replaceable reflectors, but have no coolant holes. Boron pins are installed into all replaceable blocks of the 9th layer for neutron shielding.

The dummy blocks are initially loaded into the locations of the fuel columns before fuel loading. The external shape of the dummy blocks is identical to the fuel graphite blocks, but the dummy blocks contain higher impurity (i.e., boron in graphite) than that of the fuel blocks. In fully-loaded core, all dummy blocks are replaced with fuel assemblies.

The core is surrounded by 12 permanent reflector blocks whose form is a large polygonal graphite block (see Figure 2.2). The width of the across flats of the core including the permanent reflector blocks is 4.25 m. The permanent reflector blocks have some holes for irradiation tests and neutron detection, and gaps: the void fraction is 0.7% due to the holes. Outside the permanent reflector blocks, there are side shielding blocks containing B_4C and carbon composite.

3. DESCRIPTION OF MATERIALS DATA

3.1 Materials Data of Fuel Assembly

The principal fuel assembly structural material is IG-110 graphite in the form of a right hexagonal prism having a density of 1.77 g/cm^3 with 0.40 ppm natural boron equivalent impurity. [4] The material of the fuel sleeve (clad) is identical to the fuel graphite block, but the impurity is slightly lower than that of the fuel graphite block (0.37 ppm versus 0.40 ppm). A total of 12 different enriched uranium fuels are used in the HTTR core. Thus, the fuel compact and coated fuel particles are distinguished by the uranium enrichment. The material data of the fuel compact and coated fuel particles are provided in Tables 3.1 and 3.2.

There are two different burnable poisons (H-1 and H-II). The material of the BP is B_4C and carbon composite and the densities of H-1 and H-II are 1.79 g/cm^3 and 1.83 g/cm^3, respectively. The natural boron weight percents of H-1 and H-II are 2.22 % and 2.74 %, respectively. The graphite disk between the BP pellets has a density of 1.77 g/cm^3 with 0.37 ppm of boron equivalent impurity.

Table 3.1. Materials Data of Fuel Compacts [4]

Enrichment (%)	Packing fraction (%)	Density (g/cm^3)	Impurity (ppm)
3.4	29.6	1.697	0.95
3.9	30.4	1.686	0.91
4.3	30.5	1.686	0.90
4.8	30.3	1.683	0.88
5.2	30.5	1.690	0.90
5.9	30.3	1.685	0.51
6.3	29.9	1.683	0.54
6.7	30.3	1.687	0.50
7.2	30.8	1.682	0.85
7.9	28.8	1.703	0.87
9.4	29.8	1.686	0.89
9.9	29.3	1.698	0.90

Table 3.2. Materials Data of Coated Fuel Particles [4]

Enrichment (%)		3.4	3.9	4.3	4.8	5.2	5.9
Kernel	Enrichment (%)	3.301	3.864	4.290	4.794	5.162	5.914
	Density (g/cm^3)	10.08	10.75	10.78	10.76	10.76	10.77
	Diameter (μm)	609.0	594.4	593.6	594.9	591.8	592.4
	Impurity (ppm)	0.92	0.89	0.92	0.94	1.24	0.96
1st layer	Density (g/cm^3)	1.158	1.091	1.112	1.110	1.118	1.112
	Thickness (μm)	59.1	61.7	61.3	60.9	60.4	60.3
2nd layer	Density (g/cm^3)	1.873	1.879	1.905	1.907	1.893	1.909
	Thickness (μm)	30.9	30.4	30.5	30.3	30.7	30.8
3rd layer	Density (g/cm^3)	3.206	3.207	3.206	3.205	3.205	3.204
	Thickness (μm)	29.8	28.9	29.2	29.1	29.4	29.3
4th layer	Density (g/cm^3)	1.855	1.858	1.869	1.905	1.846	1.890
	Thickness (μm)	46.4	45.7	46.2	45.2	45.7	45.9
Enrichment (%)		6.3	6.7	7.2	7.9	9.4	9.9
Kernel	Enrichment (%)	6.254	6.681	7.189	7.820	9.358	9.810
	Density (g/cm3)	10.74	10.73	10.77	10.82	10.79	10.81
	Diameter (μm)	593.5	593.2	594.0	608.1	593.4	591.4
	Impurity (ppm)	1.13	0.95	0.90	0.92	0.88	0.88
1st layer	Density (g/cm3)	1.122	1.121	1.147	1.143	1.170	1.152
	Thickness (μm)	60.4	60.8	64.9	58.7	61.1	59.3
2nd layer	Density (g/cm3)	1.909	1.902	1.894	1.878	1.902	1.873
	Thickness (μm)	31.1	31.0	31.0	29.2	31.9	30.5
3rd layer	Density (g/cm3)	3.205	3.208	3.202	3.201	3.207	3.202
	Thickness (μm)	28.7	28.7	28.6	28.7	28.2	26.7
4th layer	Density (g/cm3)	1.870	1.86	1.867	1.869	1.848	1.853
	Thickness (μm)	45.0	46.1	46.2	45.6	46.0	46.3

3.2 Materials Data of Reflector, Control Rods Guide and Dummy Blocks

The material of the permanent reflector blocks is PGX graphite that has a density of 1.732 g/cm^3 and an impurity content of 1.91 ppm. [4] The material data of the replaceable reflector, control rods guide, and dummy blocks are provided in Table 3.3. The densities of these blocks are similar to those for the fuel graphite block, but the impurity of the dummy block is much higher than that of the fuel graphite blocks.

The material of the control rod sleeve is Alloy 800H with density of 7.95 g/cm^3. The neutron absorber is B_4C and carbon composite: its total weight of neutron absorber is 2351.2 g and the absorber (B-10) mass is 135.8 g.

Table 3.3. Materials Data of Fuel Compacts [4]

	Type	ID	Material	Density (g/cm^3)	Impurity (ppm)
Replaceable reflector block	A 1 1/3	RB-1	IG-110 graphite	1.766	0.37
	A 1 2/3	RB-3		1.760	
	A 1 3/3	RB-5		1.765	
	A 2 1/3	RB-2		1.769	
	A 2 2/3	RB-4		1.751	
	A 2 3/3	RB-6		1.761	
	B 1/2	RB-7		1.755	
	B 2/2	RB-11		1.756	
	C 1/2	RB-10		1.763	
	C 2/2	IB-4		1.788	
	D 1/4	RB-8		1.761	
	D 2/4	IB-1		1.759	
	D 3/4	IB-2		1.762	
	D 4/4	RB-9		1.763	
Control rods guide block	A 1/2	CB-1	IG-110 graphite	1.776	0.37
	A 2/2	CB-0		1.768	
	B	CB-2		1.757	
	C	CB-3		1.772	
	D	CB-4		1.762	
	E 1/2	CB-5		1.756	
	E 2/2	CB-6		1.761	
Dummy block	0	DB-1	IG-11 graphite	1.767	2.5 (3.1) [a)]
	A	DB-2		1.764	3.1
	B-1	DB-3		1.764	3.1
	B-2	DB-4		1.765	3.1
	Simple	DB-5		1.767	2.5 (3.1) [a)]

a) The impurity of the dummy block was increased to 3.1 ppm from 2.5 ppm by re-measurement [6]

4. EXPERIMENTAL MEASUREMENTS

Experimental measurements performed in the HTTR start-up core are described below and the measured values are summarized in Table 4.1. [1,5] The notation in the parenthesis denotes the experiment ID specified by JAERI.

- Initial Criticality (HTTR-FC): In this experiment, the number of fuel columns is measured for the first criticality. The fuel are loaded into the core clockwise, from outer ring, one-by-one (fuel loading order is described in Figure 2.2). A small excess reactivity at the first criticality was also measured. In the experiment, the first criticality was obtained with 19 fuel columns.

- Control Rod Position at Criticality (HTTR-CR): The control rod insertion depths were measured at the critical condition for the thick annular core with 24 fuel columns and for the fully-loaded core with 30 fuel columns. Here, the control rod depth is defined by the distance from the control rod boundary to the bottom reflector. All control rod insertion levels are adjusted on the same level except for the three pairs at E01, E09, and E17. These three pairs were fully withdrawn at the operating condition.

- Excess Reactivity (HTTR-EX): The excess reactivity was measured using the inverse kinetic method. The approach to the criticality was observed by monitoring the inverse of neutron multiplication factor. The core was regarded as critical when the neutron density is maintained constant after removing the temporary neutron source. After the first criticality, the increment in reactivity was measured. The excess reactivity of the core was obtained by the addition of all increments of the reactivity from the first criticality to the fully-loaded core. A significantly high uncertainty was reported for the measured excess reactivity of the fully-loaded core (greater than 3.6% Δk).

Table 4.1. Measured Data in HTTR Start-up Core [1,5]

Measurement	Measured value
Number of fuel columns for first criticality	19
Control rod depth for thick annular core (cm) [a)]	221.5 ± 0.5
Control rod depth for fully-loaded core (cm) [a)]	177.5 ± 0.5
Excess reactivity of fully-loaded core	12% Δk/k
K-effective of thick annular core	1.1363 ± > 3.6%

a) Control rod depth is defined by the distance from the control rod boundary to the bottom reflector

5. BENCHMARK SPECIFICATION

5.1 Description of Model

A benchmark model was established utilizing the real geometry and material data of the HTTR start-up core. However, since the HTTR core is too complicated to be a practical problem, minor simplifications were assumed in this work. It is possible to eliminate some complexity and obtain a benchmark model without losing the essential physics of the experiment.

As shown in Figure 2.2, the core boundary of the HTTR is formed by the permanent reflector blocks, which are 12-polygonal blocks. This geometry cannot be made by assembling right hexagonal prisms. Thus, the core boundary is changed in the benchmark model as shown in Figure 5.1. In this figure, the permanent reflector blocks are modeled as hexagonal prisms whose external shape is identical to the fuel (or replaceable reflector) blocks. The material of the hexagonal permanent reflector blocks is the same as that specified for the actual permanent reflector blocks and the total volume of the permanent reflector blocks is conserved in this model. The layer-by-layer configurations of the fully-loaded core are provided in Figures 5.2 – 5.9.

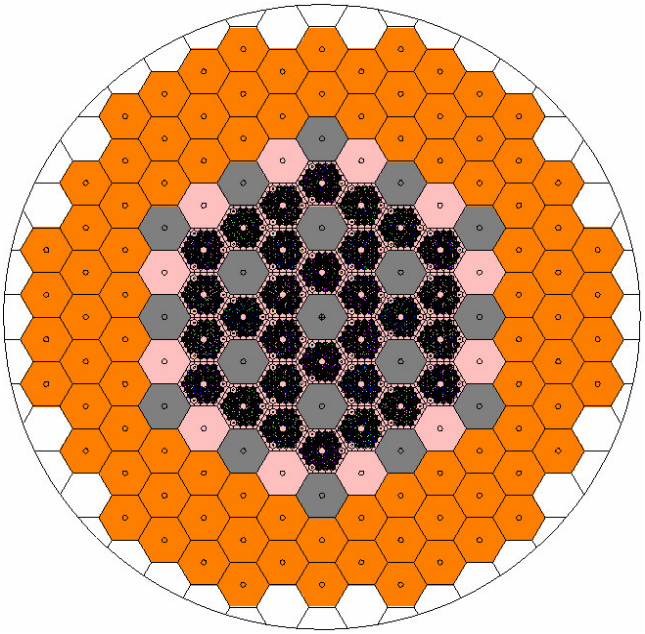

Figure 5.1. Core Layout for HTTR Benchmark Model

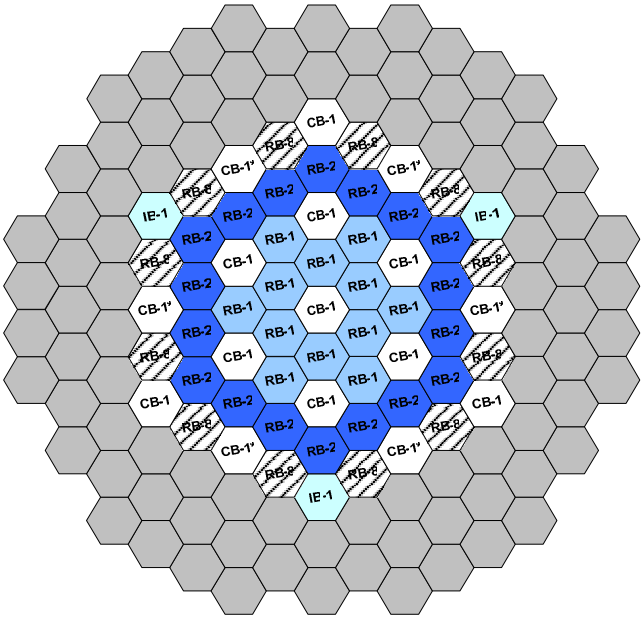

Figure 5.2. Horizontal View of Layers 1 and 2

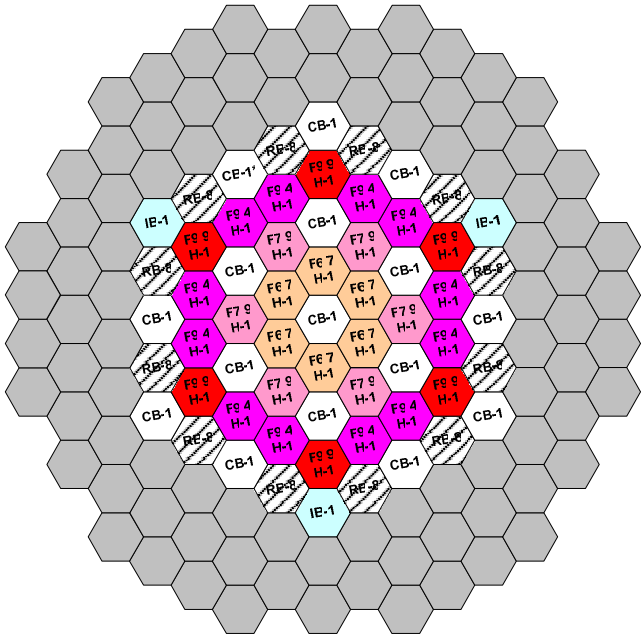

Figure 5.3. Horizontal View at 3rd Layer

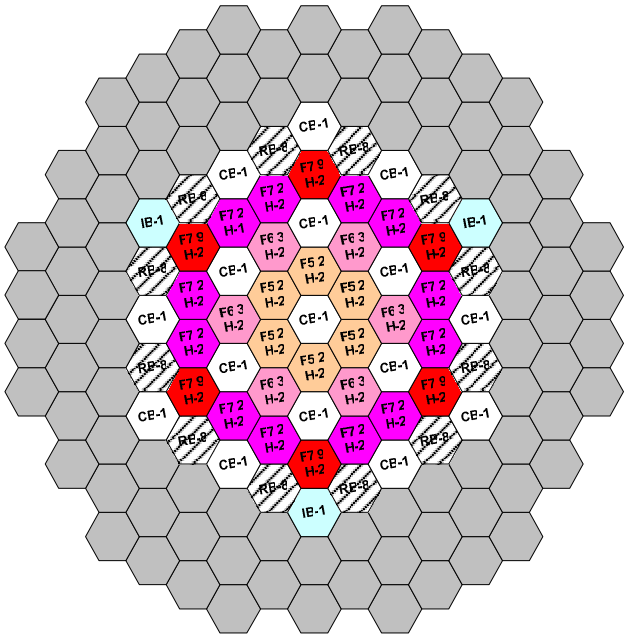

Figure 5.4. Horizontal View at 4th Layer

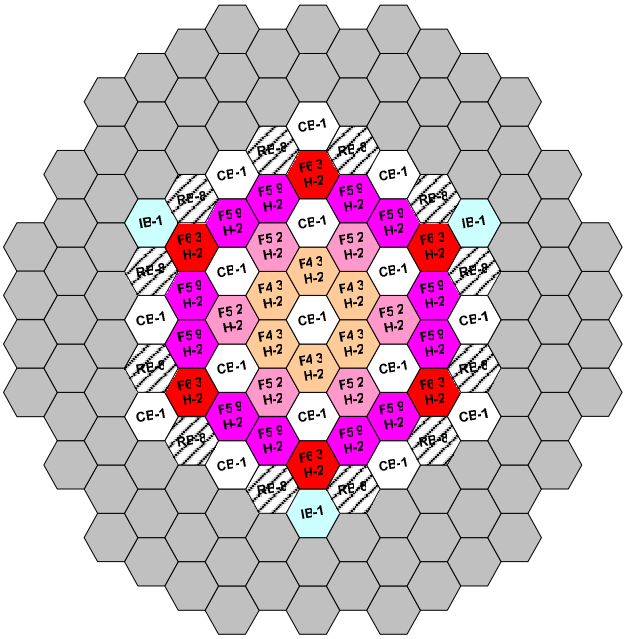

Figure 5.5. Horizontal View at 5th Layer

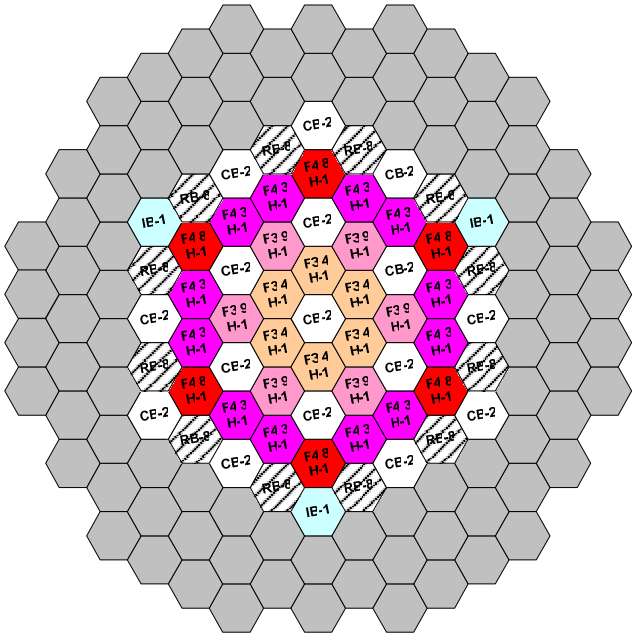

Figure 5.6. Horizontal View at 6th Layer

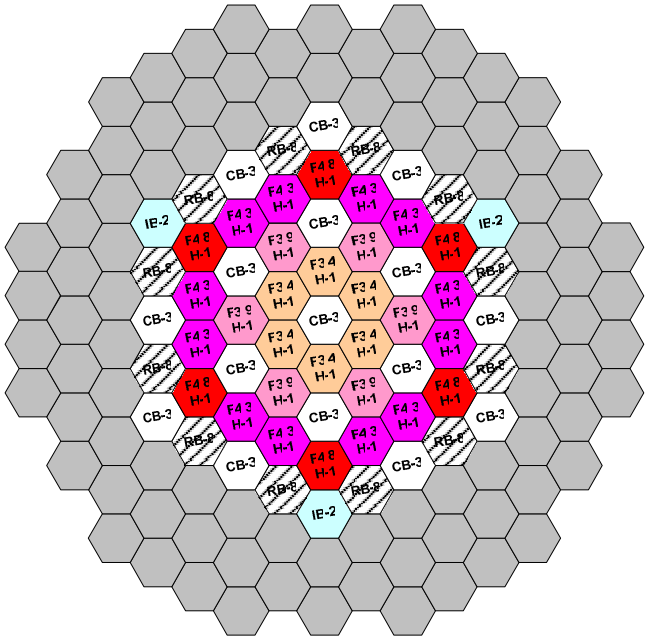

Figure 5.7. Horizontal View at 7th Layer

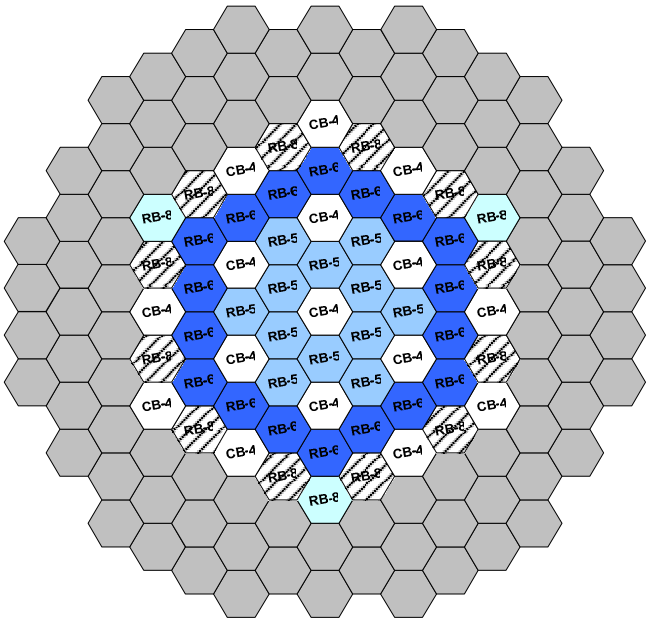

Figure 5.8. Horizontal View at 8th Layer

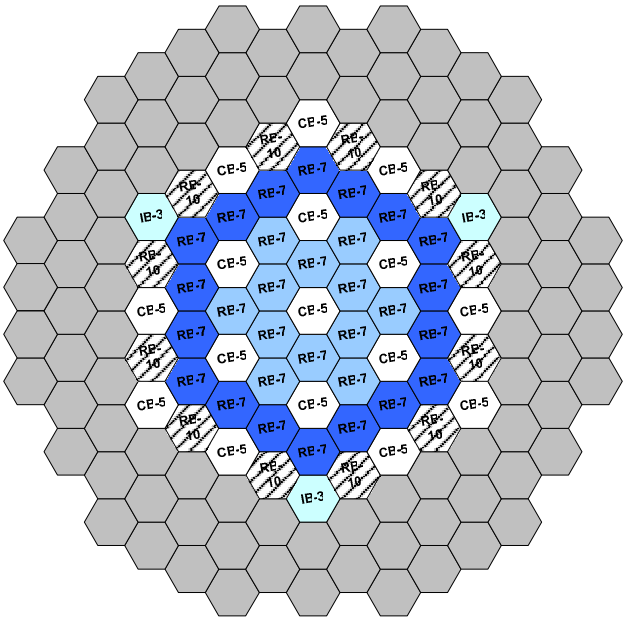

Figure 5.9. Horizontal View at 9th Layer

In the HTTR core, the outer boundary of the permanent blocks is coated with boron-carbide (B_4C) and carbon composite for the purpose of neutron shielding. In addition, boron pins are installed into lower parts of the blocks in the 9th layer for neutron shielding. Since References 4 and 5 recommended neglecting the neutron shielding in calculation models, the boron carbide coating and boron pins are ignored in the benchmark model.

Figure 2.4 shows the fuel graphite blocks. A fuel-handling hole is located at the center of each graphite block. The geometry of the fuel-handling hole is too complicated axially. In the benchmark model, the fuel-handling hole is smeared into the graphite axially. Thus, the graphite number density at the center of the graphite block is reduced as much as the volume fraction of the fuel-handling hole; the volume fraction is about 43%.

Each fuel hole is filled by 14 fuel compacts and the top and bottom of the fuel holes are encapsulated by plugs. The plug diameter is the same as the fuel hole diameter and the length is 1.7 cm (note that the height of the fuel graphite block is 58 cm and the fuel compact length is 3.9 cm). In addition, the top and bottom of the BP rods are encapsulated by the dowels. The dowel diameter is the same as for the BP hole and its length is 4.0 cm. The material data of the plug and dowel are not provided in the HTTR references. Thus, the material data of the plug and dowel are assumed to be the same with the fuel graphite block.

5.2 Materials Data

In Section 3, the materials data of the HTTR core were given for the materials densities and impurities. However, these values may result in different number densities due to the use of different universal constants (such as Avogadro number, atomic weight number, etc). To minimize the uncertainty of the material data, the number densities are provided for this benchmark. Atom densities were calculated by JAERI utilizing the material data given in Section 3. [4] The materials for which such calculations have been done include fuel compacts, fuel rods, fuel graphite blocks, burnable poisons, all reflector blocks, control rod and control rods guide blocks, and dummy blocks (see Tables 5.1 to 5.5). In these calculations, the fuel compact was divided into six materials, such as a kernel, four coating layers of the CFPs, and graphite matrix of the fuel compact.

Table 5.1. Number Densities of Fuel Compact (#/cm-barn)

Enrichment		3.40	3.9	4.3	4.8	5.2	5.9
Kernel	U-235	8.0367E-4	9.3638E-4	1.0429E-3	1.1627E-3	1.2522E-3	1.4357E-3
	U-238	2.3280E-2	2.3038E-2	2.3008E-2	2.2834E-2	2.2750E-2	2.2586E-2
	O	4.8188E-2	4.7948E-2	4.8102E-2	4.7993E-2	4.8004E-2	4.8044E-2
	B-10	1.1010E-7	1.0602E-7	1.0994E-7	1.1207E-7	1.4783E-7	1.1456E-7
	B-11	4.4317E-7	4.2673E-7	4.4251E-7	4.5108E-7	5.9515E-7	4.6111E-7
Buffer	C	5.8060E-2	5.4701E-2	5.5754E-2	5.5654E-2	5.6055E-2	5.5754E-2
IPYC	C	9.3909E-2	9.4210E-2	9.5514E-2	9.5614E-2	9.4912E-2	9.5714E-2
SiC	Si	4.8151E-2	4.8166E-2	4.8151E-2	4.8136E-2	4.8136E-2	4.8121E-2
	C	4.8151E-2	4.8166E-2	4.8151E-2	4.8136E-2	4.8136E-2	4.8121E-2
OPyC	C	9.3007E-2	9.3157E-2	9.3709E-2	9.5514E-2	9.2556E-2	9.4762E-2
Matrix	C	8.5085E-2	8.4534E-2	8.4534E-2	8.4383E-2	8.4734E-2	8.4483E-2
	B-10	2.4543E-8	2.3506E-8	2.2830E-8	2.1702E-8	1.8432E-8	6.9024E-9
	B-11	9.8790E-8	9.4614E-8	9.1893E-8	8.7353E-8	7.4189E-8	2.7783E-8
Homogeneous fuel compact	U-235	6.4509E-5	7.4887E-5	8.3358E-5	9.3663E-5	1.0049E-4	1.1448E-4
	U-238	1.8659E-3	1.8396E-3	1.8362E-3	1.8366E-3	1.8229E-3	1.7983E-3
	B-10	2.6099E-8	2.4835E-8	2.4642E-8	2.4133E-8	2.4651E-8	1.3937E-8
	B-11	1.0505E-7	9.9963E-8	9.9189E-8	9.7138E-8	9.9222E-8	5.6098E-8
	C	7.6139E-2	7.5473E-2	7.5649E-2	7.5631E-2	7.5665E-2	7.5751E-2
	O	3.8607E-3	3.8291E-3	3.8392E-3	3.8605E-3	3.8468E-3	3.8255E-3
	Si	2.0505E-3	2.0718E-3	2.0943E-3	2.0890E-3	2.1200E-3	2.0902E-3

Enrichment		6.3	6.7	7.2	7.9	9.4	9.9
Kernel	U-235	1.5149E-3	1.6163E-3	1.7460E-3	1.9085E-3	2.2773E-3	2.3912E-3
	U-238	2.2455E-2	2.2325E-2	2.2291E-2	2.2246E-2	2.1812E-2	2.1740E-2
	O	4.7939E-2	4.7883E-2	4.8073E-2	4.8309E-2	4.8179E-2	4.8262E-2
	B-10	1.3454E-7	1.1297E-7	1.0745E-7	1.1037E-7	1.0526E-7	1.0544E-7
	B-11	5.4155E-7	4.5474E-7	4.3249E-7	4.4423E-7	4.2370E-7	4.2441E-7
Buffer	C	5.6255E-2	5.6205E-2	5.7509E-2	5.7308E-2	5.8662E-2	5.7760E-2
IPYC	C	9.5714E-2	9.5363E-2	9.4962E-2	9.4160E-2	9.5363E-2	9.4210E-2
SiC	Si	4.8136E-2	4.8181E-2	4.8091E-2	4.8076E-2	4.8166E-2	4.8091E-2
	C	4.8136E-2	4.8181E-2	4.8091E-2	4.8076E-2	4.8166E-2	4.8091E-2
OPyC	C	9.3759E-2	9.3258E-2	9.3609E-2	9.7371E-2	9.2656E-2	9.2907E-2
Matrix	C	8.4383E-2	8.4584E-2	8.4333E-2	8.5386E-2	8.4534E-2	8.5135E-2
	B-10	5.7948E-9	6.6972E-9	2.1174E-8	2.1236E-8	2.2699E-8	2.3061E-8
	B-11	2.3325E-8	2.6957E-8	8.5228E-8	8.5478E-8	9.1367E-8	9.2824E-8
Homogeneous fuel compact	U-235	1.2041E-4	1.2899E-4	1.3793E-4	1.5269E-4	1.7780E-4	1.8843E-4
	U-238	1.7822E-3	1.7790E-3	1.7583E-3	1.7771E-3	1.7004E-3	1.7105E-3
	B-10	1.4730E-8	1.3658E-8	2.3131E-8	2.3934E-8	2.4146E-8	2.4594E-8
	B-11	5.9288E-8	5.4973E-8	9.3106E-8	9.6338E-8	9.7191E-8	9.8995E-8
	C	7.5690E-2	7.5746E-2	7.5606E-2	7.6443E-2	7.6005E-2	7.6407E-2
	O	3.8052E-3	3.8159E-3	3.7924E-3	3.8596E-3	3.7564E-3	3.7979E-3
	Si	2.0372E-3	2.0533E-3	2.0566E-3	1.9428E-3	1.9802E-3	1.8622E-3

To evaluate the double heterogeneous effect, the number densities of the homogeneous fuel compacts were also included in this benchmark model. The neutron detector insertion holes (about 0.7% volume fraction) are smeared into the permanent reflector blocks. The impurity

content of the dummy block that was initially specified as 2.5 ppm has been increased to 3.1 ppm due to results from re-measurement in which the number of samples was increased from 1 to 18. [5] In this benchmark, the original impurity content was used in calculating the number density (the effect of impurity increment will be discussed in Section 6).

Table 5.2. Number Densities of Graphite Block and Control Rods (#/cm-barn)

		Graphite sleeve	Graphite block	H-1 of BP	H-II of BP	Disk of BP	Permanent block	Control absorber
Kernel	B-10	7.1811E-9	7.8482E-9	4.4613E-4	5.6049E-4	7.1771E-9	3.6414E-8	7.2842E-9
	B-11	2.8905E-8	3.1590E-8	1.7640E-3	2.2162E-3	2.8889E-8	1.4657E-7	2.9320E-8
	C	8.8745E-2	8.8745E-2	8.7599E-2	8.8693E-2	8.8695E-2	8.6232E-2	8.9046E-2

Table 5.3. Number Densities in Replaceable Reflector Blocks (#/cm-barn)

Type		A 1 1/3	A 1 2/3	A 1 3/3	A 2 1/3	A 2 2/3	A 2 3/3	B 1/2
ID		RB-1	RB-3	RB-5	RB-2	RB-4	RB-6	RB-7
Kernel	C	8.8545E-2	8.8244E-2	8.8494E-2	8.8695E-2	8.3779E-2	8.8294E-2	8.7993E-2
	B-10	7.2432E-9	7.2186E-9	7.2391E-9	7.2555E-9	7.1817E-9	7.2227E-9	7.1981E-9
	B-10	2.9155E-8	2.9056E-8	2.9138E-8	2.9204E-8	2.8907E-8	2.9072E-8	2.8973E-8
Type		B 2 2/2	C 1/2	C 2/2	D 1/4	D 2/4	D 3/4	D 4/4
ID		RB-11	RB-10	IB-3	RB-8	IB-1	IB-2	RB-9
Kernel	C	8.8043E-2	8.8394E-2	8.8394E-2	8.8294E-2	8.8194E-2	8.8344E-2	8.8394E-2
	B-10	7.2022E-9	7.2309E-9	7.3334E-9	7.2227E-9	7.2145E-9	7.2268E-9	7.2309E-9
	B-11	2.8990E-8	2.9105E-8	2.9518E-8	2.9072E-8	2.9039E-8	2.9089E-8	2.9105E-8

Table 5.4. Number Densities of Control Rods Guide Blocks (#/cm-barn)

Type		A 1/2	A 2/2	B	C	D	E 1/2	E 2/2
ID		CB-1	CB-0	CB-2	CB-3	CB-4	CB-5	CB-6
Kernel	C	8.9046E-2	8.8645E-2	8.8093E-2	8.8845E-2	8.8344E-2	8.8043E-2	8.8294E-2
	B-10	7.2842E-9	7.2514E-9	7.2063E-9	7.2678E-9	7.2268E-9	7.2022E-9	7.2227E-9
	B-11	2.9320E-8	2.9188E-8	2.9006E-8	2.9254E-8	2.9089E-8	2.899E-8	2.9072E-8

Table 5.5. Number Densities of Dummy Blocks (#/cm-barn)

Type			A	B-1	B-2	Simple
ID		DB-1	DB-2	DB-3	DB-4	DB-5
Kernel	B-10	4.9164E-8	6.0618E-8	6.0618E-8	6.0652E-8	4.8772E-8
	B-11	1.9787E-7	2.4399E-7	2.4399E-7	2.4413E-7	1.9631E-7
	C	8.8595E-2	8.8444E-2	8.8444E-2	8.8484E-2	8.8595E-2

5.3 Temperature and Nitrogen Issue

Since the HTTR start-up core experiments were performed at room temperature [1,4,5], the room temperature value (293 K) is used in the benchmark model.

The thin annular core consists of 18 fuel columns. In the experiment, the first criticality of the HTTR was obtained with 19 fuel columns.[1] Thus, the thin annular HTTR core should be sub-critical. In the preliminary evaluation [6,7], which was performed by JAERI using the MVP continuous energy Monte Carlo code, the required fuel columns were estimated as 16 ± 1. To resolve the discrepancies between the experiment and MVP calculations (19 versus 16), a re-evaluation has been performed. [6] From this reevaluation, JAERI found that two factors were wrong in the preliminary evaluations: boron impurity in the dummy graphite blocks and the nitrogen in the porous graphite. The boron impurity of the dummy graphite block was assumed to be 2.5 ppm originally, but it was found to be 3.1 ppm in the re-measurement (the effect of the boron impurity will be discussed in Section 6). Nitrogen remains in the porous graphite at room temperature, but it is primarily released from the porous graphite when the core temperature increases. Nitrogen acts as a neutron absorber; however, it was ignored in the preliminary evaluations. The reevaluation using MVP code gave 18 ± 1 fuel columns to be critical and the eigenvalues of the annular core were 1.00593 and 1.00287 with JENDL 3.2 and JENDL 3.1 nuclear data libraries, respectively. The uncertainty level was 3σ=0.15% Δk. Since the HTTR references do not discuss the detailed nitrogen mass in the porous graphite, the nitrogen content of the porous graphite is ignored in this benchmark model.

6. EVALUATION OF BENCHMARK SPECIFICATION

6.1 Reference Monte Carlo Calculations

The whole-core geometry of the HTTR has been explicitly modeled in MCNP4C calculations, including explicit representation of fuel and reflector blocks, coolant channels, the gap between graphite blocks, plugs in fuel holes, dowels in BP holes, axial heterogeneity of the burnable poison rods, etc. Figure 6.1 shows two fuel compact models that have been employed in this study: in the first (homogeneous model), the coated fuel particles are smeared with the compact graphite matrix using volume weighting without accounting explicitly for the self-shielding effect of CFPs, while in the second (the heterogeneous model) the CFPs are explicitly modeled. The difference in the k_{eff} values of these two models is defined as the double heterogeneous effect in this work (see Section 6.1.7). In MCNP4C calculations, the number of neutron histories per batch is 10,000 and the number of batches is 500 (i.e., total five million histories were traced). Before accumulating the tally, the first 5 batches were discarded. The ENDF/B-VI neutron library data was primarily used for these benchmark calculations, but JEF2.2 neutron library data was also used to evaluate neutron library effects (see Section 6.1.6).

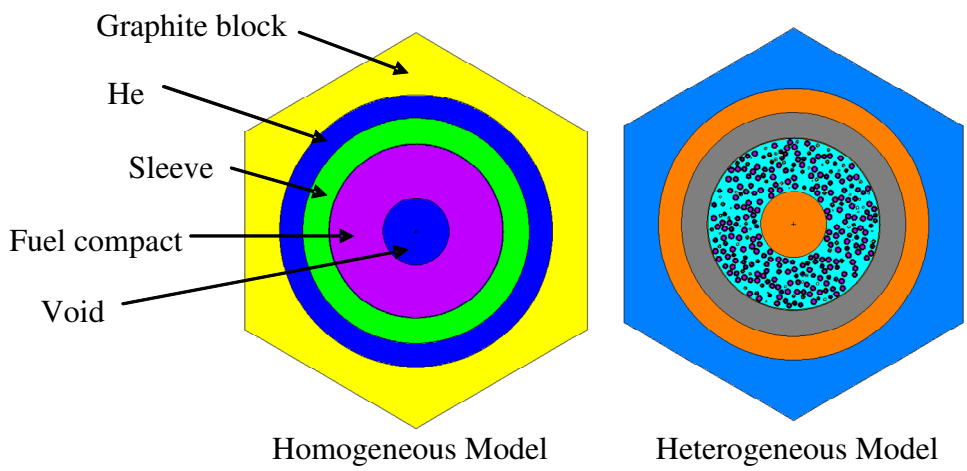

Figure 6.1. Fuel Compact Models

6.1.1 Number of Columns Required for First Criticality

Corresponding to the experimental measurements, three major parameters (number of fuel columns for the first criticality (HTTR-FC), control rods position at criticality (HTTR-CR), and the excess reactivity (HTTR-EX)) of the benchmark model were evaluated. First, the required number of fuel columns for the first criticality was evaluated and the result is summarized in Table 6.1. The result obtained from the MCNP4C calculation is similar to the result of JAERI's preliminary calculation. As mentioned in the previous section, the benchmark model ignored the revised impurity content of the dummy blocks and the nitrogen content in the porous graphite. Thus, the specification of the benchmark model is similar to that used in JAERI's preliminary calculation. Finally, a review of literature [5] indicated that other MCNP4 calculations and analysis for this core (performed by other groups) observed such low values (ranging from 15-16) for the number of columns required for first criticality.

Table 6.1. Comparison of Number of Columns for First Criticality

Organization	Code	Number of columns	Eigenvalue
JAERI –Japan	Experiment	19	Critical
JAERI – Japan	MVP	16 ± 1 [a)]	?
JAERI – Japan		18 ± 1 [b)]	1.006 ± ?
ANL (this study)	MCNP4C	16	1.002 ± 0.001

a) Preliminary results (2.5 ppm impurity of dummy block and nitrogen in porous graphite is ignored).
b) Re-evaluated after adjustment of impurity of dummy block and nitrogen effect.

6.1.2 Position of Control Rods for Critical Configurations

The position (insertion depth) of the control rods have also been evaluated at the critical conditions for the cores with 24 and 30 fuel columns. The results are presented in Table 6.2. The MCNP4C calculation estimated lower positions for the control rods compared with the experimental measurements. Note that the depth of the control rod position is the distance between the boundary of the control rod and the bottom reflector. The reason for the lower calculated control rod positions compared to the experimental measurements is because MCNP4C over-estimated the excess reactivity, most likely because of inadequate information of

impurities and the neglect of the nitrogen in the porous graphite. The ANL results are consistent with other MCNP4 results in open literature [5].

Table 6.2. Control Rods Positions at Critical Conditions

Organization	Code	Position (cm)	
		24 fuel columns	30 fuel columns
JAERI –Japan	Experiment	221.5 ± 0.5	177.5 ± 0.5
JAERI – Japan	MVP	208.0	180.0
ANL (this study)	MCNP4C	203.0	167.0

6.1.3 Core Excess Reactivity

The core k_{eff} values have been calculated for the thin annular (18 columns), thick annular (24 columns) and fully-loaded (30 columns) cores in order to determine the core excess reactivity. The results are summarized in Table 6.3. For the fully-loaded core, the k_{eff} value inferred from experimental measurement is 1.1363 (± >3.6%). The MCNP4C value obtained in this study is 1.15714 (±0.00037). The uncertainty (experimental, etc) associated with the inferred measurement value is quite high, and the calculated value is within 1σ of the "measured" value. The calculated k_{eff} value is however significantly higher (1.8%Δk/k) than the "measured" value.

Table 6.3. Eigenvalues of HTTR Core Calculations

Number of fuel columns	Eigenvalue with ENDF/B-VI	Excess Reactivity (%Δk/k)
18 (Thin annular)	1.02366 ± 0.00056	2.3
24 (Thick annular)	1.11702 ± 0.00047	10.5
30 [a)] (Fully-loaded)	1.15714 ± 0.00037	13.6

a) Eigenvalue of experiment with inverse multiplication factor method is 1.13630 ± >3.6%.

6.1.4 Comparison to Other Monte Carlo Results

In Table 6.4, the results from this work are compared with other Monte Carlo results obtained under the IAEA Coordinated Research Program on Evaluation of High Temperature

Gas Cooled Reactor [5]. The materials data used in the IAEA CRP are consistent with those used in this benchmark model (i.e., the original impurity content of the dummy block was used and nitrogen in the porous graphite was ignored).

Similar differences between calculation and measurement that are seen in this study were observed for the other evaluations. The excess reactivity evaluated from the KENO and MCNP Monte Carlo calculations is about 1.5 - 1.8 % higher than that inferred from measurement, while the TRIPOLI-4 Monte Carlo calculation is 0.8 % higher. In Reference 5, several causes of the differences between the Monte Carlo calculations and experiment are cited: (1) uncertainty of impurities in graphite block, (2) air or nitrogen content in graphite pores, (3) coated fuel particle modeling (regular and random distribution), and 4) choice of neutron library data.

Table 6.4. Comparison of Monte Carlo Calculations for Full-Core Case

Organization	Code	Neutron Library	Eigenvalue	Excess reactivity (% Δk/k)
JAERI –Japan	Experiment		1.1363 ± >3.6%	12.0
CEA – France	TRIPOLI 4 [a)]	JEF2.2	1.1463 ± 0.0009	12.8
IRI – Netherlands	KENO	JEF2.2	1.1584 ± 0.0005	13.7
IBRAE – Russia	MCNP4A	ENDF/B-VI	1.1567 ± ?	13.6
Turkey	MCNP4B	ENDF/B-VI	1.1564 ± 0.0010	13.5
ANL (this study)	MCNP4C	ENDF/B-VI	1.1571 ± 0.0004	13.6
	MCNP4C	JEF2.2	1.1605 ± 0.0006	13.8
	MCNP5	ENDF/B-VI	1.1579 ± 0.0004	13.6

a) 1.13833 ± 0.0009 after adjusting the impurities and the air content in pores.

These result and the others presented above indicate significant differences between the code results and the measured core criticality. In our attempt to discern the reasons for the differences, sensitivity studies were performed. The results of those studies are summarized in the following sections.

6.1.5 Impact of Regular Lattice versus Random CFP Modeling

For modeling simplicity and computational efficiency, the random distribution of coated fuel particles in the graphite matrix has been approximated by regular lattice distributions using the lattice geometry option of MCNP4C. In previous studies, [8,9] it was observed that the

MCNP4C eigenvalues obtained with regular lattice distributions are consistently smaller than those obtained with random distributions. Although the regular lattice and random distribution models resulted in statistically meaningful eigenvalue differences, their magnitudes were generally small. Using a two-dimensional core problem (which was specified for the 5th layer of the HTTR core), the difference in the k_{eff} values from the regular lattice and random distribution models was evaluated. The difference was found to be about 150 pcm, with the regular lattice model giving a lower eigenvalue. Physics reasoning suggests that the impact will be smaller for the *whole-core* configuration (other core regions have lower spatial importance). Due to this small difference and because of the impracticality of using the random distribution model for whole-core Monte Carlo calculations (data storage requirements and significantly large computational tracking zones), the regular lattice distribution model was utilized to evaluate the HTTR cores.

6.1.6 Impact of Nuclear Data Library

The impact of nuclear data on the results has been evaluated using JEF2.2 data library in addition to the ENDF/B-VI library that was utilized for most of the current evaluation. The results of this study are summarized in Table 6.5. The eigenvalue difference between the calculations using the ENDF/B-VI and JEF2.2 libraries is about 250 - 270 pcm. So the data effect is not large, and would not account for the differences observed between the cases using ENDF/B-VI and JEF2.2 data in Table 6.4.

Table 6.5. Comparison of k_{eff} Obtained with Different Libraries

Number of fuel columns	Eigenvalue with ENDF/B-VI	Eigenvalue with JEF2.2
18 (Thin annular)	1.02366 ± 0.00056	1.02652 ± 0.00059
24 (Thick annular)	1.11702 ± 0.00047	1.12041 ± 0.00045
30 (Fully-loaded)	1.15714 ± 0.00037	1.16048 ± 0.00059

6.1.7 Impact of Homogeneous versus Heterogeneous Compact Modeling

In the MCNP4C model used in this work, the CFPs have been modeled explicitly (using primarily the regular lattice model). It was however unclear what some of the other results used; explicit (heterogeneous) or smeared CFP-graphite-matrix compact (homogeneous) model, difference between which is termed "double heterogeneity". Additionally, we wanted an estimate of the double heterogeneity effect in order to determine the relevance of the HTTR to the VHTR. The results of the calculations for the three cores are summarized in Table 6.6. The double heterogeneity effect is seen to increase with the number of fuel columns (535 versus 743 pcm). The magnitude of the double heterogeneity effect for the HTTR is about a factor of 4 – 5 lower than that observed for the prismatic block-type VHTR [9]. Note that the homogeneous model predicts a lower value of the core k_{eff}.

Table 6.6. Eigenvalues of HTTR Core Calculations

Number of fuel columns	Homogeneous	Heterogeneous	Double Heterogeneity Effect (pcm $\Delta\rho$)
18 (Thin annular)	1.01808 ± 0.00058	1.02366 ± 0.00056	535
24 (Thick annular)	1.10945 ± 0.00058	1.11702 ± 0.00047	611
30 (Fully-loaded)	1.14727 ± 0.00058	1.15714 ± 0.00037	743

6.1.8 Impact of Impurity on Core Criticality

To assess the effect of the uncertainty in the impurity content of the dummy graphite block, the thin-annular core was re-evaluated using the updated information (i.e., increase in the impurity content). (Note that the uncertainty in the impurity content of the dummy blocks does not affect the k_{eff} of the fully-loaded core because all dummy blocks are replaced by the fuel blocks in this core configuration.) By increasing the impurity content of the dummy block (3.1 ppm versus 2.5 ppm [6]), the k-effective value of the thin annular core was decreased from 1.02366 to 1.01732 (±0.0006). This result indicates that the k-effective value is very sensitive to

the impurity content of the graphite blocks. It is therefore necessary that in addition to specification of core constituents an accurate indication of the impurity content be specified.

6.2 Whole-Core Deterministic Calculations

Whole-core deterministic models have been developed for analyzing the HTTR core. Descriptions of the models and results are presented in this section.

6.2.1 Descriptions of the DRAGON and DIF3D codes

Currently, only a few lattice codes allow the detailed treatment of the double heterogeneity effect inherent in the HTGR design at the assembly level. Two modern tools that contain models for representing coated fuel particles are the WIMS8 [10] and DRAGON [11] codes. A distinction between the WIMS8 and DRAGON models for the HTGR assembly is that the WIMS8 code does not provide the particulate-fuel double heterogeneity treatment at the assembly level like DRAGON (but at the pin level). A two-step scheme is therefore necessary in the WIMS8 calculation for the assembly. [9] Thus, the DRAGON code was selected as the lattice code in this study.

The DRAGON code has a collection of models for simulating the neutronics behavior of a unit cell or a fuel lattice in a nuclear reactor. The typical functionalities found in most modern lattice codes are contained in DRAGON code. These include interpolation of microscopic cross sections supplied by means of standard libraries; resonance self-shielding calculations in multidimensional geometries; multi-group and multi-dimensional neutron flux calculations which can take into account neutron leakage; transport-transport or transport-diffusion equivalence calculations; and modules for editing condensed and homogenized nuclear properties for reactor calculations. The code also performs isotopic depletion calculations. The code user must however supply cross sections in one of the following standard formats: DRAGON, MATXS (TRANSX-CTR), WIMSD4, WIMS-AECL, and APOLLO. Macroscopic cross sections can also be read by DRAGON via the input data stream. At ANL, the 69- and 172-group cross section libraries created in WIMSD4-format by the Reduced Enrichment for Research and Test Reactors (RERTR) project are used with the DRAGON code.

It is noted that in the DRAGON full-assembly model for HTGR hexagonal block, the block is formed by a collection of pin-cell sized hexagons. Each pin-cell contains the fuel compact and its surrounding block graphite. When all the fuel and coolant-hole pin-cells are represented, the block graphite content is not totally accounted for and therefore an extra ring of pin-cell sized hexagons is used to represent the remaining graphite. The number density of the graphite in these peripheral cells is modified to preserve the graphite content of the assembly block. Due to the use of the pin-cell sized hexagons, the DRAGON assembly model has jagged boundaries, not the flat boundaries of the hexagonal block.

An assessment of the accuracy of the DRAGON code when used for analyzing the Very High Temperature Reactor (VHTR) fuel element has been done by comparing results from the code to those from the high fidelity MCNP4C code. [12] Results show that eigenvalues, neutron spectra, and magnitude of the double heterogeneity effect predicted by DRAGON generally agree well with the reference values obtained from MCNP4C calculations. [8,9]

There are a number of well-established deterministic tools for whole-core calculations. In this study, the DIF3D code [13], which was developed at ANL, was used for the whole-core calculations. The DIF3D code has several flux solvers such as finite-difference and nodal diffusion theory solvers, and the VARIANT nodal transport solver. The applicability of the DIF3D code for high temperature gas-cooled reactor whole-core calculations was assessed in a VHTR optimization study [14] and in a recent feasibility study of deep-burn transmutation [15]. The code model was found to provide sufficient accuracy.

6.2.2 Lattice and Core Modeling

The HTTR core has been evaluated using the DRAGON and DIF3D coupled calculations. The microscopic multigroup cross sections needed by the DIF3D code were generated by DRAGON calculations. For the standard fuel assembly, the DRAGON code solves the 172-group transport equations using a two-dimensional hexagon geometry and a reflective boundary condition. The code uses the multigroup flux obtained for the given problem to condense the microscopic cross sections (averaged over the assembly) into 6 neutron group data. However, for the control rods guide and reflector blocks, the DRAGON code cannot solve the

transport equations directly because there is no fission source in the non-fueled graphite blocks. For this reason, the cross sections of the control rods guide and reflector blocks were generated from an approximate two-dimensional model (see Figure 6.2). In this model, in order to provide the appropriate neutron spectra to the non-fueled blocks, one fuel assembly is connected to the control rods guide and reflector blocks and a reflective boundary condition is imposed.

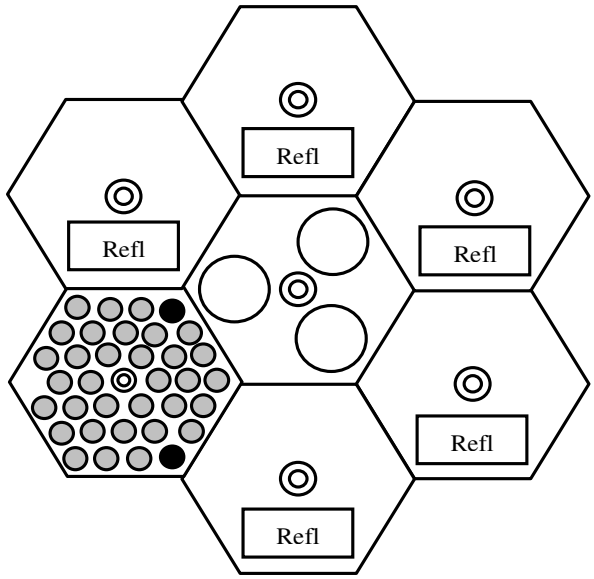

Figure 6.2. An Approximation Model for Generating Cross Sections of Control Rod Guide and Reflector Blocks

For the whole-core calculations, the Hexagonal-Z (Hex-Z) geometry option of DIF3D was utilized. The HTTR core has complicated radial and axial heterogeneities: 12 different fuel types, some in assemblies with 33 pins and some with 31 pins, two types of BP rods, fuel rods and BP rods encapsulated by plugs and dowels, axial and radial reflector blocks, etc. In the Hex-Z core model, the radial heterogeneity in each hexagonal block is not explicitly modeled in the DIF3D code since cross sections have been rigorously homogenized by smearing all materials in the DRAGON lattice calculations. Axially, the regions of fuel plugs and dowels are modeled explicitly. However, due to the axial heterogeneity of the BP rods, two fuel block models were developed according to the BP homogenization approach (see Figure 6.3). The axial heterogeneity of the BP rod is shown in Figure 2.6; graphite disks are sandwiched between two BP pellets. In Figure 6.3, the BP rods (neutron absorber and graphite disks) are smeared with

fuel rods and graphite block in the homogeneous BP model (left figure), while the neutron absorbers and graphite disks are separately smeared with fuel and graphite in the explicit BP model (right figure). Thus, there are three material layers axially defined in the simple BP model and five material layers in the standard BP model.

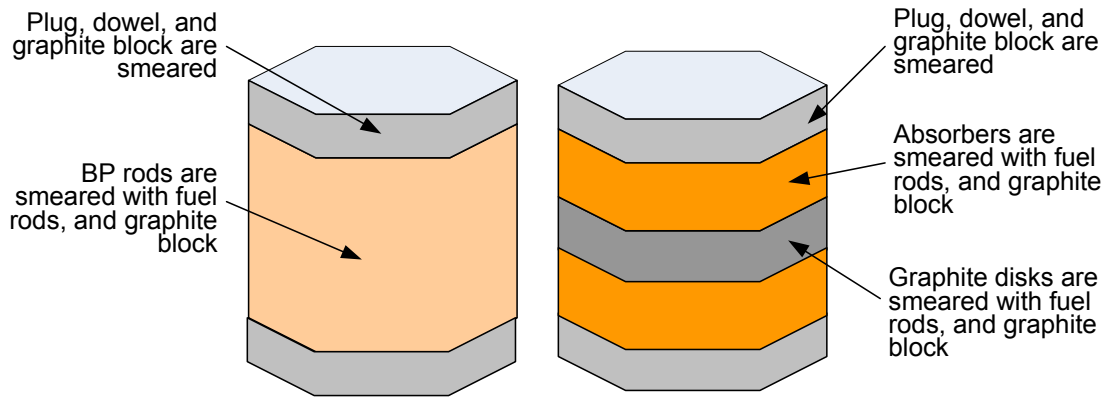

Figure 6.3. Fuel Block Models According to Axial BP Homogenization Approach

6.2.3 Results of Deterministic Calculations

Comparison of Spectra

As indication of the relevance of the HTTR to the VHTR [14], the fuel parameters and assembly-wise spectrum of the two systems have been compared and are summarized in Table 6.7 and Figure 6.4.

Table 6.7. Comparison of HTTR and VHTR Fuel Parameters

Parameter	HTTR Model	VHTR Model
Kernel diameter (μm)	~ 600	425
Particle diameter (μm)	~ 930	845
Packing fraction (%)	~ 30	25
U enrichment (%)	3.4 – 9.9	14.0
Number of BP rods	2 with B_4C	0
Impurity of graphite block	~ 1.0 ppm	Not modeled
C/U-235	2570 – 1780	~ 2400
Fast-to-thermal flux ratio [a)]	3.5 – 7.5	2.61

a) Cut-off energy is 0.4 eV

The uranium enrichment of the HTTR fuel is lower than that of the VHTR fuel, but the graphite-to-fissile (C/U-235) ratios of the HTTR fuel assemblies are similar or lower than that of the VHTR assembly because the packing fraction and kernel diameter are bigger. Due to the burnable poisons and impurity of the graphite, the thermal fluxes of the HTTR fuel assemblies are lower than that of the VHTR (see the spectrum and fast-to-thermal flux ratio). Note that the burnable poison and impurity of the graphite block were not modeled in the VHTR assembly model used in this comparison. In addition, due to the difference in the operating temperatures, the thermal flux of the VHTR is shifted to higher energy; HTTR tests were done at the cold state.

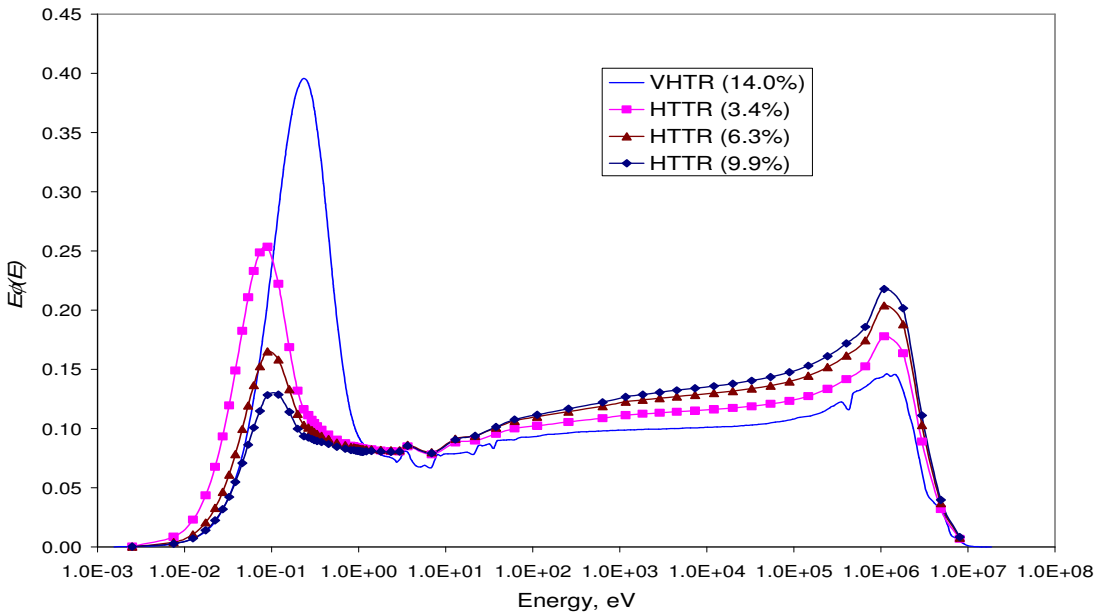

Figure 6.4. Spectra of HTTR Assemblies

Comparison of Criticality for the Fully-Loaded Core

The k-effective values of the fully-loaded core have been calculated and the results compared with other deterministic calculations [16]. Table 6.8 is a summary of the results. In these calculations, the high order variational nodal option (5th-order flux approximation, quadratic source approximation, and P_3 angular flux expansion) of the DIF3D code was utilized with one hexagon per node and about 2.0 cm in height. Generally, the deterministic calculations gave an overestimation of the k_{eff} of the fully-loaded HTTR core and the overestimation increases with increase in the number of neutron energy groups.

The result of the DRAGON/DIF3D calculation with explicit BP model is about 3.4% Δk/k higher compared to the value inferred from measurement and about 1.6% Δk/k higher than the result of the MCNP4C calculation. Two possibilities are suspected for these large differences between the measurement and the deterministic calculations. The first possibility is the composition uncertainty (such as impurity and nitrogen in graphite), which was already observed in the Monte Carlo calculations. In Table 6.8, this effect is about 1.8% Δk/k (see the difference between the measurement and MCNP4C calculation).

Table 6.8. Eigenvalue Comparison for Deterministic HTTR Core Calculations

Code	Equation	Spatial refinement	k-effective
Experiment			1.1363 ± 3.6%
MCNP4C(this study)		Explicit Hexagonal-Z	1.1571 ± 0.0004
BOLD VENTURE	13 group diffusion	Cylindrical-Z, 6 rings, Finite difference	1.1885
CRONOS	8 group diffusion	Hexagonal-Z	1.1698
CITATION	4 group diffusion	Triangle-Z, Finite difference	1.1607
PANTHER	2 group diffusion	Triangle-Z, Finite element	1.1595
DIF3D (this study)	6 group diffusion	Hexagonal-Z, variational nodal option with explicit BP model	1.1750
	6 group diffusion	Hexagonal-Z, variational nodal option with homogeneous BP model	1.1619

The second possibility is the approximation made in the flux solvers used for the deterministic calculations and the cross sections for the reflectors. There is significant streaming through the large holes of the control rods guide blocks and irradiation blocks (there are 19 control rods guide and irradiation columns among total 61 columns). However, the streaming effect was significantly underestimated in the DIF3D calculations. Similarly, the method introduced in this study to obtain the control block and reflector cross sections (see Figure 6.2) is not adequate to capture the streaming effect. In addition, the flux solvers of the deterministic codes are not accurate to estimate the reaction rates of the highly heterogeneous HTTR core: the evidence of this is observed from the results of the two axial BP models. In Table 6.6, the impact of homogenizing the BP rods (i.e., the k-effective difference between the homogeneous and explicit BP models) is about 1.1% Δk/k: similar results have been observed in the European benchmarking study [16].

7. CONCLUSIONS

A preliminary evaluation of the High Temperature Engineering Test Reactor (HTTR) start-up experiments has been performed. Monte Carlo and deterministic models were developed and used for the analysis of the four critical configurations of the HTTR, which were attained along the path to full-core loading. Data in open literature was used as basis for these evaluations. The results obtained show a significant difference (1.8% $\Delta k/k$) in the core criticality calculated by the MCNP code and the experimental measurement; larger differences of about 2.3 – 3.4 $\%\Delta k/k$ were found for the deterministic codes. These are consistent with some of the values reported for an HTTR experiment evaluation previously arranged by the IAEA.

The lack of more detailed data was a major limitation to the effort because it was not possible to discern the major sources of the differences observed between calculation and measurement data for the experiments. Due to the potential relevance of the HTTR data in future licensing of the VHTR, it is recommended that avenues be pursued to obtain more detailed data from JAERI (Japan). This could be done under the bilateral or multilateral platform provided by the Generation IV International Forum or under the activities of international organizations.

8. REFERENCES

1. "*Status of the HTTR Project*," Japan Atomic Energy Research Institute, Home page of HTTR, http://www2.tokai.jaeri.go.jp/httr/eng/index_main_eng.html, (2004).
2. S. Saito, et al, "*Design of High Temperature Engineering Test Reactor (HTTR)*," JAERI-1332, Japan Atomic Energy Research Institute (1994).
3. K. Yamashita, et al, "*Nuclear Design of the High-Temperature Engineering Test Reactor (HTTR)*," Nuclear Science and Engineering **122**, 212 (1996).
4. N. Nojiri, et al, "*Benchmark Problem's Data for HTTR's Start-up Core Physics Experiment IAEA Benchmark*," JAERI-memo 10-1005, Japan (1998).
5. "*Evaluation of High Temperature Gas Cooled Reactor Performance: Benchmark analysis related to initial testing of the HTTR and HTR-10*," IAEA-TECDOC-1382, IAEA (2003).
6. N. Fujimoto, K. Yamashita, H. Nojiri, M. Takeuchi, S. Fujisaki, "*Annular Core Experiments in HTTR's Start-up Core Physics Tests*," Nuclear Science and Engineering, **150**, 310 (2005).
7. N. Nojiri, et al, "*Preliminary Analyses of HTTR's Start-up Physics Tests by Monte Carlo Code MVP*," JAERI-Tech 98-032, Japan Atomic Energy Research Institute (1998).
8. T. K. Kim, W. S. Yang, T. A. Taiwo, and M. A. Smith, "*Preliminary Assessment of Lattice Physics Capabilities for VHTR Analysis*," Trans. Am. Nucl. Soc., **91** (2004).
9. T. K. Kim, W. S. Yang, M. A. Smith, T. A. Taiwo, and H. S. Khalil, "*Assessment of Monte Carlo and Deterministic Codes for Next Generation Nuclear Plant (NGNP) Core Modeling*," Gen-IV report, Argonne National Laboratory, April 15, 2004.
10. "*WIMS – A Modular Scheme for Neutronics Calculations*," User's Guide for Version 8, ANSWER/WIMS(99)9, The ANSWERS Software Package, AEA Technology.

11. G. Marleau, et al, "*A User Guide for DRAGON*," Technical report IGE-174 Rev. 4, Ecole Polytechnique de Montréal, September 1998 (1998).

12. "*MCNP – A General Monte Carlo N-Particle Transport Code*," Version 4C, Los Alamos National Laboratory, LA-13709-M.

13. K. L. Derstine, "*DIF3D: A Code to Solve One-, Two-, and Three-Dimensional Finite-Difference Diffusion Theory Problems*," ANL-82-64, Argonne National Laboratory, 1984.

14. T. K. Kim, W. S. Yang, T. A. Taiwo and H. S. Khalil. "*Equilibrium Cycle Analysis in Support of Fuel Specification for Next Generation Nuclear Power Plant*," ICAPP-05, Seoul, Korea, May 15-19, 2005.

15. T. K. Kim, T. A. Taiwo, R. N. Hill, W. S. Kim and F. Venneri, "*A Feasibility Study of Reactor-Based Deep-Burn Concepts*," ANL-AFCI-155, Argonne National Laboratory, August, 2005.

16. X. Raepsaet et al. "*Analysis of the European Results on the HTTR's Core Physics Benchmarks*," Nuclear Engineering and Design, **222**, 173 (2003).

HTR10-GCR-RESR-001 **ANL-GenIV-059**
CRIT

EVALUATION OF THE INITIAL CRITICAL CONFIGURATION OF THE HTR-10 PEBBLE-BED REACTOR

Evaluator

William K. Terry
Idaho National Laboratory

Internal Reviewers

Soon-Sam Kim
J. Blair Briggs

Independent Reviewers

Yuliang Sun
Institute of Nuclear Energy Technology
Tsinghua University

Temitope Taiwo
Argonne Laboratory

Status of Compilation / Evaluation / Peer Review

Chapter	Page	Compiled	Independent Review	Working Group Review	Approved
1.0 DETAILED DESCRIPTION	4				
1.1 Description of the Critical and / or Subcritical Configuration	6				
1.2 Description of Buckling and Extrapolation Length Measurements	16				
1.3 Description of Spectral Characteristics Measurements	16				
1.4 Description of Reactivity Effects Measurements	16				
1.5 Description of Reactivity Coefficient Measurements	16				
1.6 Description of Kinetics Measurements	16				
1.7 Description of Reaction-Rate Distribution Measurements	16				
1.8 Description of Power Distribution Measurements	16				
1.9 Description of Isotopic Measurements	16				
1.10 Description of Other Miscellaneous Types of Measurements	16				
Chapter	**Page**	**Evaluated**	**Independent Review**	**Working Group Review**	**Approved**
2.0 EVALUATION OF EXPERIMENTAL DATA	17				
2.1 Evaluation of Critical and / or Subcritical Configuration Data	19				
2.2 Evaluation of Buckling and Extrapolation Length Data	38				
2.3 Evaluation of Spectral Characteristics Data	38				
2.4 Evaluation of Reactivity Effects Data	38				
2.5 Evaluation of Reactivity Coefficient Data	38				
2.6 Evaluation of Kinetics Measurements Data	38				
2.7 Evaluation of Reaction Rate Distributions	38				
2.8 Evaluation of Power Distribution Data	38				
2.9 Evaluation of Isotopic Measurements	38				
2.10 Evaluation of Other Miscellaneous Types of Measurements	38				

Chapter	Page	Compiled	Independent Review	Working Group Review	Approved
3.0 BENCHMARK SPECIFICATIONS	39				
3.1 Benchmark-Model Specifications for Critical and / or Subcritical Measurements	39				

3.2 Benchmark-Model Specifications for Buckling and Extrapolation Length Measurements	50				
3.3 Benchmark-Model Specifications for Spectral Characteristics Measurements	50				
3.4 Benchmark-Model Specifications for Reactivity Effects Measurements	50				
3.5 Benchmark-Model Specifications for Reactivity Coefficient Measurements	51				
3.6 Benchmark-Model Specifications for Kinetics Measurements	51				
3.7 Benchmark-Model Specifications for Reaction-Rate Distribution Measurements	51				
3.8 Benchmark-Model Specifications for Power Distribution Measurements	51				
3.9 Benchmark-Model Specifications for Isotopic Measurements	51				
3.10 Benchmark-Model Specifications of Other Miscellaneous Types of Measurements	51				
Chapter	**Page**	**Compiled**	**Independent Review**	**Working Group Review**	**Approved**
4.0 RESULTS OF SAMPLE CALCULATIONS	52				
4.1 Results of Calculations of the Critical or Subcritical Configurations	52				
4.2 Results of Buckling and Extrapolation Length Calculations	52				
4.3 Results of Spectral Characteristics Calculations	52				
4.4 Results of Reactivity Effect Calculations	52				
4.5 Results of Reactivity Coefficient Calculations	52				
4.6 Results of Kinetics Parameter Calculations	53				
4.7 Results of Reaction-Rate Distribution Calculations	53				
4.8 Results of Power Distribution Calculations	53				
4.9 Results of Isotopic Calculations	53				
4.10 Results of Calculations of Other Miscellaneous Types of Measurements	53				
Chapter	**Page**	**Compiled**	**Independent Review**	**Working Group Review**	**Approved**
5.0 REFERENCES	53				
Appendix A: Computer Codes, Cross Sections, and Typical Input Listings	54				
Appendix B: Calculation of Base-case Atomic Number Densities in the Core Region	79				
Appendix C: Nuclear Constants	85				

EVALUATION OF THE INITIAL CRITICAL CONFIGURATION OF THE HTR-10 PEBBLE-BED REACTOR

IDENTIFICATION NUMBER: HTR10-GCR-RESR-001 CRIT

KEY WORDS: Pebble-bed reactor, criticality, research reactor, benchmark evaluation, Chinese Reactors, HTR-10, graphite-moderated reactors, HTGRs

1.0 DETAILED DESCRIPTION

The HTR-10 is a small (10 MWt) pebble-bed research reactor intended to develop pebble-bed reactor (PBR) technology in China. It will be used to test and develop fuel, verify PBR safety features, demonstrate combined electricity production and co-generation of heat, and provide experience in PBR design, operation, and construction.

Table 1 gives major design features of the reactor, and Figure 1 illustrates the reactor layout. The reactor was not at power during the subject experiment, and some key features, such as the composition of the gas in the void spaces, were different from the specifications in Table 1, as explained in detail below. However, the data in Table 1 serve to characterize the reactor, and they are therefore included here.

Table 1. Reactor design features (from Reference 1)

Reactor thermal power	MW	10
Primary helium pressure	MPa	3.0
Reactor core diameter	cm.	180
Average core height	cm.	197
Average helium temperature at reactor outlet	°C	700
Average helium temperature at reactor inlet	°C	250
Helium mass flow rate at full power	kg/s	4.3
Main steam pressure at steam generator outlet	MPa	4.0
Main steam temperature at steam generator outlet	°C	440
Feed water temperature	°C	104
Main steam flow rate	t/hr	12.5
Number of control rods in side reflector		10
Number of absorber ball units in side reflector		7
Nuclear fuel		UO_2
Heavy metal loading per fuel element	g	5
Enrichment of fresh fuel element	%	17
Number of fuel elements in equilibrium core		27,000
Fuel loading mode		multi-pass

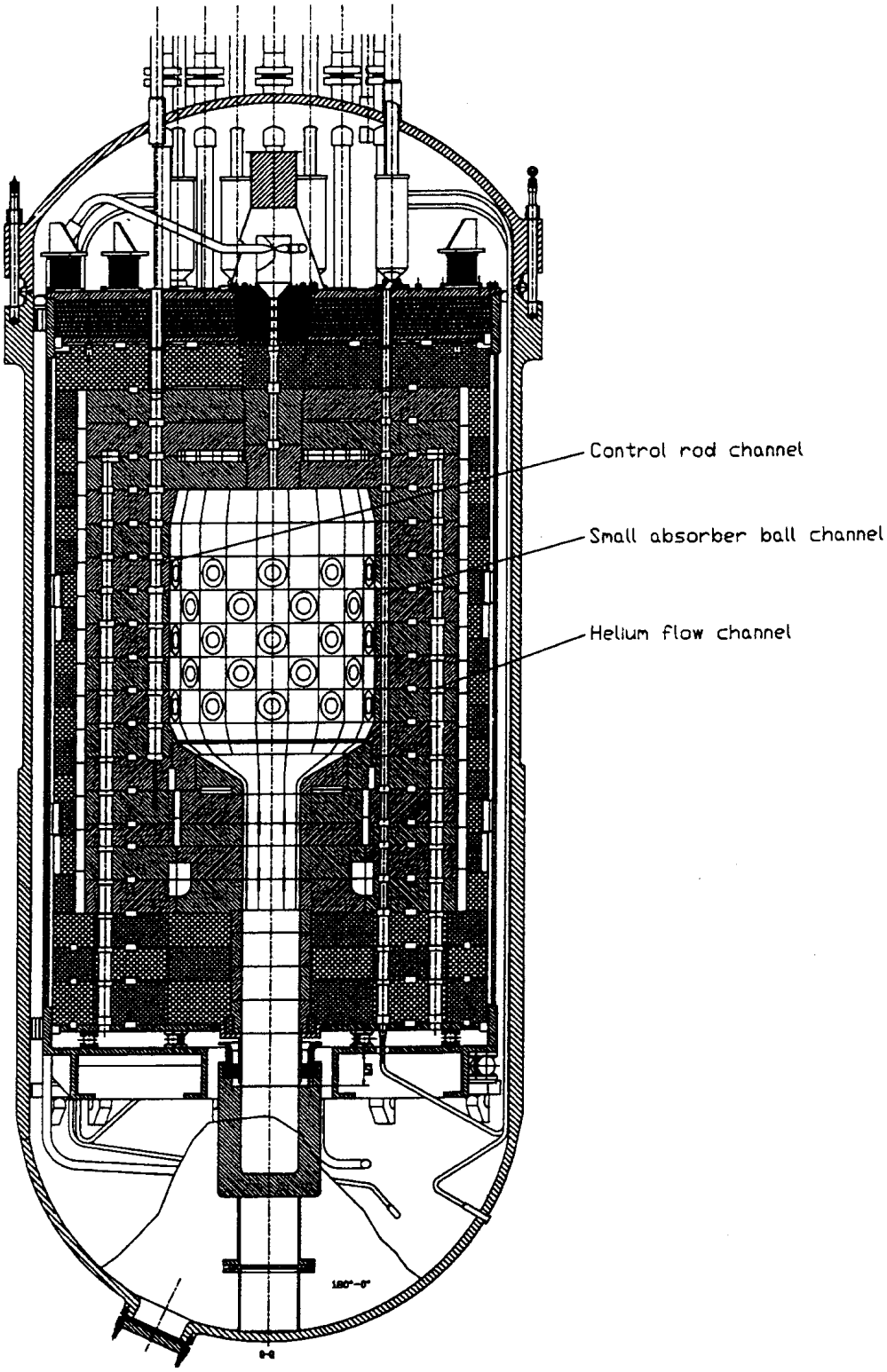

Figure 1. Layout of HTR-10 (from Reference 1)

As a test reactor intended to demonstrate all the technologies associated with PBRs, the HTR-10 contains a complete cooling system that supplies hot helium to a steam generator for generation of electricity and supply of district heating. In a later experimental phase, the HTR-10 will supply heat to both a steam cycle and a gas-turbine cycle. The primary coolant loop contains three pressure vessels: the reactor vessel, the steam generator vessel, and the hot gas duct. In the initial criticality experiment, only the core and the reflector are modeled.

The HTR-10 first became critical on 1 December 2000. This evaluation assesses the usefulness of the data obtained in the initial criticality experiment as a benchmark for reactor physics codes. It is concluded that the experiment is an acceptable benchmark.

In the initial critical condition, all control rods were withdrawn. Measurements of control rod worth were also made on the cold clean core. The control rod worth experiments have not yet been evaluated.

1.1 Description of the Critical Configuration

Like any PBR, the HTR-10 is fueled by billiard-ball-size spheres containing fuel particles embedded in a matrix. During reactor operation, the fuel spheres are introduced at the top and slowly flow downwards through the core region. As shown in Figure 1, the HTR-10 core is a cylindrical cavity above a conical zone (the "conus") that funnels pebbles into a discharge tube. The core, conus, and discharge tube are surrounded by graphite blocks (the reflector), most of which contain boron and some of which are penetrated by various borings for coolant flow, control rods, emergency shutdown absorber balls, and other purposes. In the initial critical experiment, the voids in the core and reflector were filled by moist air rather than the helium with which the reactor is cooled while in operation, and the conus was filled with "dummy" balls – spheres the same size as fuel spheres but made only of graphite. In the cylindrical core, a mixture of fuel balls and dummy balls in the ratio of 57:43 was added until the core became critical. During this initial fuel loading, pebbles were not removed at the bottom, so the pebbles remained stationary after they settled into position in the core. A small Am-Be source (4.4×10^7 neutrons/s) was provided to assist startup, and the neutron flux was tracked by neutron counters. Criticality was achieved when 16,890 balls (fuel and dummy) had been loaded. This is equivalent to a level core height of 123.06 cm.

1.1.1 Overview of Experiment

The HTR-10 is located at the Institute of Nuclear Energy Technology (INET), a unit of Tsinghua University, near Beijing. The HTR-10 project was approved by the Chinese State Council in March 1992, ground was broken in 1994, and construction was

completed in 2000. Initial criticality was achieved on 1 December 2000. The experiment was performed by the INET.

In advance of the actual experiment, data were distributed worldwide for interested groups to use in benchmarking calculations with various computer codes. The benchmark problem specifications differed in several respects from the experiment as it was run. Some compositions provided in the benchmark specifications were different from the as-built compositions, the benchmark and as-run temperatures were different, and the void spaces in the actual experiment were filled with air instead of helium. The results of the benchmark efforts are reported in Reference 1.

The initial criticality experiment has a total uncertainty in k_{eff} of slightly more than 0.005. It is judged acceptable as a benchmark.

1.1.2 Description of Experimental Configuration

Dimensions and material data describing the initial critical experiment were provided by the HTR-10 research group in Reference 1. Dimensional data are presented in this subsection, and material data are provided in the next one. Figure 2 shows the construction of the fuel pebble and the TRISO fuel particles embedded in the fuel zone matrix of the fuel pebble. Table 2 shows the dimensions of the various components of the fuel pebble and fuel particle illustrated in Figure 2. Table 3 shows the nominal dimensions of all components in the core and reflector, together with tolerance limits, observed ranges, and standard deviations where they are known. The nominal compositions are taken from Reference 1, and the uncertainties are taken from Reference 2. Reference 2 presents data obtained by 1997, so it might not reflect tolerances or observations in the year of the experiment, but it contains the only information found on the tolerance specifications for the HTR-10.

Table 2. Dimensions of Pebbles and Fuel Particles

Diameter of ball	6.0 cm
Diameter of fuel zone	5.0 cm
Volumetric filling fraction of balls in the core	0.61
Radius of the kernel(mm)	0.25
Coating layer materials (starting from kernel)	Buffer/PyC/SiC/PyC
Coating layer thickness(mm)	0.09/0.04/0.035/0.04
Diameter of dummy (no fuel) elements	6.0 cm

As noted above, the reflector region comprises numerous graphite blocks of different compositions. The variations in the volume-averaged compositions of the blocks arise both from different boron concentrations and from different sizes and placements of borings. Reference 1 contains a mapping of the various blocks into model regions, with average material densities provided. This mapping, with dimensions shown, is presented

in Figure 3; this figure differs slightly from the analogous figure in Reference 1, as explained in Section 3.

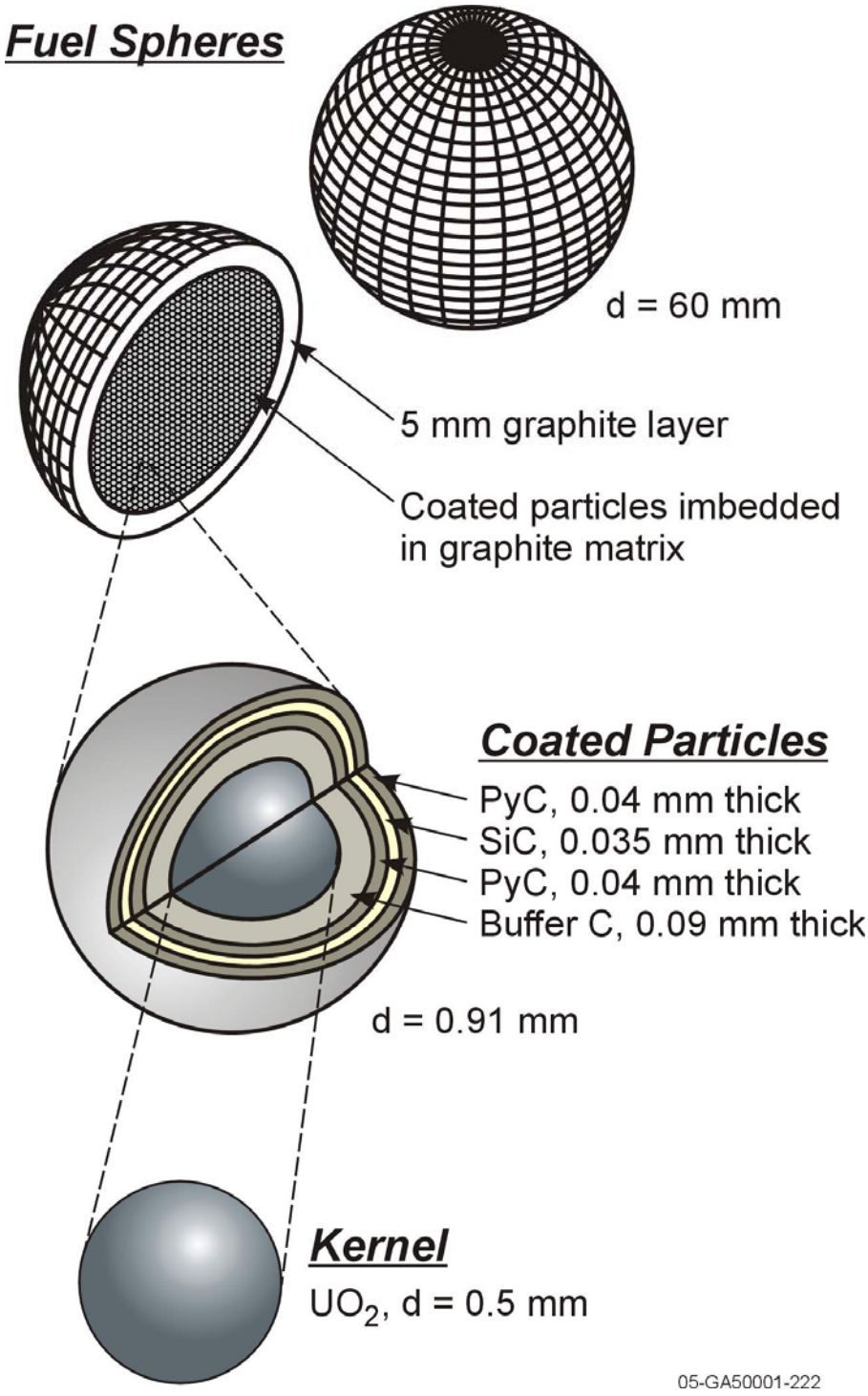

Figure 2. Illustration of Fuel Spheres and TRISO Coated Particles

Table 3. Nominal values and variations in dimensions

Item	Nominal Value	Design Tolerances	Observed Range	Standard Deviation
Core height	123 cm	n/a	n/a	n/a
Diameter of core cavity	180 cm	n/a	n/a	n/a
Height of core cavity	221.818 cm	n/a	n/a	n/a
Height of conus	36.946 cm	n/a	n/a	n/a
Dimensions of graphite blocks	Various	n/a	n/a	n/a
Outer diameter of graphite reflector	380.0 cm	n/a	n/a	n/a
Overall height of graphite reflector	610.0 cm	n/a	n/a	n/a
Diameter of cold helium flow channels	8.0 cm	n/a	n/a	n/a
Radial location of cold helium flow channels	144.6 cm	n/a	n/a	n/a
Height of cold helium flow channels	505.0 cm	n/a	n/a	n/a
Diameter of control rod and irradiation channels	13.0 cm	n/a	n/a	n/a
Height of control rod and irradiation channels	450.0 cm	n/a	n/a	n/a
Radial location of control rod and irradiation channels	102.1 cm	n/a	n/a	n/a
Diameter of round part of KLAK channels	6.0 cm	n/a	n/a	n/a
Width of oval part of KLAK channels	6.0 cm	n/a	n/a	n/a
Length (in plane of cross section) of oval part of KLAK channels	16.0 cm	n/a	n/a	n/a
Diameter of hot gas duct	30.0 cm	n/a	n/a	n/a
Elevation of hot gas duct axis	480.0 cm	n/a	n/a	n/a
Length of hot gas duct	100.0 cm	n/a	n/a	n/a
Radius of fuel discharge tube	25.0 cm	n/a	n/a	n/a
Length of fuel discharge tube	221.236 cm	n/a	n/a	n/a
Diameter of fuel pebble	6.0 cm	5.98-6.0	5.98-6.0	n/a
Diameter of kernel	0.5 mm	0.5	0.501	0.025 des, 0.0102 exp
Thickness of buffer layer	0.09 mm	0.09	0.0902	0.018 des, 0.0044 exp
Thickness of IPyC layer	0.04 mm	0.03-0.05	0.0368-0.0424	n/a
Thickness of SiC layer	0.035 mm	0.031-0.039	0.0324-0.0376	n/a
Thickness of OPyC layer	0.04 mm	0.03-0.05	0.039-0.045	n/a
Packing fraction	0.61	n/a	n/a	n/a

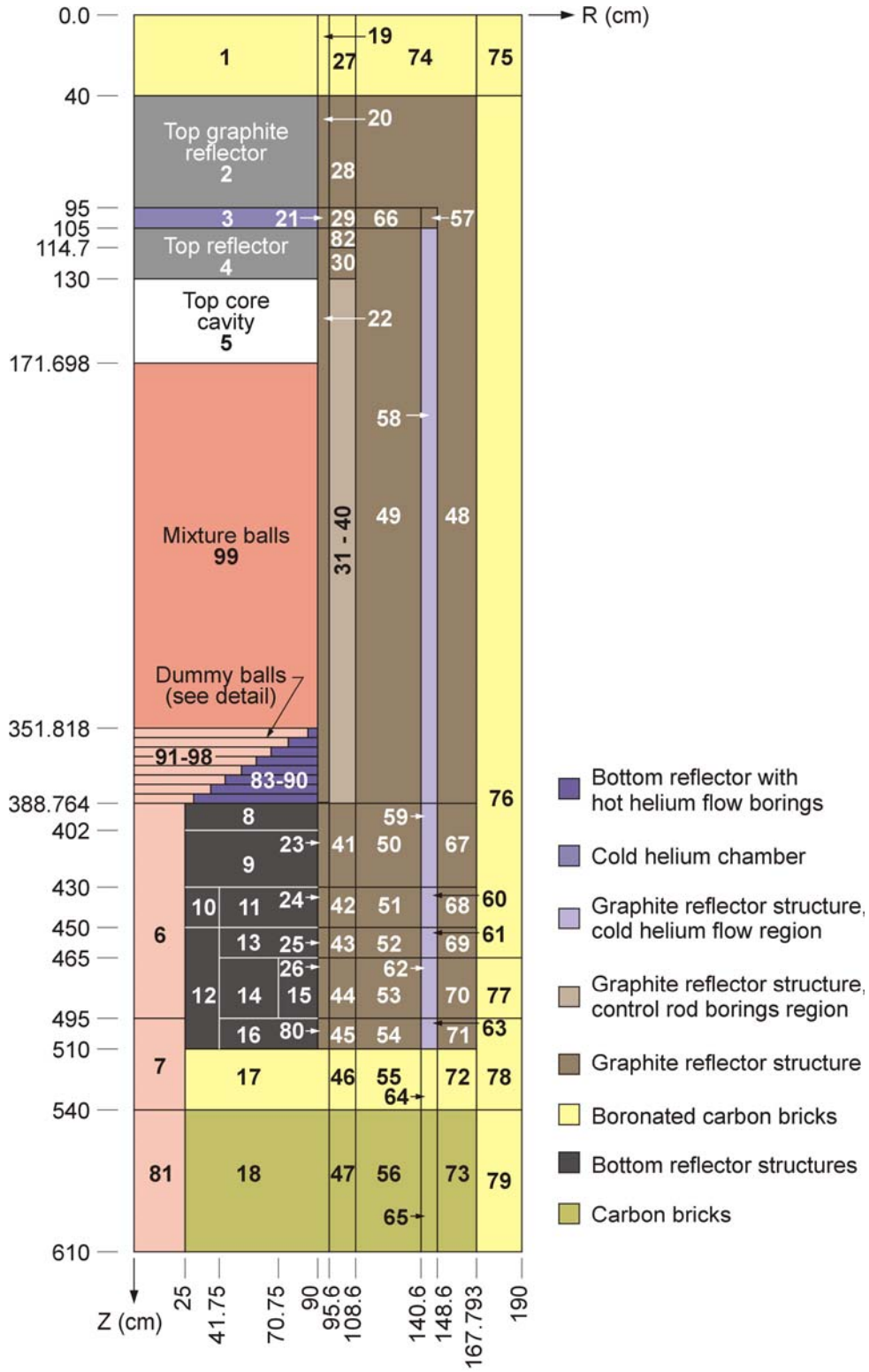

Figure 3(a). Zones of HTR-10 for modeling (dimensions are in cm)

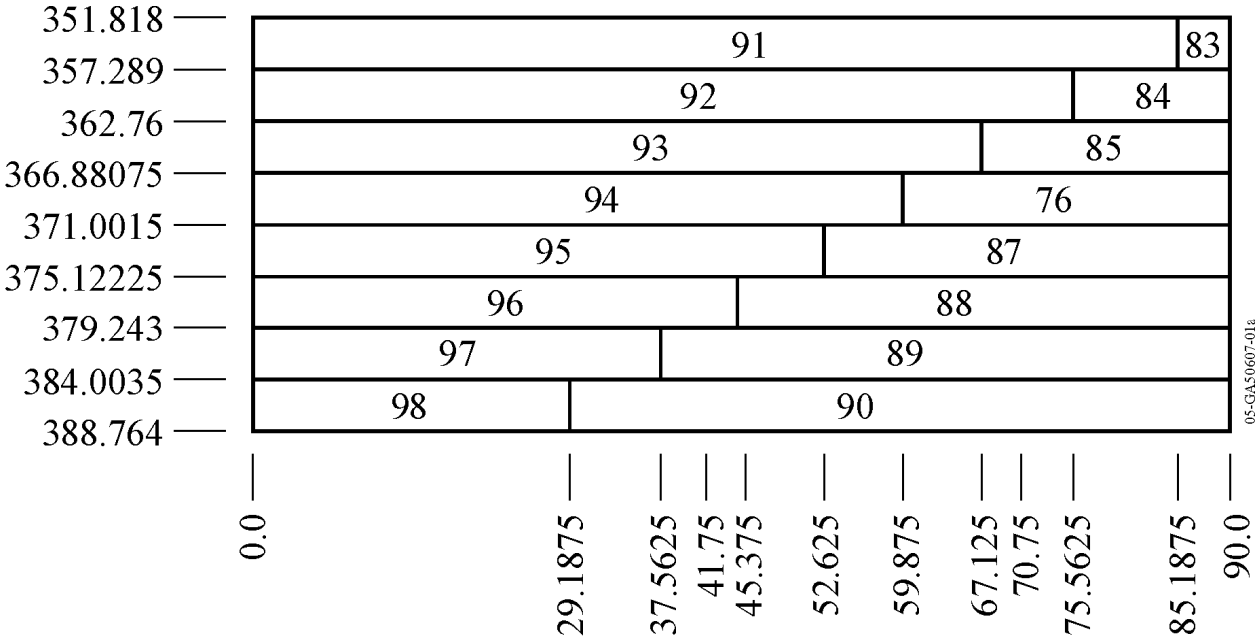

Figure 3(b). Detail in conus region (dimensions are in cm)

Figure 4 shows a horizontal cross section at an elevation within the core, displaying the borings for coolant flow channels, control rod and experiment channels, and emergency shutdown absorber ball channels. Figure 4 also shows the cross section of the emergency shutdown absorber ball channels in the section next to the core (above and below the core region, these channels are circular in cross section).

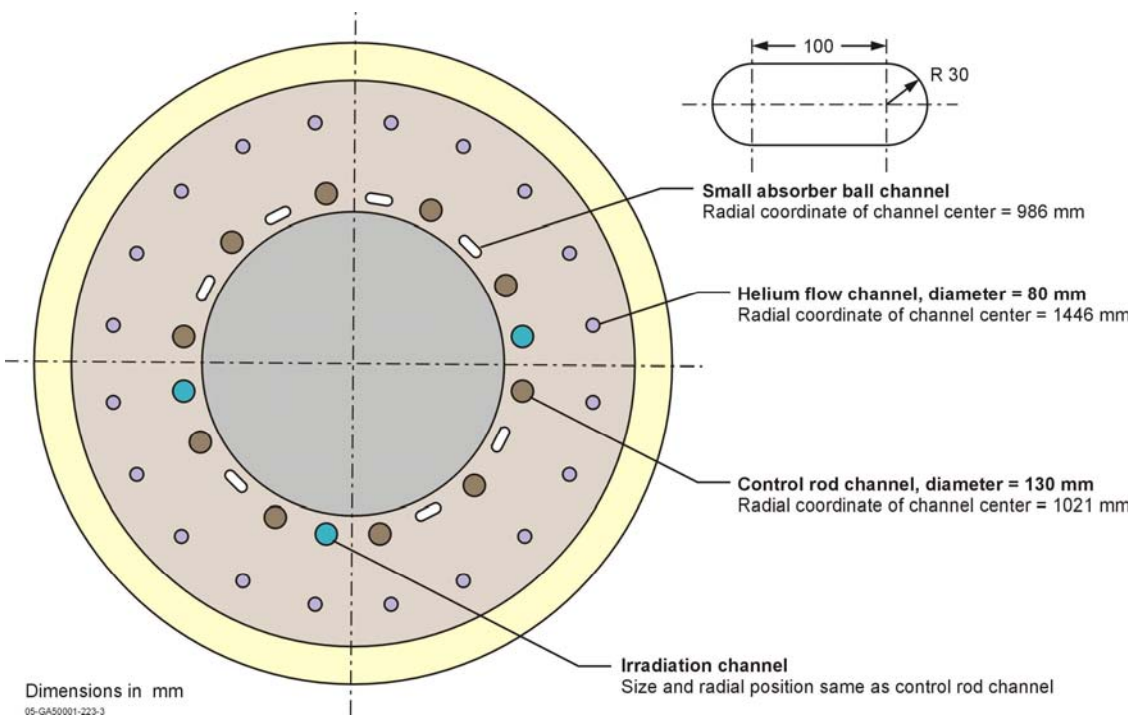

Figure 4. Cross section of reactor in core region

1.1.3 Description of Material Data

The nominal data for the fuel and dummy ball materials, in the actual as-built configuration, are given in Table 4. The material data for the reflector region are given in Table 5 for the zones shown in Figure 3.

The only materials specified in Table 5 are carbon and natural boron. The relative boron fraction varies among reflector zones, especially where highly boronated graphite is used to absorb neutrons near the periphery of the reflector. The graphite density also varies, because many of the zones have voids for various purposes. Since the control rods were withdrawn in the initial criticality experiment, and since no emergency neutron absorber balls had been introduced into the reflector, all the voids were assumed to be filled with air.

Although the HTR-10 is cooled by helium in operation, in the initial criticality experiment the voids in the reactor were filled with "moist" air at a total pressure of 0.1013 MPa and a temperature of 15 °C. The word "moist," which was used by the HTR-10 modeling group, is taken to mean saturated, as the water vapor density specified at the nominal temperature of 27 °C (see Section 1.1.4) is in fact the saturation density.

Table 4. Nominal material properties of fuel and dummy pebbles as built (from Reference 1)

Density of graphite in matrix and outer shell	1.73 g/cm3
Heavy metal (uranium) loading (weight) per ball	5.0 g
Enrichment of 235U (weight)	17 %
Equivalent natural boron content of impurities in uranium	4 ppm
Equivalent natural boron content of impurities in graphite	1.3 ppm
Volumetric filling fraction of balls in the core	0.61
UO2 density(g/cm3)	10.4
Coating layer materials (starting from kernel)	Buffer/PyC/SiC/PyC
Coating layer density(g/cm3)	1.1/1.9/3.18/1.9
Density of graphite in dummy balls	1.84 g/cm3
Equivalent natural boron content of impurities in graphite in dummy balls	0.125 ppm

Table 6 specifies the compositions of all the components in the reactor. Tolerance limits and observed ranges are shown where they are known. The nominal compositions are taken from Reference 1, and the uncertainties are taken from Reference 2. As noted above for the dimensions, Reference 2 presents data obtained by 1997, so it might not reflect tolerances or observations in the year of the experiment, but it contains the only information found on the tolerance specifications for the HTR-10.

1.1.4 Temperature Information

The initial criticality experiment was run with a clean cold core. In the benchmark specifications provided in advance of the experiment, the temperature was given as 20 °C, and the composition of the air actually occupying the void spaces in the reactor was specified at 27 °C, but the actual temperature on the day of the experiment was 15 °C . The actual temperature, 15 °C , is used in this evaluation.

1.1.5 Additional Information Relevant to Critical and Subcritical Measurements

No additional information is applicable.

Table 5. Compositions of zones shown in Figure 3 (from Reference 1, with revisions)

No. of zone	Carbon density (a/b-cm)	Natural boron density (a/b-cm)	Remarks
83-90	0.851047E-01	0.456926E-06	Bottom reflector with hot helium flow borings
1	0.729410E-01	0.329811E-02	Boronated carbon bricks
2	0.851462E-01	0.457148E-06	Top graphite reflector
3	0.145350E-01	0.780384E-07	Cold helium chamber
4	0.802916E-01	0.431084E-06	Top reflector
5			Top core cavity
6,7,91-97	0.572501E-01	0.277884E-08	Dummy balls, simplified as graphite of lower density
8	0.781408E-01	0.419537E-06	Bottom reflector structures
9	0.823751E-01	0.442271E-06	Bottom reflector structures
10	0.843647E-01	0.298504E-03	Bottom reflector structures
11	0.817101E-01	0.156416E-03	Bottom reflector structures
12	0.850790E-01	0.209092E-03	Bottom reflector structures
13	0.819167E-01	0.358529E-04	Bottom reflector structures
14	0.541118E-01	0.577456E-04	Bottom reflector structures
15	0.332110E-01	0.178309E-06	Bottom reflector structures
16	0.881811E-01	0.358866E-04	Bottom reflector structures
17,55,72, 74,75,76, 78,79	0.765984E-01	0.346349E-02	Boronated carbon bricks
18,56,73	0.797184E-01	0.000000E+00	Carbon bricks
19	0.761157E-01	0.344166E-02	Boronated carbon bricks
20	0.878374E-01	0.471597E-06	Graphite reflector structure
21	0.579696E-01	0.311238E-06	Graphite reflector structure
22,23,25, 49, 50,52,54, 66, 67,69,71, 80	0.882418E-01	0.473769E-06	Graphite reflector structure
24,51,68	0.879541E-01	0.168369E-03	Graphite reflector structure
26	0.846754E-01	0.454621E-06	Graphite reflector structure
27	0.589319E-01	0.266468E-02	Boronated carbon bricks
28,82	0.678899E-01	1.400000E-05	Graphite reflector structure
29	0.403794E-01	1.400000E-05	Graphite reflector structure
30,41	0.678899E-01	0.364500E-06	Graphite reflector structure
31-40	0.634459E-01	0.340640E-06	Graphite reflector, control rod borings region
42	0.676758E-01	0.125331E-03	Graphite reflector structure
43,45	0.861476E-01	0.462525E-06	Graphite reflector structure
44	0.829066E-01	0.445124E-06	Graphite reflector structure
46	0.747805E-01	0.338129E-02	Boronated carbon bricks
47	0.778265E-01	0.000000E+00	Carbon bricks
48	0.582699E-01	0.312850E-06	Graphite reflector structure
53	0.855860E-01	0.459510E-06	Graphite reflector structure
57	0.728262E-01	0.391003E-06	Graphite reflector structure
58,59,61, 63	0.760368E-01	0.408240E-06	Graphite reflector, cold helium flow region
60	0.757889E-01	0.145082E-03	Graphite reflector, cold helium flow region
62	0.737484E-01	0.395954E-06	Graphite reflector, cold helium flow region
64	0.660039E-01	0.298444E-02	Boronated carbon bricks
65	0.686924E-01	0.000000E+00	Carbon bricks
70	0.861500E-01	0.462538E-06	Graphite reflector structure
77	0.749927E-01	0.339088E-02	Boronated carbon bricks
81	0.847872E-01	0.000000E+00	Dummy balls, but artificially taken as carbon bricks

Table 6. Nominal values and variations in compositions

Item	Nominal Value	Design Tolerances	Observed Range	Standard Deviation
Uranium fuel loading (g/fuel pebble)	5.0 g	4.9-5.1	4.95-5.05	n/a
Density of graphite matrix in fuel pebble	1.73 g/cm3	1.73-1.77	1.73	n/a
Total ash in fuel element	0	≤300.0 ppm	130-190	n/a
Lithium in fuel element	0	≤0.3 ppm	0.007-0.023	n/a
Boron in fuel element	1.3 ppm	≤3.0 ppm	0.15	n/a
Density of graphite matrix in reflector	1.76 g/cm3	n/a	n/a	n/a
Density of boron in natural graphite reflector elements	4.8366 ppm	n/a	n/a	n/a
Ratio of oxygen to uranium in kernel	2	<2.01	n/a	n/a
Density of kernel	10.4 g/cm3	>10.4	10.83	n/a
Density of buffer layer	1.1 g/cm3	≤1.1	1.02	0.03 exp
Density of IPyC layer	1.9 g/cm3	1.8-2.0	1.80-1.92	n/a
Density of SiC layer	3.18 g/cm3	≥3.18	3.19-3.23	n/a
Density of OPyC layer	1.9 g/cm3	1.8-2.0	1.85-1.89	n/a
Composition of coolant	1.149e-3 g/cm3	n/a	n/a	n/a
Moisture content of coolant	2.57E-5 g/cm3	n/a	n/a	n/a

1.2 Description of Buckling and Extrapolation Length Measurements

No buckling or extrapolation length measurements were reported.

1.3 Description of Spectral Characteristics Measurements

No spectral characteristics were measured.

1.4 Description of Reactivity Effects Measurements

With a slight excess reactivity (i.e., at a total loading of 17,000 pebbles, or 110 more than the critical count), a control rod worth calibration experiment was carried out. One "typical" control rod was inserted a distance of 223 cm from its withdrawn position. The integral worth of the control rod was measured to be 1.4693%.

1.5 Description of Reactivity Coefficient Measurements

No reactivity coefficient measurements were made.

1.6 Description of Kinetics Measurements

No kinetics parameters were measured.

1.7 Description of Reaction-Rate Distribution Measurements

No reaction-rate distribution measurements were made.

1.8 Description of Power Distribution Measurements

No power distribution measurements were made.

1.9 Description of Isotopic Measurements

No isotopic measurements were made.

1.10 Description of Other Miscellaneous Types of Measurements

No other measurements have been reported.

2.0 EVALUATION OF EXPERIMENTAL DATA

The overall uncertainty in a calculated parameter that is a function of multiple input parameters is given by[(1)]

$$u_c^2(k_{eff}) = \sum_{i=1}^{N} (\Delta k_i)^2 + 2\sum_{i=1}^{N-1} \sum_{j=i+1}^{N} (\Delta k_i)(\Delta k_j) r_{i,j} \tag{1}$$

In Equation 1, Δk_i is the change in k_{eff} when parameter i is changed by the increment u_i, the standard uncertainty in the parameter, and $r_{i,j}$ is the correlation coefficient for parameters i and j.

Data on dimensions and materials are given in Table 4 (Section 1.1.2). Most of the data are given only as nominal values, with no information provided about tolerances, observed variations, or standard deviations. Where standard deviations are available, they are used for calculating the u_i. Where observed ranges are given, but not standard deviations, the limiting values of the observed ranges are usually applied, and plausible distribution functions are assumed for finding the u_i. Where only tolerances are given, their limiting values are used, along with plausible distribution functions. Where no guidance is given on the variability of a parameter, conservative engineering judgment is used. All uncertainties are adjusted to values of 1σ.

One category of unknown dimensional uncertainties includes the dimensions of the graphite blocks from which the reflector is constructed. In typical milling operations, tolerances on the order of tenths of millimeters are common. Cumulative uncertainties from stacking a set of ten or so blocks milled with such tolerances would be on the order of millimeters or less. For conservatism, a tolerance of ±1 cm is usually assumed for dimensions specifying the positioning of graphite reflector elements. Because borings have to line up much more precisely than that, a tolerance of 0.25 cm is usually assumed for the locations and radii of the various channels in the core.

Usually, no information is given about the distribution function of the deviation of a parameter from its nominal value. In most cases, it is assumed for convenience that the most relevant quantity is uniformly distributed. For example, if the change in k_{eff} from its nominal value is proportional to the change in the volume of a spatial region, then it is assumed that the deviation of the volume of that region from its nominal value is uniformly distributed.

The following subsections discuss the calculation of the uncertainties in the parameters listed in Table 4. The values of k_{eff} are computed in the as-run critical configuration and in the configuration with each parameter assigned its maximum variation (or its standard deviation

---

(1) " ICSBEP Guide to the Expression of Uncertainties," Larry G. Blackwood, Independent Reviewer, Revision 1, September 30, 2004, p. 29. This guide has not been published, but it is available to anyone involved in the IRPhEP.

when available), one parameter at a time. The bases for the choices of the parameter values are discussed. Only a few parameters are important enough that reasonable variations in them produce relatively large variations in k_{eff}; these parameters are discussed at greater length.

The value of k_{eff} computed for a given configuration depends on the microscopic cross sections used in the calculation. The calculated microscopic cross sections are somewhat sensitive to the fast and thermal buckling values used in the input to COMBINE, the cross section processing code[(1)] used in this evaluation. The buckling values were found by a buckling search, as explained in subsection 3.1.1. In most cases, variations in the problem specifications were small enough that the same cross sections were used for both the critical baseline configuration and the perturbed configuration. However, in some cases, new cross sections were calculated for a perturbed case. The baseline value of k_{eff} is 1.03257.

The baseline value of k_{eff} computed for this evaluation is farther from 1.0 than one would like to see. PEBBED,[(2)] the code used to calculate k_{eff}, has been validated extensively,[(3)] but its results are naturally dependent on the quality of the cross sections supplied to it. Calculation of cross sections in graphite systems presents problems that have not yet been resolved. Another possible source of inaccuracy is the shape of the upper surface of the core. Pebbles fall onto the upper surface at discrete drop points, where mounds build up, and they roll down a mound until they lodge more or less randomly on the surface. PEBBED assumes a planar upper core surface, like all the benchmark models reported in Reference 1. The error introduced by this assumption is not known. However, it introduces a constant bias in the results, and the uncertainty analysis should be unaffected by this bias.

Another possible source of inaccuracy in the PEBBED results is the use of only two spectral zones in the model – one in the core, and the other in the reflector. This might be inadequate, even in the HTR-10 initial startup core, which is uniform in composition. Again, however, this representation introduces in the results a constant bias that will not affect the uncertainties calculated when dimensional or compositional parameters are varied.

---

(1) Robert A. Grimesey, David W. Nigg, and Richard L. Curtis, *COMBINE/PC – A Portable ENDF/B Version 5 Neutron Spectrum and Cross-Section Generation Program*, EGG-2589, Rev. 1, Idaho National Engineering Laboratory, February 1991.

(2) W. K. Terry, H. D. Gougar, and A. M. Ougouag, "Direct Deterministic Method for Neutronics Analysis and Computation of Asymptotic Burnup Distribution in a Recirculating Pebble-Bed Reactor," Annals of Nuclear Energy 29 (2002), pp. 1345-1364.

(3) Hans D. Gougar, Abderrafi M. Ougouag, and William K. Terry, "Validation of the Neutronic Solver within the PEBBED Code for Pebble Bed Reactor Design," proc. *Mathematics and Computation, Supercomputing, Reactor Physics and Nuclear and Biological Applications,* Palais des Papes, Avignon, France, September 12-15, 2005, American Nuclear Society, LaGrange Park, IL (2005)

Another minor source of inaccuracy in the PEBBED results is the assumption that the core density is uniform. Of course, the pebble packing fraction is only about 61%, so on the scale of a pebble diameter the density is highly nonuniform, but on the scale of the core dimensions, this nonuniformity is not expected to make much difference. However, spheres in a container are not distributed uniformly throughout. It has been observed experimentally[(1)] that the packing fraction varies from zero at the edges through several damped oscillations to approach an asymptotic value of about 61% over a distance of about five sphere diameters. The effects of these inhomogeneities have been studied for a simple hypothetical PBR reactor configuration.[(2)] It was found that the difference in the calculated value of k_{eff} was about $5x10^{-4}$ for that reactor. The packing fraction itself is uncertain, but the uncertainty in this parameter is addressed in the analysis.

For perspective, the results of the international benchmark collaboration are noted, as given in Reference 1. The objective of the initial criticality benchmark was to predict the initial critical core height. The measured height was 123.06 cm, and the assumed temperature for the predictions was 20 °C. Predictions by various groups ranged from 107 cm to 137.3 cm. These values range from -13% to +12% of the core height. It is reported in subsection 2.1.1 below that a difference of 0.1% in the core height produces a difference of $3.7x10^{-4}$ in k_{eff}. If the relationship between the difference in k_{eff} and the difference in core height were linear over the entire range of core heights, the errors in k_{eff} would vary from -0.048 to +0.044, corresponding to a range in k_{eff} of 0.952 to 1.044. Computation of k_{eff} in PBRs is evidently not straightforward, and considerable research seems needed before accuracy is routinely obtained comparable to that in computations for light water reactors.

2.1 Evaluation of Critical Configuration Data

The following subsections contain evaluations of the critical configuration measurements described in Section 1.1. In many cases, the assumptions on the uncertainties in experimental parameters are very crude. However, the only important parameters are those whose uncertainties lead to uncertainties of more than 10^{-3} in k_{eff}. When reasonable and conservative assumptions lead to smaller uncertainties than that in k_{eff}, little is to be gained by trying to be more precise.

In all cases where tolerances or observed variations apply to large numbers of objects (pebbles and fuel particles or portions thereof), both systematic errors (applying to all the objects equally)

---

(1) R. F. Benenati and C. B. Brosilow, "Void Fraction Distribution in Beds of Spheres," *A. I. Ch. E. Journal* **8**, No. 3, pp. 359-361 (1962).

(2) W. K. Terry, A. M. Ougouag, Farzad Rahnema, and Michael Scott McKinley, "Effects of spatial variations in packing fraction on reactor physics parameters in pebble-bed reactors," American Nuclear Society Mathematics & Computation Division Conference, Gatlinburg, Tennessee, April 6-11, 2003.

and random errors (different from one pebble to the next) will occur. For the fuel particles and their subregions especially, the uncertainties from the random errors are extremely small (the tolerance limit for the random error divided by the square root of the number of fuel particles, √(4751x16,890) = 8957.9 (see Appendix B)). For errors in properties of pebbles, the uncertainty in the random component is equal to the tolerance limit for the random component divided by the square root of the number of pebbles, or 129.96. In all cases, division by such large numbers would make the random component of the uncertainty negligible. However, since nothing is known about how the errors are divided between the systematic and random components, it is assumed throughout that the errors are all systematic. This assumption provides the analysis with a large degree of conservatism.

When a variable x is judged to be distributed uniformly between the bounding values μ and $\mu+a$, the standard deviation in x can be shown to be $a/\sqrt{3}$.(1) (The reference actually proves the claim for a uniform distribution from $\mu-a$ to $\mu+a$, but the extension of the proof to the half-interval is trivial.) Then the standard deviation of a linear function $f(x)$ is $f(a/\sqrt{3})$. This observation is used repeatedly in the following analysis.

2.1.1 Core Height and Core Diameter

The core height is a calculated parameter, based on the number of balls contained in the core. As discussed above, the upper core surface is actually a mound, but it is modeled as a plane at an elevation consistent with the core volume and a cylindrical core shape. The total number of balls (fuel and dummy) in the cylindrical core region at criticality was given as 16,890, and no information was given on the accuracy of the count. The core height was computed from the number of balls and the nominal core diameter at an assumed packing fraction of 0.61.

The number of pebbles in the core is

$$N_p = \frac{\pi f_p R_c^2 H_c}{V_p} \quad , \qquad (2)$$

where f_p =packing fraction,
R_c = core radius,
H_c = core height,
and V_p = pebble volume.

Then, in part, k_{eff} is a function of the packing fraction, core radius, core height, and pebble volume. The dependencies of k_{eff} on pebble volume and packing fraction are treated in subsequent subsections. In this subsection, pebble volume and packing fraction are held

(1) " ICSBEP Guide to the Expression of Uncertainties," Larry G. Blackwood, Independent Reviewer, Revision 1, September 30, 2004, p. 29. This guide has not been published, but it is available to anyone involved in the IRPhEP.

constant. It is convenient to treat core radius and core height together; it is reasonable to treat them as independent (uncorrelated) variables.

No estimate is given on the uncertainty in the number of balls in the core, but engineering judgment suggests that a counting accuracy of less than 1% would be very poor, while an accuracy of 0.1% (at one standard deviation) might be acceptable. The latter figure corresponds to a miscount of about 17 balls in the core. PEBBED calculations (based on changes of 1 cm in radius and height) show that a change in the core radius leads to a change in k_{eff} of 1.10643×10^{-5} per ball, while a change in core height leads to a change in k_{eff} of 2.16393×10^{-5} per ball. (This difference in sensitivity is due to the relatively short and wide configuration of the core at initial criticality). Then for a miscount of 17 balls,

$u_{core\ radius} = 1.9 \times 10^{-4}$
and
$u_{core\ height} = 3.7 \times 10^{-4}$.

2.1.2 Height of Core Cavity

This parameter is the height of the cavity in which the core resides, which includes the void space above the core, not the height of the core itself. The effect on k_{eff} of variations in this parameter is assessed by raising the datum plane at the top of the core cavity. No other computational cells are affected by this change. No guidance is given on the possible variation in core cavity height, but this parameter depends on the precision with which the graphite components of the reflector are milled. As noted above, a very conservative value of 1 cm is assumed for most graphite dimensional uncertainties. If the top of the core cavity is raised by 1 cm, k_{eff} changes by -4.2×10^{-4}. For lack of specific knowledge about how errors in core cavity height might be distributed, it is conservatively assumed that the distribution is uniform. Then the standard deviation in core height errors and the resulting change in k_{eff} are the limiting value divided by √3 (cf. Footnote (a)):

$u_{core\ cavity} = -2.4 \times 10^{-4}$.

2.1.3 Height of Conus

An uncertainty in the height of the conus is represented by moving the datum plane at the top of the conus upwards by 2.7355 cm, an increment that fits conveniently with the PEBBED nodalization, and by moving the datum plane at the top of the core by an equal amount. Thus, the active core height does not change. The shift roughly amounts to one pebble radius, which corresponds to a miscount of about 375 pebbles, an unlikely amount. For this assumed uncertainty, the change in k_{eff} is found to be 1.05×10^{-3}. Conservatively assuming a uniform distribution function for errors in conus height, one divides this number by √3 to find (to the nearest significant figure)

$u_{conus} = 6.1\text{x}10^{-4}$.

2.1.4 Dimensions of Graphite Blocks

As discussed in Section 2.0, tolerances of about 0.1 mm are assumed for milling the graphite blocks. Such tolerances appear reasonable in view of the necessity of coolant, control rod, and emergency absorber ball channels to line up. Except in the outer periphery of the reflector, where boronated carbon bricks are used to reduce neutron leakage into the surroundings, the only differences among adjacent blocks are in their void fraction; uncertainties in void fraction are accounted for below where the sizes and locations of the different borings are varied. Uncertainties in the inner and outer reflector diameters and the inner and outer reflector axial dimensions are also treated in other subsections. The importance of neutrons is low in the outer periphery. Therefore, it is not necessary to analyze the effects of uncertainties in the internal boundaries between reflector blocks.

2.1.5 Outer Diameter of Graphite Reflector

The outer diameter of the reflector could differ from the nominal value by an accumulation of off-nominal radial dimensions in graphite blocks at several radial locations or by off-nominal radial dimensions at a single radial location. Two cases of the latter possibility were explored. First, the outermost zone was increased 1 cm in radius; this led to an increase in k_{eff} of $1.8\text{x}10^{-4}$. Second, with the outermost zone again at its nominal thickness, the next-to-outermost zone was increased 1 cm in radius; this led to a decrease in k_{eff} of $1.4\text{x}10^{-4}$.

The outermost zone consists of boronated carbon bricks, installed for the purpose of capturing neutrons that would otherwise escape into the surrounding pressure vessel (which was not represented in the model provided in Reference 1 by the Chinese research group). Even though boron has a high absorption cross section for thermal neutrons, increasing the thickness of the boronated carbon bricks provides more scattering sites from which neutrons can be scattered back towards the core. In other words, nothing is as good an absorber as a vacuum boundary condition, so replacing vacuum with anything increases k_{eff}. However, increasing the thickness of the region inside the boronated graphite layer is found to decrease k_{eff}. It is surmised that this additional layer of low-boron graphite softens the neutron energy spectrum slightly, which increases the absorption of neutrons in the boronated carbon bricks and decreases the number of neutrons that can be reflected back into the core.

The larger effect is taken as the uncertainty in k_{eff} resulting from differences in the reflector outer diameter from the nominal value. The change in k_{eff} is proportional to the change in the cross-sectional area of the outermost zone. If the error in the cross-sectional area is uniformly distributed, a reasonable assumption, then the uncertainty in k_{eff} associated with uncertainty in reflector outside diameter is $1.8\text{x}10^{-4}/\sqrt{3}$, or (to the nearest significant figure)

$u_{refl\ O.D.} = 1.0\text{x}10^{-4}$.

2.1.6 Height of Graphite Reflector

In this case, because of the large height of the reflector, a greater uncertainty was assumed in the height: ±1%, which is a dimensional uncertainty of ±6.1 cm. Increasing the axial thickness of the first axial region increases k_{eff} by $1.0\text{x}10^{-5}$. Increasing the axial thickness of the last region by 6.1 cm causes no change in k_{eff}. Whatever distribution function applies, the error at the standard deviation is smaller, but when it is rounded to the nearest significant figure the value returns to $1\text{x}10^{-5}$.

$u_{refl\ ht} = 1\text{x}10^{-5}$.

2.1.7 Diameter of Cold Helium Flow Channels

The nominal diameter of the helium flow channels is 8.0 cm; tolerance information is not given. A very conservative tolerance of ±0.5 cm is assumed; more realistic tolerances would be of the order of a fraction of a millimeter.

The helium flow channels occupy portions of Regions 58-65 in Figure 3. From Table 2, one can infer the void fraction in each region (Regions 22, etc., have no voids) and the part of the void space taken by the flow channels in each region. Then a reduction in the flow channel diameter can be used to find the new void fraction and the new nuclide number densities in each region. It is found that a simultaneous reduction of 0.5 cm in all the flow channel diameters produces an increase in k_{eff} of $2\text{x}10^{-5}$. If the error in cross-sectional area is assumed to be distributed uniformly, then the uncertainty in k_{eff} is $2\text{x}10^{-5}/\sqrt{3}$, or, to the nearest significant figure,

$u_{He\ flow\ dia} = 1\text{x}10^{-5}$.

2.1.8 Radial Location of Cold Helium Flow Channels

The helium flow channels occupy the entire radial span of Regions 58-65; i.e., r = 140.6-148.6 cm. (No tolerance information is given.) Therefore, the radial location of the channels can be adjusted by moving the inner and outer boundaries of these regions by equal amounts. The flow channels must line up well in axially adjacent blocks in order for the coolant to flow smoothly, so the tolerances in radial location must be quite small. For conservatism, it is assumed that the tolerance is 0.25 cm. An outward shift in the radial location of the flow channels produces a reduction of $4.0\text{x}10^{-5}$ in k_{eff}. If the error in radial location is distributed uniformly, then the uncertainty in k_{eff} is $4.0\text{x}10^{-5}/\sqrt{3}$, or, to the nearest significant figure,

$u_{He\ rad\ loc} = -2\text{x}10^{-5}$.

2.1.9 Height of Cold Helium Flow Channels

The cold helium flow channels extend to the bottom of the model in Figure 3. To change their height, one must extend them or contract them at the top. It was assumed for modeling convenience that the cold helium flow channels were extended through the entire axial span of region 57 of Figure 3, an increase of 10 cm. This is a very conservative assumption. This adjustment caused no change at all in k_{eff}.

$u_{He\ chan\ ht} = 0.0$

2.1.10 Diameter of Control Rod and Irradiation Channels

The control rod and irradiation channels are located at the same radial position and have the same diameter and axial extent. They occupy the entire radial span of Regions 27-31, 41, 42, and 82, or r = 95.6-108.6 cm. No tolerance range is given. The diameter is conservatively assumed to be 0.5 cm smaller than nominal. The same approach is applied as to the helium flow channels, discussed in Section 2.1.7 above. The change in k_{eff} is $6.1\text{x}10^{-4}$, and the uncertainty is $6.1\text{x}10^{-4}/\sqrt{3}$:

$u_{C\ R\ dia} = 3.5\text{x}10^{-4}$.

2.1.11 Height of Control Rod and Irradiation Channels

The control rod and irradiation channels extend from the top of the core through Region 42 of Figure 3. The region below Region 31 is Region 43, which is 15 cm in height. Because neutrons are more important near the core than in the helium flow channel regions, it is excessively coarse to assume a perturbation in the height of the control rod and irradiation channels that extends the entire length of Region 43. It is assumed instead, still conservatively, that the perturbed channels extend 2 cm into Region 43. This perturbation does not change k_{eff}.

$u_{C\ R\ ht.} = 0.0$

2.1.12 Radial Location of Control Rod and Irradiation Channels

No tolerances are given on the location of the control rod and irradiation channels. If the inner and outer boundaries of the annulus containing these channels are moved outwards by 0.25 cm, the change in k_{eff} is $1.1\text{x}10^{-4}$. Assuming a uniform error distribution in the radial location of the channels, one finds the uncertainty in k_{eff} to be

$u_{C\ R\ loc} = 6\text{x}10^{-5}$.

2.1.13 Dimensions of KLAK Channels

The HTR-10 has two independent shutdown systems: the normal control rods and a supply of small spherical absorbers, often called "KLAK" from the German acronym for small absorber balls ("kleine aufsauger Kugeln"), that can be dropped into seven channels located in the same radial regions of the model as the control rod and irradiation channels. The KLAK channels run the entire length of the model. In the core and conus axial range, the channel cross sections are ovals 6 cm wide and 16 cm long, with the long sides oriented in the circumferential direction of the reactor. Above and below that axial range, the KLAK channels are cylindrical, with a diameter of 6 cm. No tolerance ranges are given.

The channels occupy a 6 cm radial zone in model regions 13 cm in radial extent. The KLAK channels can move in a range of 7 cm radially in these regions without changing the region densities. Such large perturbations in the KLAK channel locations are implausible. Therefore, the effects of radial mislocations of the KLAK channels are not modeled. However, the effects of perturbations in the size of the channels indicate that the effects of such mislocations are probably very small.

For the KLAK channels, an uncertainty of 10% (in standard deviation) was assumed in the cross-sectional area for all regions. This corresponds to about 5% in linear dimensions ($\sqrt{1.1}$ = 1.04881), or about 1.5 mm in radius in the cylindrical sections and 8 mm in the long direction in the oval section. The uncertainties in k_{eff} were computed from such increases in the sizes of the three sections of the KLAK channels.

Upper cylindrical section: $u_{KLAK\ upper} = 0.0$

Oval section : $u_{KLAK\ middle} = -2.8\text{x}10^{-4}$.

Lower cylindrical section: $u_{KLAK\ lower} = 0.0$.

2.1.14 Dimensions of Hot Gas Duct

The hot gas duct extends from r=90 cm to the outer edge of the reflector, in regions 26, 44, 53, 62, 70, and 77 in an axial zone from z=465 cm to z=495 cm. The nominal diameter of the duct, 30 cm, spans this axial range. No tolerance ranges are given.

Because the duct is large, a large perturbation of 1 cm was assumed in the diameter. The same approach described above for the cold helium flow channels was applied to the duct diameter. The changed duct diameter had no effect on k_{eff}.

The effect of a perturbation in the length of the duct was examined by assuming the duct to extend through the radial extent of Region 15, which is adjacent to Region 26. This assumption extends the length of the duct by 19.25 cm, which is completely unrealistic. However, the

perturbation caused no change in k_{eff}, so more realistic perturbations would also have no effect.

A shift in the axial location of the duct could be accomplished by changing the locations of the datum planes at *z*=465 cm and *z*=495 cm, but this change would affect the nuclide number densities in other regions besides those containing the duct. An axial shift could also be represented by calculating perturbed nuclide number densities in regions adjacent to the nominal location of the duct, into which the duct would move in the perturbation, but this approach would alter the nuclide number densities throughout the adjacent regions, which would give distorted neutron flux distributions. Because of the lack of influence the other changes in duct dimensions have on k_{eff}, it is simply assumed that realistic shifts in hot gas duct axial position also have no effect.

$u_{hot\ gas\ duct} = 0.0$

2.1.15 Radius of Fuel Discharge Tube

The fuel discharge tube occupies regions 6, 7, and 81 in Figure 3. Its nominal radius is 25 cm; no tolerance range is given. The uncertainty in discharge tube radius is modeled by moving the radial boundary of Regions 6, 7, and 81 outwards by 0.25 cm. There is no effect on k_{eff}.

$u_{discharge\ radius} = 0.0.$

2.1.16 Height of Fuel Discharge Tube

The fuel discharge tube extends to the bottom of the model. The effect of increasing the height of the model has already been examined. A perturbation in the fuel discharge tube height is redundant.

$u_{discharge\ height} = 0.0$

2.1.17 Diameter of Fuel Pebble

The HTR-10 fuel pebble is a sphere 6 cm in diameter, consisting of an inner fuel zone 5 cm in diameter and an outer unfueled layer. The inner fuel zone consists of a graphite matrix containing an average of 8335 TRISO coated fuel particles. The outer layer contains only graphite. The core also contains dummy graphite balls, which are also 6 cm in diameter; the ratio of fuel balls to dummy balls is 57:43.

The tolerance range on fuel pebble diameter is 5.98-6.0 cm; this is also the observed range. The uncertainty in k_{eff} resulting from uncertainty in fuel pebble diameter is evaluated by reducing the pebble diameter to 5.98 cm.

There are several ways to do this, but the greatest changes in average nuclide densities in the core region are produced by keeping the diameter of the fuel zone constant and reducing the thickness of the outer graphite layer. For example, reducing the diameter of the fuel zone and keeping the outer graphite layer thickness constant would shrink the fuel zone volume almost in proportion to the shrinkage in total pebble volume; then the average nuclide densities in the core would be almost unaffected and k_{eff} would hardly change at all. The average densities are further changed by assuming that the dummy balls are also reduced to 5.98 cm in diameter. The result of making those changes is to decrease k_{eff} by 2.12×10^{-3}.

As noted in Section 2.1, the error within the tolerance range presumably comprises a systematic component and a random component. However, no information is available on how the error is apportioned between the systematic and random components. The most conservative approach is to assume that the error is all systematic. The uncertainty in the systematic component is equal to the tolerance limit for the systematic component divided by $\sqrt{3}$, assuming that the systematic error in volume is uniformly distributed (the change in k_{eff} is proportional to the volume change, not the linear change). Then the uncertainty in k_{eff} is $-2.12 \times 10^{-3}/\sqrt{3}$, or

$$u_{FPdia} = -1.22 \times 10^{-3} .$$

It merits comment that k_{eff} is reduced by packing more fuel balls, which each contain the same amount of fuel as the nominal pebbles, into the same volume of core. Evidently the HTR-10 is undermoderated, so that the loss of moderation caused by reducing the amount of graphite in the core overshadows the increase in the macroscopic fission cross section obtained by increasing the amount of fuel. A study of the effect of changing the relative amounts of fuel and moderator in PBRs has found that the usual formula of 5 cm for the fuel zone diameter and 6 cm for the fuel pebble diameter does not provide optimal moderation, at least for some fuel particle packing fractions.[(1)]

2.1.18 Diameter of Kernel

The nominal kernel diameter is 0.5 mm, and the measured standard deviation is 0.0102 mm. The 1-σ kernel is 6.2457% larger in volume than the nominal kernel. However, there is a tolerance in pebble fuel loading of 5.0±0.1 g/pebble. This is only a variation of ±2%. Therefore, if all of the kernels were allowed to reach their 1σ diameter, the limit on fuel loading would be exceeded. Hence, the limit on fuel loading (see Section 2.1.23) bounds the effects of uncertainties in the fuel kernel diameter, and the fuel kernel diameter is not used in the uncertainty analysis.

---

(1) Abderrafi M. Ougouag, Hans D. Gougar, William K. Terry, Ramatsemela Mphahlele, and Kostadin N. Ivanov, "Optimal Moderation in the Pebble-Bed Reactor for Enhanced Passive Safety and Improved Fuel Utilization," proc. *PHYSOR 2004, The Physics of Fuel Cycles and Advanced Nuclear Systems: Global Developments,* American Nuclear Society, Chicago, IL, April 25-29, 2004.

2.1.19 Thickness of Buffer Layer

The buffer layer is a relatively porous layer of carbon immediately surrounding the kernel. Its porosity is intended to provide room for fission product gases without excessive pressure buildup. In the HTR-10 fuel, the buffer layer thickness is nominally 0.09 mm, and the experimentally observed standard deviation is 0.0044 mm. In the uncertainty analysis, it was assumed that all the buffer layers in the core were increased by one standard deviation from the nominal value, and that all the other layers in the fuel particles kept their original volumes. The new core average nuclide densities were computed, and k_{eff} was found to decline by $-3.0\text{x}10^{-5}$. It is assumed that the error in buffer volume is uniformly distributed; then the uncertainty in k_{eff} is $-3.0\text{x}10^{-5}/\sqrt{3}$, or, to the nearest significant figure,

$u_{buffer\ thickness} = -2\text{x}10^{-5}$.

The reason for the decrease in k_{eff} is that the expanded buffer layer displaces matrix material, since the diameter of the fuel zone is held constant. Then there is a decrease in carbon density in the core, which reduces moderation.

2.1.20 Thickness of IPyC Layer

Outside the buffer layer, the TRISO particle consists of three hard and dense layers that provide a miniature containment vessel for fission products. The first of these is the inner pyrolytic carbon (IPyC) layer. Its nominal thickness is 0.04 mm, its tolerance range is 0.03-0.05 mm, and its observed range of variation is 0.0368-0.0424 mm. For conservatism, it was assumed that all of the IPyC layers in the core were expanded to their maximum allowable thickness, while all the other layers retained their nominal volumes. The density of the pyrolytic carbon layers is greater than that of the matrix material, so expansion of the layers increases the carbon density in the core and enhances moderation. Therefore, k_{eff} increases slightly; the change is $3\text{x}10^{-5}$. If the volume error is uniformly distributed, then to the nearest significant figure,

$u_{IPyC\ thickness} = 2\text{x}10^{-5}$.

2.1.21 Thickness of SiC Layer

The second hard and dense layer outside of the buffer zone is the silicon carbide layer. This is the strongest layer in the fuel particle and the principal containment shell. It has a nominal thickness of 0.035 mm, a tolerance range of 0.031-0.039 mm, and an observed range of 0.0324-0.0376 mm. Standard deviations are not given. First, it was assumed that all of the SiC layers in the core were expanded to their maximum allowable thickness, while all the other layers retained their nominal volumes. This perturbation produced a decrease in k_{eff} of $-3.4\text{x}10^{-4}$.

In cases like the IPyC layer, where even perturbations up to the maximum tolerance value produce only very small changes in k_{eff}, it is both conservative and inconsequential to use the maximum allowable perturbation to compute the uncertainty in k_{eff}. However, when such a perturbation produces a larger change in k_{eff}, it is more reasonable to assume the maximum observed perturbation. The computed change in k_{eff} and the fractional volume change were applied were used to calculate

$$\frac{dk_{eff}}{d\overline{V}} = -2.70499x10^{-3}. \tag{3}$$

Then an increase of the SiC thickness to its maximum observed value gives a change in k_{eff} of $-2.2x10^{-4}$. If the change in SiC volume is assumed to be distributed uniformly, then

$u_{SiC\ thickness} = -1.3x10^{-4}$.

2.1.22 Thickness of OPyC Layer

The final hard and dense layer in the TRISO particle, and its outermost shell, is the outer pyrolytic carbon (OPyC) layer. This shell has a nominal thickness of 0.04 mm, a tolerance range of 0.03-0.05 mm, and an observed range of 0.039-0.045 mm. It was assumed that all the OPyC layers in the core were increased to their maximum allowable values while all the other layers retained their nominal volumes. This assumption led to an increase of $5x10^{-5}$ in k_{eff}. If the change in the OPyC volume is distributed uniformly,

$u_{OPyC\ thickness} = 3x10^{-5}$.

2.1.23 Uranium Fuel Loading

The nominal uranium loading in the HTR-10 fuel is 5 g per pebble. The tolerance range is 4.9-5.1 g, and the observed range is 4.95-5.05 g. The tolerance range was used to estimate the derivative

$$\frac{dk_{eff}}{d\overline{m}_U} = 0.179 \quad , \tag{4}$$

where $\overline{m}_U$ is the normalized uranium mass in the pebble.

The observed variation in $\overline{m}_U$ is ±1%, so the associated variation in k_{eff} is $1.79x10^{-3}$. If the deviation of the uranium loading from the nominal value is distributed uniformly within the observed range, the uncertainty in k_{eff} is

$1.79x10^{-3}/\sqrt{3}$, or

$u_{U\ loading}$ = 1.03x10^{-3} .

2.1.24 Density of Graphite Matrix in Fuel Pebble

The density of the graphite matrix in the fuel pebble is nominally 1.73 g/cm^3. The tolerance range is 1.73-1.77 g/cm^3, and only the nominal value was observed. It is not plausible to assume that there is no uncertainty in the graphite density, but the observation of only one value suggests that a uniform distribution is not appropriate. For this case, a triangular distribution was assumed, with the mode (i.e., the most frequently observed value) equal to the nominal value and the distribution function declining to zero at the maximum tolerance value.

The variance in the triangular distribution is given by(1)

$$\sigma^2 = \frac{a^2 + b^2 + c^2 - ab - ac - bc}{18}, \tag{5}$$

where *a* and *b* are the limits of the interval on which the distribution function is defined, and *c* is the mode.

This formula was applied to the deviation of the graphite density from 1.73 g/cm^3, so that *a*=0, *b*=0.04, and *c*=0. Then σ^2 = 8.88889x10^{-5} and σ = 0.009428. The uncertainty is found by computing k_{eff} at one standard deviation away from the nominal value. Thus, the value of the graphite matrix density at which k_{eff} is to be evaluated is 1.739428 g/cm^3. The boron content of the graphite matrix is assumed to remain at 1.3 ppm. The fuel matrix graphite is only one component of the carbon in the core region. All the other carbon components are assumed to be unaffected. When the new graphite and boron densities are used in PEBBED, the associated uncertainty in k_{eff} is found to be

$u_{fuel\ graphite\ density}$ = 1.13x10^{-3}.

2.1.25 Total Ash in Fuel Element

The fuel specifications permit small amounts of unspecified impurities. Without knowing what they are, it is impossible to assess their effects quantitatively. However, it is not necessary to do so. The tolerance limits on the boron content of the fuel and reflector are actually limits on equivalent boron content, which includes the unspecified impurities.

2.1.26 Lithium in Fuel Element

(1) M. Evans, Nicholas Hastings, and Brian Peacock, *Statistical Distributions*, 3rd Edition, John Wiley and Sons, New York, 2000, pp. 187-188.

The nominal fuel element contains no lithium, but a trace amount of up to 0.3 ppm is permitted, and concentrations of 0.007-0.023 ppm are observed.

The maximum allowable amount of lithium was assumed, not only in the fuel elements but also in the dummy balls. A new cross section set was generated, and the revised multiplication constant was computed. The change in k_{eff} is 1.7×10^{-5}. The deviation of the lithium concentration from zero to the maximum allowable value is assumed to be uniform. Then the uncertainty in k_{eff} is $1.7 \times 10^{-5}/\sqrt{3}$, or

$u_{Li} = 1 \times 10^{-5}$.

2.1.27 Boron in Fuel Element

The nominal boron concentration in the fuel graphite is 1.3 ppm, while the tolerance limit is 3.0 ppm. The only observed value reported in Reference 2 for the boron in the fuel element graphite matrix is 0.15 ppm. As in the case of the fuel matrix graphite density, it requires judgment to choose a distribution function for the boron concentration. When, in contrast, the boron content in the dummy balls was found to differ substantially from the nominal value (the nominal value was 1.3 ppm, while the as-built value is reported as 0.125 ppm), the deviation was noted in the experiment report (Reference 1). One would expect that a deviation almost as great in the fuel element matrix boron would also have been reported. The nominal value is almost in the middle of the tolerance range. It is very conservative to assume a uniform distribution between the minimum and maximum values of 0 and 3.0 ppm, respectively, and to find k_{eff} at the maximum of 3.0 ppm.

When this value is used to adjust the boron concentration in all components of the fuel element except the kernels, for which a value of 4 ppm was used as reported in Reference 1, the change in k_{eff} from the baseline value is -7.43×10^{-3}. The uncertainty for a uniform distribution is $-7.43 \times 10^{-3}/\sqrt{3}$, or

$u_{fuel\ boron} = -4.29 \times 10^{-3}$.

2.1.28 Density of Graphite Matrix in Reflector

The nominal graphite density in the reflector material is 1.76 g/cm^3; no information is given on tolerances, observed ranges, or standard deviations. It is assumed that the total tolerance range is the same as for the graphite matrix in the fuel pebbles, i.e., 0.04 g/cm^3, but that the nominal value is centered in the range. So the assumed tolerance range becomes 1.76±0.02 g/cm^3. Furthermore, it is assumed that the deviation from the nominal value is distributed uniformly within this range. The boron content is assumed to vary in proportion to the carbon density.

With these assumptions, when k_{eff} is evaluated at a density of 1.78 g/cm^3, the change in k_{eff} becomes 1.09×10^{-3}, and the uncertainty is found to be $1.09 \times 10^{-3}\sqrt{3}$, or

$u_{reflector\ graphite} = 6.3\text{x}10^{-4}$.

2.1.29 Density of Boron in Reflector Natural Graphite

Here, the boron is assumed to vary independently from the carbon density. The nominal boron concentration is 4.8366 ppm by weight; no information is given on tolerances, observed ranges, or standard deviations. This value applies to the natural graphite in the reflector, and not to boronated carbon bricks or other structures in which the boron concentration is elevated above the natural level.

The change in k_{eff} was calculated for a 10% deviation in boron density from the nominal value. The result was $-5.00\text{x}10^{-3}$. This is a very large effect, showing that k_{eff} is quite sensitive to the boron concentration, as one would expect. Accordingly, it is unlikely that a tolerance of ±10% would be considered acceptable. It is likely to be still conservative to assume a tolerance range of ±5%, which would approximately halve the change in k_{eff}. If the distribution function is uniform, the uncertainty is $-5.00\text{x}10^{-3}/2\sqrt{3}$, or

$u_{reflector\ boron} = -1.44\text{x}10^{-3}$.

2.1.30 Ratio of Oxygen to Uranium in Kernel

The nominal value is the stoichiometric ratio of 2.0; the tolerance limit is 2.01. It is assumed that the distribution is uniform from the nominal value to the limit. The multiplication factor is found to change by $1\text{x}10^{-5}$, so that the uncertainty is $1\text{x}10^{-5}/\sqrt{3}$, or, to the nearest significant figure,

$u_{O/U} = 1\text{x}10^{-5}$.

2.1.31 Density of Kernel

The nominal kernel density is 10.4 g/cm^3, which is also the lower tolerance limit. The observed value is given in Reference 2 as 10.83 g/cm^3. The observed value is considerably higher than the nominal value, so new cross sections were computed for this uncertainty calculation. Then k_{eff} was found for a kernel density of 10.83 g/cm^3. The change in k_{eff} was found to be $5.48\text{x}10^{-3}$.

This is a very large change in k_{eff}, but the difference in kernel density from the nominal value is also quite large, namely 4.13%. There is a tolerance range on fuel loading per pebble, as discussed in subsection 2.1.24 above, of 4.9-5.1 g, or ±2%. Therefore, if all kernel densities were equal to the value reported in Reference 2, and if the number of kernels were unchanged, the pebble would exceed its tolerance on fuel loading. The fuel loading tolerance limit is

bounding on the average kernel density, and the effects of variations in kernel density within the fuel loading tolerance limit are included in the uncertainty reported in subsection 2.1.23.

2.1.32 Density of Buffer Layer

The nominal value of the density of the buffer layer is 1.1 g/cm^3, the tolerance range is 0-1.1 g/cm^3, the observed value given in Reference 2 is 1.02 g/cm^3, and the standard deviation is 0.03 g/cm^3. The boron concentration is assumed to remain at 1.3 ppm. A deviation of 0.1 g/cm^3 was used to calculate $dk_{eff}/d\rho_{buffer}$,but the uncertainty was evaluated at the standard deviation; to the nearest significant figure, this is

$u_{buffer\ density} = -3\text{x}10^{-5}$.

2.1.33 Density of IPyC Layer

The nominal IPyC density is 1.9 g/cm^3, the tolerance range is 1.8-2.0 g/cm^3, and the observed range is 1.8-1.92 g/cm^3. No standard deviation is given. The change in k_{eff} from the nominal value was computed from the tolerance limit of 2.0 g/cm^3, with the boron concentration unchanged at 1.3 ppm. The change in k_{eff} was found to be $6\text{x}10^{-5}$; if the probability distribution is uniform, then to the nearest significant figure,

$u_{IPyC\ density} = 3\text{x}10^{-5}$.

2.1.34 Density of SiC Layer

The nominal SiC density is 3.18 g/cm^3, the tolerance range is ≥3.18 g/cm^3, the observed range is 3.19-3.23 g/cm^3, and no standard deviation is given. For conservatism, the change in k_{eff} was computed for the upper tolerance limit and found to be $-2\text{x}10^{-5}$. If the distribution in the range from 3.18-3.23 g/cm^3 is uniform, then to the nearest significant figure,

$u_{SiC\ density} = 1\text{x}10^{-5}$.

2.1.35 Density of OPyC Layer

The nominal OPyC density is 1.9 g/cm^3, the tolerance range is 1.8-2.0 g/cm^3, and the observed range is 1.85-1.89 g/cm^3. The derivative $dk_{eff}/d\rho_{OPyC}$ was calculated at the tolerance limit of 2.0 g/cm^3, but the distribution was assumed uniform between 1.85g/cm^3 and 1.9 g/cm^3 for simplicity and conservatism; then the change in k_{eff} is $-4.5\text{x}10^{-5}$ and the uncertainty is that value divided by √3; to the nearest significant figure, this is

$u_{OPyC\ density} = 3\text{x}10^{-5}$.

2.1.36 Composition of Coolant

The coolant in actual reactor operation is helium, but in the initial criticality experiment the voids in the reactor were occupied by ambient air, which was specified as "moist" air at a total pressure of 0.1013 MPa and a temperature of 15 °C. The specified pressure of 0.1013 MPa is standard sea level atmospheric pressure, 29.92 in Hg. As mentioned in subsection 1.1.3, the term "moist" is taken to mean saturated. Therefore, the baseline composition is saturated air at 15 °C and 0.1013 MPa.

There are two potential causes of uncertainty in the specification of the coolant. First, the air was probably not fully saturated. Second, the air pressure was probably not standard sea level pressure. The second possibility is treated in the next subsection. A check of weather data in Beijing on the Internet shows a wide variability in the relative humidity, from low humidity (e.g., around 20%) to nearly saturated. The lowest possible value of relative humidity is zero. The change in k_{eff} from saturated air to totally dry air was found to be $-3\text{x}10^{-5}$. Assuming a uniform distribution between the extremes of humidity, one finds, to the nearest significant figure,

$u_{water\ vapor} = 2\text{x}10^{-5}$.

2.1.37 Air Pressure

Standard sea level pressure is 29.92 in. Hg (0.1013 MPa). Sea level pressure typically varies about ±1 in. Hg. While larger variations are not uncommon, they represent more extreme weather than normal. Atmospheric pressure also varies with elevation above sea level; the elevation at Beijing is given on the Internet variously from 35 to 55 m. This is sufficiently close to sea level not to affect the standard atmospheric pressure significantly. A cursory search of the Internet failed to reveal a standard deviation for atmospheric pressure, so 1 in. Hg was taken as a conservative estimate. With the components of dry air made denser by a factor of 30.92/29.92, the change in k_{eff} was found to be $-3.0\text{x}10^{-4}$. This is a small change compared to some of the other uncertainties, and not worth trying to refine further.

$u_{air\ pressure} = -3.0\text{x}10^{-4}$.

2.1.38 Boron in Kernels and Dummy Balls

Reference 1 gives the boron concentration in the kernels as 4 ppm and the boron concentration in the dummy balls as 0.125 ppm. No information is given on tolerances, observed ranges, or standard deviations. No information was given on these boron concentrations in Reference 2.

It is implied that these concentrations are confidently known values. In the specifications for the

international benchmark that was performed before the initial criticality experiment, the boron concentration in the dummy balls was given as 1.3 ppm, but Reference 1 states that the actual value was 0.125 ppm instead of the previously stated value of 1.3 ppm. This implies that the corrected value is known accurately. It seems unlikely that whatever tolerance range applies to this parameter is as large as those that apply to the reflector and fuel ball matrix graphite compositions. It is customary in such circumstances to assume an uncertainty of one-half the last digit, i.e, ±0.5x0.001=±0.0005, or ±0.4%. This is too small to merit analysis.

The argument to support confidence in the value of 4 ppm for the kernel boron concentration is less compelling, but in the absence of specific data on the variability of this parameter, the given value is taken as a measurement with the customary uncertainty of one-half the last digit: ±0.5x1=±0.5. This tolerance was applied to the kernel graphite, with a resulting change in k_{eff} of $-7x10^{-5}$. Assuming a uniform error distribution, one finds

$u_{kernel\ boron} = -4x10^{-5}$.

2.1.39 Packing Fraction

The average packing fraction is assumed to be 0.61, as has been observed experimentally.[5] But other packing fractions are theoretically possible, and a numerical study has shown that shifts in packing fraction, as might happen in an earthquake, can induce substantial changes (of the order of 1%) in k-effective.[1] Evidently an increase in packing fraction causes a reduction in leakage even though the total mass of the core remains constant.

The statistical variation in packing fraction in a bed of spheres is not known. It is unlikely that the packing fraction will exceed 0.64, which corresponds to the maximally random jammed state.[2] This is the condition where the pebbles are as closely packed as possible while remaining randomly arranged. Closer packing requires organized lattice structure.

In this analysis, it is assumed that the packing fraction varies uniformly in the range from 0.60-0.62. This assumption is believed to be conservative. When the inventory of core constituents remains constant, a change in packing fraction entails a change in core height. This change is uncorrelated with the change analyzed in subsection 2.1.1, because there the change in core height was assumed to result from an inaccurate pebble count. The change in k_{eff} from an increase in packing fraction to 0.62 is found to be $3.3x10^{-3}$, when the core height changes as

---

(1) A. M. Ougouag and W. K. Terry, "A Preliminary Study of the Effect of Shifts in Packing Fraction on k-effective in Pebble-Bed Reactors," American Nuclear Society Mathematics & Computation Division Conference, Salt Lake City, Utah, September 9-13, 2001.

(2) S. Torquato, T. M. Truskett, and P. G. Debenedetti, "Is Random Close Packing of Spheres Well Defined?" Phys. Rev. Lett. 84, p. 2064, 6 March 2000.

needed to keep the core material inventories constant. For a uniform distribution, the corresponding uncertainty in k_{eff} is

$u_{packing\ fraction} = 1.90\text{x}10^{-3}$.

2.1.40 Overall Uncertainty in k_{eff}

When Eq. 1 is applied to all the uncertainties calculated in subsections 2.1.1-2.1.39, assuming that all the uncertainties are uncorrelated (a reasonable and pragmatically necessary assumption), the result is

$u_{overall} = 5.41\text{x}10^{-3}$, or about 0.5%.

This number was obtained by making consistently conservative assumptions on the variability of parameters on which k_{eff} may depend. The parameters that could have the largest effect are the various boron densities, the graphite matrix density, the fuel loading, and the pebble diameter. It is unlikely that any of the boron densities, on average, are as far from the nominal value as the tolerance range permits. Therefore, the initial criticality measurement in HTR-10 is judged to be an acceptable benchmark.

Table 7 summarizes the results of the uncertainty calculations.

Table 7. Individual and total uncertainties

Item	**Uncertainty (u_i) (NA means not applicable – see text)**
Core radius	1.9e-4
Core height	3.7e-4
Height of core cavity	2.4e-4
Height of conus	6.1e-4
Dimensions of graphite blocks	NA
Outer diameter of graphite reflector	1.0e-4
Height of graphite reflector	1e-5
Diameter of cold helium flow channels	1e-5
Radial location of cold helium flow channels	-2e-5
Height of cold helium flow channels	0
Diameter of control rod and irradiation channels	3.5e-4
Height of control rod and irradiation channels	0
Radial location of control rod and irradiation channels	6e-5
Diameter of KLAK channels (upper)	0
Dimensions of KLAK channels (middle)	-2.8e-4
Diameter of KLAK channels (lower)	0
Dimensions of hot gas duct	0
Radius of fuel discharge tube	0
Height of fuel discharge tube	0
Diameter of fuel pebble	1.22e-3
Diameter of kernel	NA
Thickness of buffer layer	-2e-5
Thickness of IPyC layer	2e-5
Thickness of SiC layer	-1.3e-4
Thickness of OPyC layer	3e-5
Uranium fuel loading	1.03e-3
Density of graphite matrix in fuel pebble	1.13e-3
Total ash in fuel element	NA
Lithium in fuel element	1e-5
Boron in fuel element	-4.29e-3
Density of graphite matrix in reflector	6.3e-4
Density of boron in reflector graphite	-1.44e-3
Ratio of O to U in kernel	1e-5
Density of kernel	NA
Density of buffer	-3e-5
Density of IPyC layer	3e-5
Density of SiC layer	1e-5
Density of OPyC layer	3e-5
Composition of coolant (saturated vs. dry air)	2e-5
Air pressure	-3e-4
Boron in kernels	-4e-5
Boron in dummy balls	NA
Packing fraction	1.9e-3
Total (root mean square)	5.41e-3

2.2 Evaluation of Buckling and Extrapolation Length Data

No buckling or extrapolation length measurements were made.

2.3 Evaluation of Spectral Characteristics Data

No spectral characteristics were measured.

2.4 Evaluation of Reactivity Effects Data

The control rod worth measurements have not yet been evaluated.

2.5 Evaluation of Reactivity Coefficient Data

No reactivity coefficients were measured.

2.6 Evaluation of Kinetics Measurements Data

No kinetics measurements were made.

2.7 Evaluation of Reaction-Rate Distributions

No reaction-rate measurements were made.

2.8 Evaluation of Power Distribution Data

No power distribution measurements were made.

2.9 Evaluation of Isotopic Measurements

No isotopic measurements were made.

2.10 Evaluation of Other Miscellaneous Types of Measurements

No other measurements were made.

3.0 BENCHMARK SPECIFICATIONS

3.1 Benchmark-Model Specifications for Critical and / or Subcritical Measurements

This section contains benchmark specifications for the critical configuration described in Section 1.1.

3.1.1 Description of the Calculational Model and Methodology

The geometry of the HTR-10 was divided into axisymmetric regions as shown in Figures 5 and 6. The definition of regions in Figure 5 is mostly as specified by the HTR-10 research group in its invitation to participants in its international benchmark project. The graphite and boron densities for the regions in Figure 5 were also supplied by the HTR-10 team in Reference 1; these are given in Table 8. The dimensions of components in the fuel and dummy pebbles are given in Table 9. The HTR-10 research group has access to the detailed design drawings and documents for their reactor; the data in these figures and tables are surely better than anything one could derive from publicly available documents. Thus, these data were used as the basis for the calculational model in this evaluation. For this evaluation, the INL code PEBBED[(1),(2)] was used to calculate k_{eff} for the nominal and perturbed configurations. PEBBED is a reactor physics and fuel management code developed by the Idaho National Laboratory (INL) specifically for PBRs. For compatibility with PEBBED, the numbering of some zones in the reflector, the conus, and the bottom reflector section with hot helium flow borings was changed slightly from the numbering assigned by the HTR-10 modeling group. Figure 5 shows the numbering used in this evaluation report. The only change that affects the fidelity of the model is the approximation of the straight, slanted surface of the conus by a series of stair-steps. This is a necessary approximation for the use of any code in cylindrical geometry; some participants in the pre-experiment benchmark program applied the same approach. The stair-steps are small, so that the effects of the approximation should be negligible; in any case, the approximation introduces a uniform bias in the results and will not corrupt the uncertainty calculation.

The PEBBED input deck for the nominal configuration is presented in Appendix A.

---

1 W. K. Terry, H. D. Gougar, and A. M. Ougouag, "Direct Deterministic Method for Neutronics Analysis and Computation of Asymptotic Burnup Distribution in a Recirculating Pebble-Bed Reactor," Annals of Nuclear Energy 29 (2002), pp. 1345-1364.

(2) H. D. Gougar, W. K. Terry, and A. M. Ougouag, *PEBBED V.4.3 Manual (DRAFT)*, Idaho National Engineering and Environmental Laboratory. This manual has not been published, but it will be provided to officially designated reviewers.

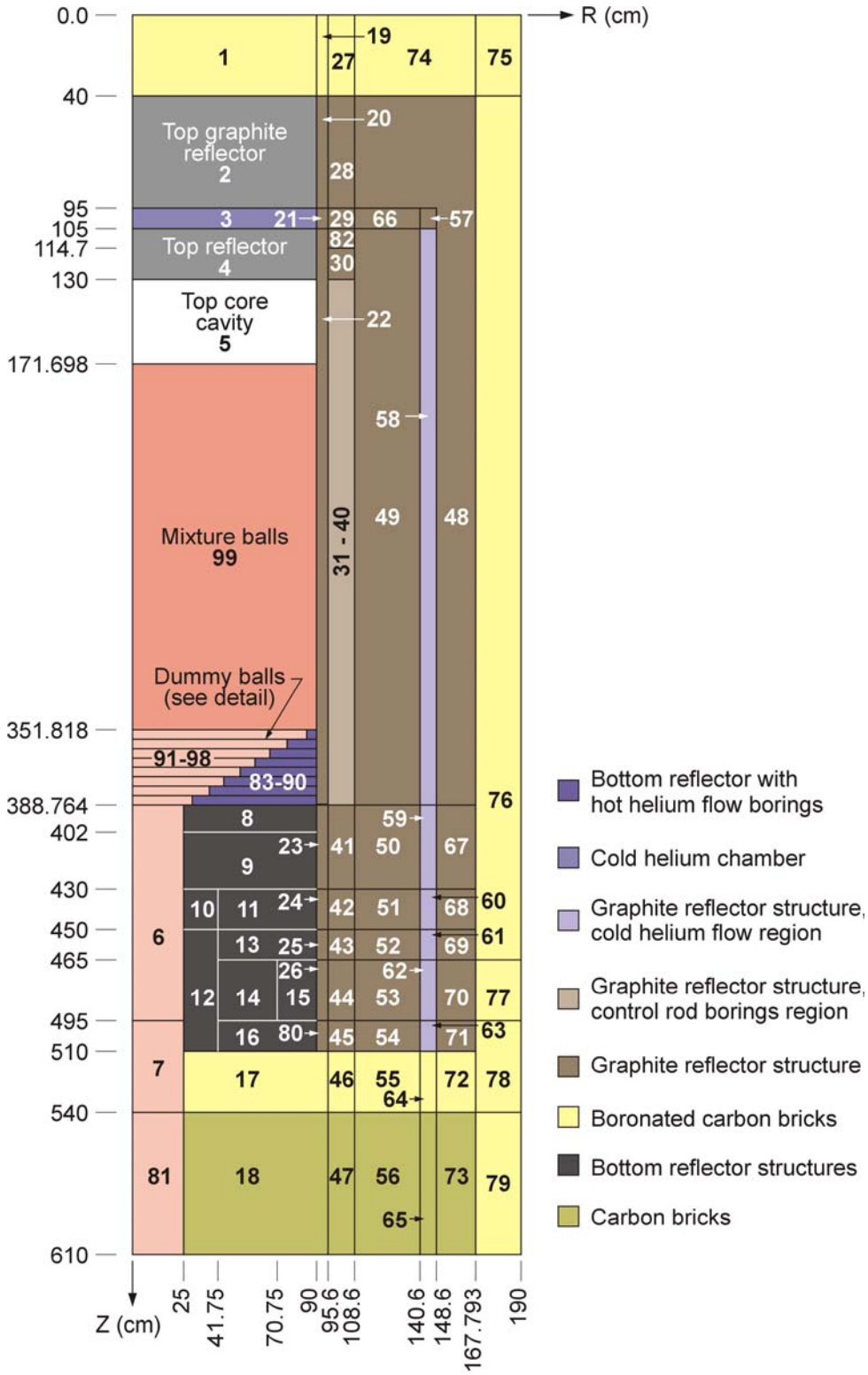

Figure 5(a). Zones of HTR-10 for modeling (dimensions are in cm)

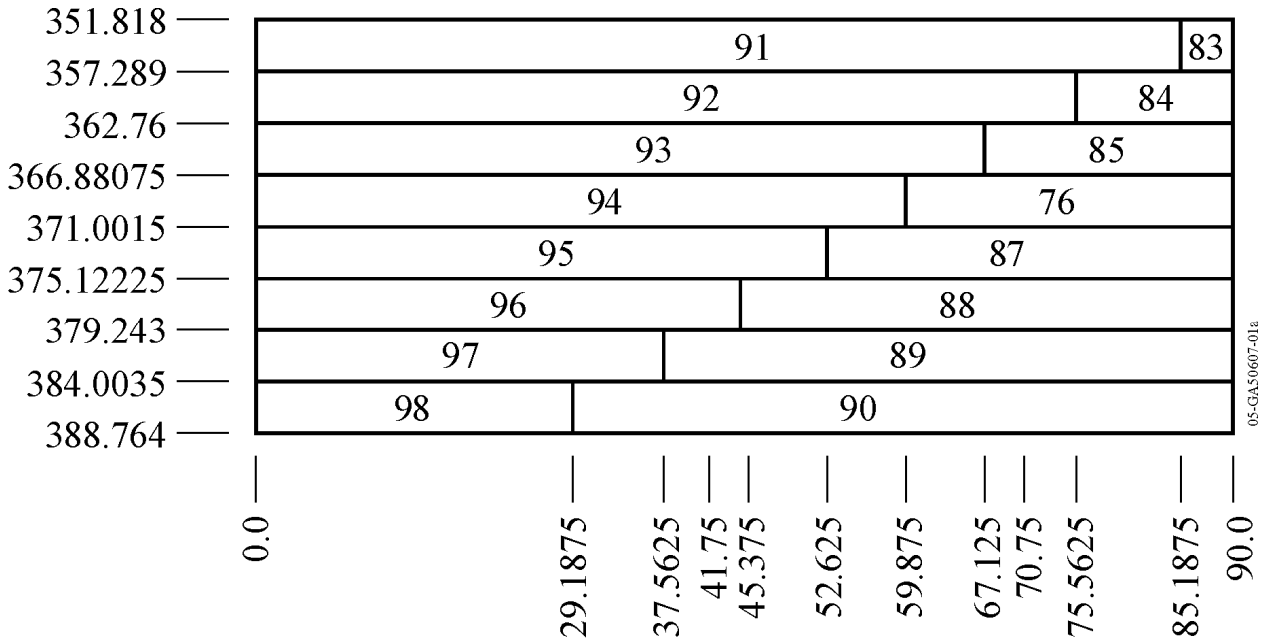

Figure 5(b). Detail in conus region (dimensions are in cm)

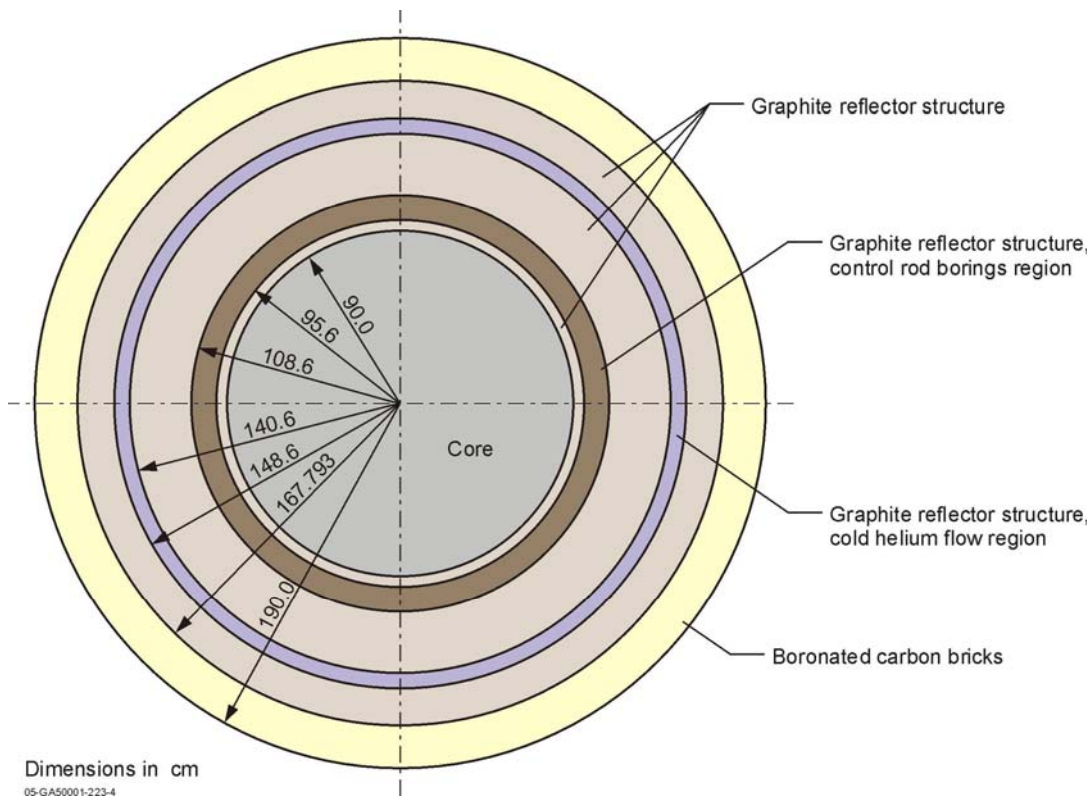

Figure 6. Cross section of reactor in core region

Table 8. Compositions of zones shown in Figure 3 (from Reference 1, with revisions)

No. of zone	Carbon density (a/b-cm)	Natural boron density (a/b-cm)	Remarks
83-90	0.851047E-01	0.456926E-06	Bottom reflector with hot helium flow borings
1	0.729410E-01	0.329811E-02	Boronated carbon bricks
2	0.851462E-01	0.457148E-06	Top graphite reflector
3	0.145350E-01	0.780384E-07	Cold helium chamber
4	0.802916E-01	0.431084E-06	Top reflector
5			Top core cavity
6,7,91-97	0.572501E-01	0.277884E-08	Dummy balls, simplified as graphite of lower density
8	0.781408E-01	0.419537E-06	Bottom reflector structures
9	0.823751E-01	0.442271E-06	Bottom reflector structures
10	0.843647E-01	0.298504E-03	Bottom reflector structures
11	0.817101E-01	0.156416E-03	Bottom reflector structures
12	0.850790E-01	0.209092E-03	Bottom reflector structures
13	0.819167E-01	0.358529E-04	Bottom reflector structures
14	0.541118E-01	0.577456E-04	Bottom reflector structures
15	0.332110E-01	0.178309E-06	Bottom reflector structures
16	0.881811E-01	0.358866E-04	Bottom reflector structures
17,55,72, 74,75,76, 78,79	0.765984E-01	0.346349E-02	Boronated carbon bricks
18,56,73	0.797184E-01	0.000000E+00	Carbon bricks
19	0.761157E-01	0.344166E-02	Boronated carbon bricks
20	0.878374E-01	0.471597E-06	Graphite reflector structure
21	0.579696E-01	0.311238E-06	Graphite reflector structure
22,23,25, 49, 50,52,54, 66, 67,69,71, 80	0.882418E-01	0.473769E-06	Graphite reflector structure
24,51,68	0.879541E-01	0.168369E-03	Graphite reflector structure
26	0.846754E-01	0.454621E-06	Graphite reflector structure
27	0.589319E-01	0.266468E-02	Boronated carbon bricks
28,82	0.678899E-01	1.400000E-05	Graphite reflector structure
29	0.403794E-01	1.400000E-05	Graphite reflector structure
30,41	0.678899E-01	0.364500E-06	Graphite reflector structure
31-40	0.634459E-01	0.340640E-06	Graphite reflector, control rod borings region
42	0.676758E-01	0.125331E-03	Graphite reflector structure
43,45	0.861476E-01	0.462525E-06	Graphite reflector structure
44	0.829066E-01	0.445124E-06	Graphite reflector structure
46	0.747805E-01	0.338129E-02	Boronated carbon bricks
47	0.778265E-01	0.000000E+00	Carbon bricks
48	0.582699E-01	0.312850E-06	Graphite reflector structure
53	0.855860E-01	0.459510E-06	Graphite reflector structure
57	0.728262E-01	0.391003E-06	Graphite reflector structure
58,59,61, 63	0.760368E-01	0.408240E-06	Graphite reflector, cold helium flow region
60	0.757889E-01	0.145082E-03	Graphite reflector, cold helium flow region
62	0.737484E-01	0.395954E-06	Graphite reflector, cold helium flow region
64	0.660039E-01	0.298444E-02	Boronated carbon bricks
65	0.686924E-01	0.000000E+00	Carbon bricks
70	0.861500E-01	0.462538E-06	Graphite reflector structure
77	0.749927E-01	0.339088E-02	Boronated carbon bricks
81	0.847872E-01	0.000000E+00	Dummy balls, but artificially taken as carbon bricks

Table 9. Dimensions of Pebbles and Fuel Particles

Diameter of ball	6.0 cm
Diameter of fuel zone	5.0 cm
Volumetric filling fraction of balls in the core	0.61
Radius of the kernel(mm)	0.25
Coating layer materials (starting from kernel)	Buffer/PyC/SiC/PyC
Coating layer thickness(mm)	0.09/0.04/0.035/0.04
Diameter of dummy (no fuel) elements	6.0 cm

PEBBED is a core design and fuel management tool written to obtain simultaneous solutions of the neutron diffusion equation and the nuclide depletion/production equations in the equilibrium core directly, without following the evolution of the nuclide number densities and the neutron flux in time. PEBBED accounts explicitly for the motion of the fuel and treats arbitrarily specified pebble recirculation patterns. In the HTR-10 startup core, the fuel was not moving; PEBBED also treats this special case.

PEBBED now offers an analytical nodal option for solving the diffusion equation. However, this option had not been fully implemented in *r*-*z* cylindrical geometry when this uncertainty analysis was begun. Therefore, the uncertainty analysis was performed with the older finite-difference option in PEBBED. PEBBED has the capability to perform full r-θ-z analysis with the finite-difference option, but this uncertainty analysis was done in *r*-*z* geometry. PEBBED will soon have full three-dimensional analytical nodal capability in cylindrical geometry.

Most of the regions in Figure 5 were subdivided into several computational mesh cells in the PEBBED model. The computational mesh can be inferred from the input file in Appendix A. The meshing was selected on the basis of prior experience with spatial convergence in verification and validation studies of PEBBED.

Cross sections for PEBBED were computed by the INL's COMBINE code,[1] so named because it combines the PHROG[2] and INCITE[1] fast and thermal spectrum codes. COMBINE uses a

1 Robert A. Grimesey, David W. Nigg, and Richard L. Curtis, *COMBINE/PC – A Portable ENDF/B Version 5 Neutron Spectrum and Cross-Section Generation Program*, EGG-2589, Rev. 1, Idaho National Engineering Laboratory, February 1991.

(2) R.L. Curtis, et al., *PHROG – A FORTRAN-IV Program to Generate Fast Neutron Spectra and Average Multigroup Constants*, Idaho Nuclear Corp., IN-1435, April 1971.

166-group cross section data base derived from the Evaluated Nuclear Data Files (ENDF/B), Version 6[(2)] over the energy range from 0.001 eV to 16.905 MeV. COMBINE solves the B-1 or B-3 approximations to the neutron transport equation, at the user's choice. The P-1 approximation may be chosen as a special case of the B-1 solution. For this evaluation, the B-1 option was chosen.

COMBINE has been improved numerous times since it was first written. The version used for this evaluation is COMBINE-6.02.[(3)] Footnote (5) is an abbreviated report, mostly containing revised material library labels and revised input instructions. Footnote (1) is still the proper source for detailed theoretical elucidation of COMBINE.

In the HTR-10 startup core, 57% of the pebbles are fuel spheres and 43% are dummy balls. The COMBINE model in the core consists of a fuel sphere surrounded by the corresponding quantities of coolant and dummy-pebble graphite in a homogeneous mixture. The fuel sphere consists of a homogenized fuel zone and a pure graphite zone. A separate COMBINE model was developed for the reflector; the COMBINE calculations in the core and the reflector produce cross sections in the two spectral zones defined in the PEBBED model – i.e., the core spectral zone and the reflector spectral zone. In the reflector, the only materials present are carbon, boron, and coolant. The proportions of carbon and boron are similar except in the boronated carbon bricks used in the outer region where the neutron importance is low. Therefore, the atomic number densities used in the COMBINE reflector model were based on only two of the regions shown in Figure 5, regions 22 and 31. The COMBINE input file for the as-run critical configuration is also contained in Appendix A.

For heterogeneous systems such as PBRs, shadowing effects are accounted for in COMBINE by Dancoff factors. The PBR is doubly heterogeneous, so both interpebble and intrapebble Dancoff factors are required. For this evaluation, the Dancoff factors were computed by the new code PEBDAN, developed at the INL specifically for PBRs by Kloosterman and Ougouag.[(4)] The

---

(1) R. L. Curtis and R. A. Grimesey, *INCITE: A FORTRAN-IV Program to Generate Thermal Neutron Spectra and Multigroup Constants Using Arbitrary Scattering Kernels*, Idaho Nuclear Corporation, IN-1062, 1967.

(2) R. Kinsey, *Data Formats and Procedures for the Evaluated Nuclear Data File ENDF*, Brookhaven National Laboratory, BNL-NCS-50496, 1979.

(3) W. Y. Yoon letter to D. W. Nigg, "COMBINE-6 CYCLE 1," WYY-01-94, January 17, 1994.

(4) J. Kloosterman and A. M. Ougouag, "Computation of Dancoff Factors for Fuel Elements Incorporating Randomly Packed TRISO Particles," INEEL/EXT-05-02593, Idaho National Engineering and Environmental Laboratory, January 2005.

input file for PEBDAN is also included in Appendix A.

COMBINE not only predicts k_∞ for the unit cell, it also predicts k_{eff} for specified values of fast and thermal buckling. Since the actual reactor is critical, the appropriate values of buckling are those for which COMBINE gives k_{eff}=1.0. A search was performed to determine these appropriate values; the result was B^2=4.958x10^{-4} for both the fast and thermal cases.

3.1.2 Dimensions

The dimensions of the model regions are shown in Figure 5. The pebble dimensions are given in Table 9. The dimensions of other regions involved in the uncertainty analysis are given in Table 10. Figure 7 shows the dimensions of the KLAK channels in the core region.

Table 10. Dimensions of regions in HTR-10 not defined elsewhere

Region	Diameter (cm)	Coordinate of center (cm)	Channel length range (cm)
Twenty helium flow channels	8.0	144.6 radius	105.0≤z≤610.0
Ten control rod channels & 3 irradiation channels	13.0	102.1 radius	0≤z≤-450.0
Seven KLAK channels, sections with circular cross section	6.0	98.6 radius	0≤z<-130.0 and 388.764<z≤-610.0
Seven KLAK channels, sections with oval cross section	See Figure 6.	98.6 radius (the long axis of the cross section is in the circumferential direction)	130.0≤z≤-388.764
Hot gas duct	30.0	z=480.0	90.0≤r≤190.0
Fuel discharge tube	25.0	r=0	388.764≤z≤610.0

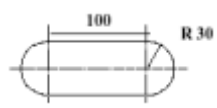

Figure 7. Cross section of KLAK channel in axial zone of the core (dimensions in mm)

3.1.3 Material Data

As shown in Figure 5, the model regions are numbered from 1 to 99. In the model of the initial critical configuration, the control rod regions in Figure 5, labeled 31-40, were consolidated into region 31, leaving a gap from 32-40. (Dividing the control rod region into several model regions allowed partial insertion of control rods, which would be required to evaluate the control rod worth experiment.)

Because the cross sections of the same nuclides will be different in the core and the reflector, which are treated as different spectral zones in the model, nuclides that appear in both zones are treated separately in the two zones, with different material numbers.

The only materials present in the model are graphite (with varying boron concentrations), fuel, and coolant. The reactor vessel and other structural components are omitted. These components are all located in regions of very small neutron importance, so their omission is reasonable. (Perusal of the PEBBED flux output file shows that the thermal neutron flux in the boronated carbon bricks is between four and eleven orders of magnitude lower than that in the core, as depicted in Figure 8; the other neutron energy groups show similar disparities.) The channels for coolant flow, control rods, and KLAK are merely borings in the reflector, so there are no structural materials associated with them.

For the reflector components, the carbon and boron atomic number densities were provided by the HTR-10 group (Reference 1); these densities are presented in Table 8. Only the total boron densities were specified; these were converted to B-10 and B-11 densities by multiplying by the natural abundance (0.199 for B-10 and 0.801 for B-11; cf. the Chart of the Nuclides[(1)]). The atomic number densities of the gaseous constituents were calculated from the stated temperature and total pressure, 15 °C and 0.1013 MPa, and the assumption that the air is saturated. The proportions of the constituents of dry air are listed below by volume[(2)]:

Nitrogen 78.084%
Oxygen 20.9476%
Argon 0.934%.

The remaining constituents of dry air are ignored.

The graphite density in regions 22,23,25,48,49,50,52,54,67,69,71,and 80 is solid density (at 1.76 g/cm^3, the specified density of the reflector graphite); the coolant volumes are determined in the other regions as the fractions of the solid density that the graphite in them occupies.

The carbon and boron atomic number densities are also tabulated in Reference 1 for the dummy balls, but the tabulated densities had to be corrected for the as-built composition (1.84 g/cm^3 instead of 1.73 g/cm^3 for carbon and 0.125 ppm instead of 1.3 ppm for boron).

The number densities in the core were calculated from the specifications given in Reference 1. First, a typical cell was defined consisting of 57% of a fuel ball, 43% of a dummy ball, and the

---

(1) *Chart of the Nuclides*, Thirteenth Edition, General Electric Company, 1984.

(2) http://www.physlink.com/Reference/AirComposition.cfm, citing the CRC Handbook of Chemistry and Physics, David R. Lide, Editor-in-Chief, 1997 Edition.

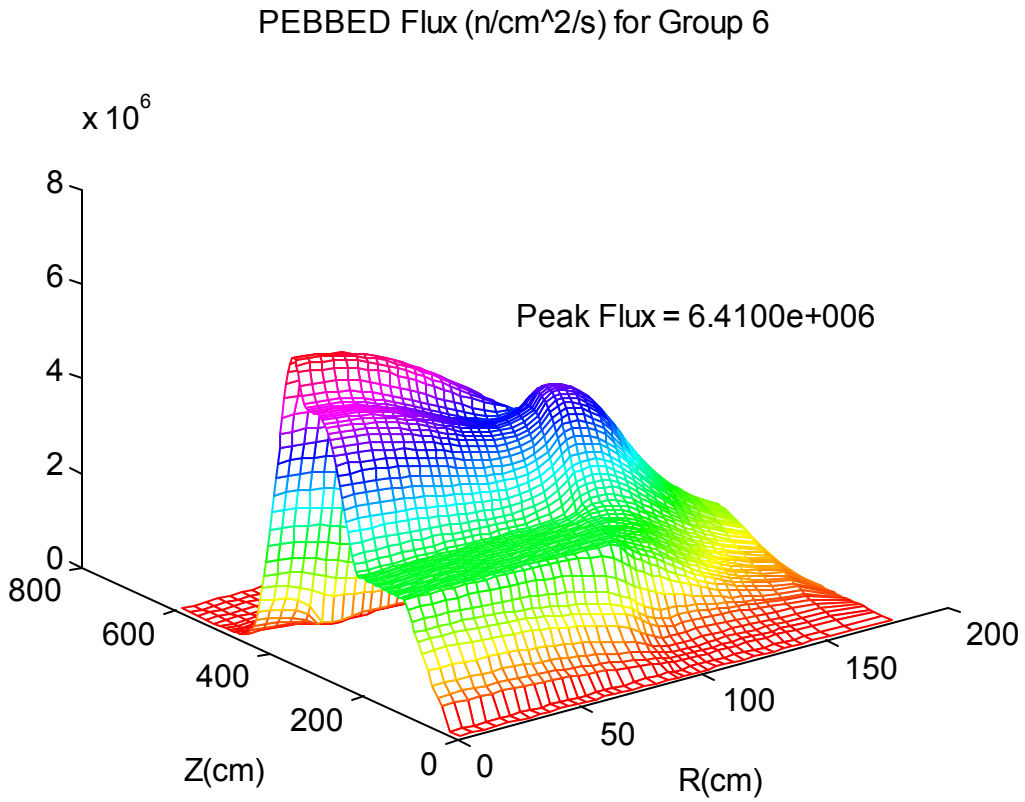

Figure 8. Thermal neutron flux in HTR-10 nominal case (the origin is at the top center of the model)

coolant volume associated with one ball, based on a packing fraction of 61% as stated in Reference 1. The volume of the cell was found to be 185.405 cm^3. Table 11 specifies the dimensions and compositions of all the components in the core region. From these data, one can calculate the average number densities of all the nuclides in the core. Because this calculation is tedious, it is sketched in Appendix B. Table 12 specifies the nominal compositions of the reflector graphite and boronated carbon bricks.

The zone-averaged atomic number densities of all nuclides in all zones in the model are given in the base-case PEBBED input in Appendix A. Tables 13-16 also give the calculated atomic number densities. Table 13 presents the homogenized number densities used in the model. Table 14 gives the number densities in the core components. The values in Table 14 are given for the reader's convenience; they were not used in this uncertainty analysis. Table 15 gives the number densities of the raw materials in the reflector – the solid reflector graphite and boronated carbon materials. Table 16 gives the number densities in air at the experiment conditions.

Table 11. Nominal material properties of fuel and dummy pebbles as built (from Reference 1)

Density of graphite in matrix and outer shell	1.73 g/cm^3
Heavy metal (uranium) loading (weight) per ball	5.0 g
Enrichment of U_{235} (weight)	17 %
Equivalent natural boron content of impurities in uranium	4 ppm
Equivalent natural boron content of impurities in graphite	1.3 ppm
Volumetric filling fraction of balls in the core	0.61
UO2 density(g/cm^3)	10.4
Coating layer materials (starting from kernel)	Buffer/PyC/SiC/PyC
Coating layer density(g/cm^3)	1.1/1.9/3.18/1.9
Density of graphite in dummy balls	1.84 g/cm^3
Equivalent natural boron content of impurities in graphite in dummy balls	0.125 ppm

Table 12. Nominal material properties of reflector materials (from Reference 1)

Density of reflector graphite	1.76 g/cm^3
Equivalent natural boron impurity in reflector graphite	4.8366 ppm
Density of boronated carbon bricks including B_4C	1.59g/cm^3
Weight ratio of B_4C in boronated carbon bricks	5%

Table 13. Homogenized atomic number densities in the model

Nuclide	Atomic number density (a/b-cm)
U-235, averaged over core	6.69520E-6
U-238, averaged over core	3.22755E-5
O-16 in kernels, averaged over core	7.79414E-5
Natural Si, averaged over core	8.51054E-5
Graphite averaged over core	5.40964E-2
B-10 averaged over core	9.92089E-9
B-11 averaged over core	3.99328E-8
Nitrogen averaged over core	1.55875E-5
O-16 in dry air, averaged over core	4.09021E-6
Argon averaged over core	9.11929E-8
Hydrogen averaged over core	3.34631E-7
O-16 from water vapor, averaged over core	1.67316E-7
Graphite at 1.76 g/cm^3	8.82418E-2
B-10 at 4.8366 ppm total boron concentration	9.42800E-8
B-11 at 4.8366 ppm total boron concentration	3.79489E-7

Table 14. Number densities in core components (not homogenized)

Nuclide	Atomic number density (a/b-cm)
U-235 in kernel	3.99198E-3
U-238 in kernel	1.92441E-2
O-16 in kernel	4.64720E-2
B-10 in kernel	4.06384E-7
B-11 in kernel	1.63575E-6
Carbon in buffer	5.51511E-2
B-10 in buffer	1.58513E-8
B-11 in buffer	6.38035E-8
Carbon in IPyC and OPyC	9.52610E-2
B-10 in IPyC and OPyC	2.73795E-8
B-11 in IPyC and OPyC	1.10206E-7
Carbon in SiC	4.77597E-2
Si (nat) in SiC	4.77597E-2
Carbon in fuel matrix	8.67377E-2
B-10 in fuel matrix	2.49298E-8
B-11 in fuel matrix	1.00345E-7
Carbon in dummy balls	9.22528E-2
B-10 in dummy balls	2.54951E-9
B-11 in dummy balls	1.02621E-8

Table 15. Number densities in solid reflector components

Nuclide	Atomic number density (a/b-cm)
Graphite at 1.76 g/cm^3	8.82418E-2
B-10 at 4.8366 ppm total boron concentration	9.42800E-8
B-11 at 4.8366 ppm total boron concentration	3.79489E-7
Carbon in boronated carbon bricks	7.65984E-2
B-10 in boronated carbon bricks	6.89235E-4
B-11 in boronated carbon bricks	2.77426E-2

Table 16. Number densities in air at experiment conditions

Nuclide	Atomic number density (a/b-cm)
Nitrogen in dry air	3.95901E-5
O-16 in dry air	1.06209E-5
Ar in dry air	2.36778E-7
Hydrogen in vapor at saturation	8.58028E-7
O-16 in vapor at saturation	4.29014E-7

3.1.4 Temperature Data

The temperature of the entire system was a uniform 15 °C.

3.1.5 Experimental and Benchmark-Model k_{eff} and / or Subcritical Parameters

The value of k_{eff} is not explicitly given in Reference 1. Instead, the core height at criticality is given. It is implied that k_{eff} is exactly equal to 1 at the measured critical core height of 123.06 cm. The effects of uncertainty in the core height specification, which is equivalent to an uncertainty in the number of pebbles in the core, are discussed in subsection 2.1.1. The approach to criticality was tracked by neutron counters, and a small Am-Be neutron source was used to provide a neutron flux for the counters to track.

3.2 Benchmark-Model Specifications for Buckling and Extrapolation-Length Measurements

No buckling or extrapolation length measurements were made.

3.3 Benchmark-Model Specifications for Spectral Characteristics Measurements

No spectral characteristics were measured.

3.4 Benchmark-Model Specifications for Reactivity Effects Measurements

The control rod worth measurements are not evaluated in this report.

3.5 Benchmark-Model Specifications for Reactivity Coefficient Measurements

No reactivity coefficient measurements were made.

3.6 Benchmark-Model Specifications for Kinetics Measurements

No kinetics parameters were measured.

3.7 Benchmark-Model Specifications for Reaction-Rate Distribution Measurements

No reaction-rate distribution measurements were made.

3.8 Benchmark-Model Specifications for Power Distribution Measurements

No power distribution measurements were made.

3.9 Benchmark-Model Specifications for Isotopic Measurements

No isotopic measurements were made.

3.10 Benchmark-Model Specifications for Other Miscellaneous Types of Measurements

No other measurements have been reported.

4.0 RESULTS OF SAMPLE CALCULATIONS

This section presents the principal results of the calculations described in Section 2. The expected value of k_{eff} is 1.0, but the calculational model gives a value of 1.03257. The uncertainty is given as a percentage deviation from the model result.

4.1 Results of Calculations of the Critical or Subcritical Configurations

As noted above, the baseline value of keff is 1.03257. The deviation from 1.0 is believed to be due to inaccuracies in the cross sections. Whatever the reason, the bias of 0.03257 is carried through the analysis.

Table 7. Principal results of calculations

Case	k_{eff}	100(C-E)/E	Uncertainty (%)
Expected value	1.00000	0.00000	N/A
Base case	1.03257	3.25700	N/A
Overall uncertainty	1.03798*	3.79800	0.52394

*This is the value of k_{eff} at $+1\sigma$. The value at -1σ, 1.02716, is equally valid.

4.2 Results of Buckling and Extrapolation Length Calculations

No buckling or extrapolation length measurements were made.

4.3 Results of Spectral-Characteristics Calculations

No spectral characteristics were measured.

4.4 Results of Reactivity-Effects Calculations

No reactivity effects were calculated.

4.5 Results of Reactivity Coefficient Calculations

No reactivity coefficients were measured.

4.6 Results of Kinetics Parameter Calculations

No kinetics parameters were measured.

4.7 Results of Reaction-Rate Distribution Calculations

No reaction-rate distributions were measured.

4.8 Results of Power Distribution Calculations

No power distributions were measured.

4.9 Results of Isotopic Calculations

Isotopic concentrations were not measured.

4.10 Results of Calculations for Other Miscellaneous Types of Measurements

No other measurements were reported.

5.0 REFERENCES

1. "Evaluation of high temperature gas cooled reactor performance: Benchmark analysis related to initial testing of the HTTR and HTR-10," IAEA-TECDOC-1382, International Atomic Energy Agency, Vienna, November 2003.

2. "Fuel performance and fission product behavior in gas cooled reactors," IAEA-TECDOC-978, International Atomic Energy Agency, Vienna, November, 1927, pp. 11-13.

APPENDICES

APPENDIX A: COMPUTER CODES, CROSS SECTIONS, AND TYPICAL INPUT LISTINGS

The codes used in this evaluation are PEBBED4, COMBINE-6, and PEBDAN. Detailed information on these codes is given in this appendix.

A.1.1 Name(s) of code system(s) used

PEBBED4

COMBINE-6 version 2

COMBDAN

A.1.2 Bibliographic references for the codes used.

H. D. Gougar, W. K. Terry, and A. M. Ougouag, *PEBBED V.4.3 Manual (DRAFT)*, Idaho National Engineering and Environmental Laboratory. This manual has not been published, but it will be provided to officially designated reviewers.
Robert A. Grimesey, David W. Nigg, and Richard L. Curtis, *COMBINE/PC – A Portable ENDF/B Version 5 Neutron Spectrum and Cross-Section Generation Program*, EGG-2589, Rev. 1, Idaho National Engineering Laboratory, February 1991.

W. Y. Yoon letter to D. W. Nigg, "COMBINE-6 CYCLE 1," WYY-01-94, January 17, 1994.

.J. Kloosterman and A. M. Ougouag, "Computation of Dancoff Factors for Fuel Elements Incorporating Randomly Packed TRISO Particles," INEEL/EXT-05-02593, Idaho National Engineering and Environmental Laboratory, January 2005.

R. Kinsey, *Data Formats and Procedures for the Evaluated Nuclear Data File ENDF*, Brookhaven National Laboratory, BNL-NCS-50496, 1979.

A.1.3 Origin of cross-section data

COMBINE uses cross sections from ENDF/B-VI.

A.1.4 Calculational methods used

PEBBED solves the neutron diffusion equation in one-, two-, or three-dimensional cylindrical or Cartesian geometry by finite-difference methods or in one- or two-dimensional cylindrical geometry by nodal methods. In PEBBED, the neutron diffusion equation is solved simultaneously with the nuclide depletion/production equations in a flowing core for a user-specified number of nuclides in the steady-state configuration of neutron flux and composition distribution. It does this by an iterative scheme without following the development of the state of the reactor in time. PEBBED also contains thermohydraulics modules for computing temperatures in normal operation and accident scenarios. However, in this evaluation, only the diffusion-theory component was needed since the fuel was all fresh and the core was stationary. Because the two-dimensional nodal option was not yet working when this evaluation was initiated, the finite-difference option was applied.

COMBINE solves the B-1 or B-3 approximation to the neutron transport equation, or the P-1 approximation as a special case of the B-1 approximation. At the user's option, it can perform an ABH thermal calculation and Nordheim, GAM-1, or Bondarenko treatment of the resolved resonance region. It uses the Wigner Rational Approximation in the unresolved resonance region. In this evaluation, the B-1 approximation was used, and the Nordheim treatment of the unresolved resonance region was chosen. The ABH option was not used. The only fissile nuclide present in the fresh HTR-10 core is u-235, so a U-235 fission spectrum was used. Self-shielding factors were not specified.

COMBINE contains an internal module for computing Dancoff factors to account for shadowing effects in doubly heterogeneous systems like PBRs. However, recent advances in treating such double heterogeneities have led to an improved method of calculating the Dancoff factors. This method is implemented in the PEBDAN code. PEBDAN results were provided as input data to the COMBINE input file.

A.1.5 Energy group structure

COMBINE begins with a 166-group energy structure from ENDF/B-6; in this evaluation, the fine group structure was collapsed to six groups in the following energy ranges:

group 1 16.905-0.111 MeV
group 2 0.111 MeV – 7100 eV
group 3 7100 – 29.0 eV
group 4 29.0 – 2.38 eV
group 5 2.38 – 0.532 eV
group 6 0.532 – 0 eV.

The two groups of lowest energy are the thermal groups.

A.1.6 Component calculations

A.1.6.1 COMBINE core spectrum and cross section calculation

Type of calculation: Unit cell
Geometry: spherical
Theory used: transport
Method used: B-1 approximation, Nordheim numerical method, Wigner rational approximation
Calculation characteristics: spectrum calculation in mixture-ball region of core, cross section calculation for each nuclide in the core (with separate nuclide labels assigned to oxygen in fuel, dry air, and water vapor), resonance materials are U-235 and U-238

A.1.6.2 COMBINE reflector cross section calculation

Type of calculation: coarse-group cross section calculation
Geometry: NA
Theory used: transport
Method used: B_1 approximation
Calculation characteristics: given U-235 fission spectrum, thermal and fast buckling values, compute group microscopic cross sections in reflector materials; no resonance materials are present

A.1.6.3 PEBDAN calculation of Dancoff factors

Type of calculation: computation of Dancoff factors
Geometry: spheres in finite media
Theory used: transport
Method used: Monte Carlo ray tracing
Calculation characteristics: given the fuel particle characteristics and packing fraction, find the intrapebble Dancoff factor; given the pebble characteristics and packing distribution, find the interpebble Dancoff factor

A.1.6.4 PEBBED calculation of k_{eff}

Type of calculation: full reactor
Geometry: cylindrical
Theory used: diffusion
Method used: finite-difference
Calculation characteristics: given detailed description of core and reflector regions, compute k-effective; six energy groups, two thermal groups, homogenized core region, reflector regions defined by HTR-10 group, two spectral zones

A.1.7 Other assumptions and characteristics – see detailed description in Section 3.1

A.1.8 Typical Input Listings for each code system type

A.1.8.1 COMBINE Input Listing

The input listing presented below is the COMBINE input for the configuration experimentally measured to be critical. It includes sections for both the core and reflector regions.

```
=  HTR-10 Spectral Zone Computation with 25mm (o.r.) fuel region   17% enrichment by wt WKT 9 Sept 05
=  Two Spectral Zones
=  Spectrum calculation and core zone
=  COMBINE V5.23 Conversion (DWN) back to v6.02 (wkt)
=  As run with moist air coolant, 15 deg C, p tot = 0.1013 MPa
1010101   0 0 1  1 12 6 1 -1 1 0 0 0 0 54 3 100
1010102   0 0 0 0
1010201   166 144 133 111 101 54
1020101   1 1 0 0 0 0 0 0 0 0 0 0
1030101   4 0 0 0 0 0 0
1030201   2 1         *U-235
1030202   2 2         *U-238
1030203   2 3         *O-16 in UO2 at 296 K
1030204   2 4         *Silicon
1030205   2 5         *Graphite in core at 296 K
1030206   2 6         *Core Boron-10
1030207   2 7         *Core Boron-11
1030208   2 8         *Core Nitrogen
1030209   2 9         *Oxygen in dry air in core
1030210   2 10        *Argon in core
1030211   2 11        *H in H2O vapor in core at 296 K
1030212   2 12        *Oxygen in water vapor in core
1041001   4.958E-4 4.958E-4  288.15         *SPECT AT 15 deg C
1042001   9228.0 92.23501  6.69520E-06 0.0 3.3333E-02 0.2318 *U-235
1042002   9237.0 92.23801  3.22755E-05 0.0 3.3333E-02 0.2318 *U-238
1042003   825.0  8.01601   7.79414E-05 0.0 3.3333E-02 0.2318 *O-16 in UO2 at 296 K
1042004   1400.0 14.00001  8.51054E-05 0.0 3.3333E-02 0.2318 *Silicon
1042005   600.0  6.01201   5.40718E-02 0.0 3.3333E-02 0.2318 *Graphite in core at 296 K
1042006   525.0  5.01001   9.92089E-09 0.0 3.3333E-02 0.2318 *Boron-10 in core
1042007   528.0  5.01101   3.99328E-08 0.0 3.3333E-02 0.2318 *Boron-11 in core
1042008   725.0  7.01401   1.51624E-05 0.0 3.3333E-02 0.2318 *Nitrogen in core
1042009   825.0  8.01601   4.06762E-06 0.0 3.3333E-02 0.2318 *O-16 in dry air in core at 296 K
1042010   1837.0 18.04001  9.06821E-08 0.0 3.3333E-02 0.2318 *Argon in core
1042011   125.0  1.01801   3.34631E-07 0.0 3.3333E-02 0.2318 *H in H2O vapor in core at 296 K
1042012   825.0  8.01601   1.67316E-07 0.0 3.3333E-02 0.2318 *O-16 in H2O vapor in core at 296 K
1043011   293.0  3.0 3.29243E-05 2.50  0.2634 -1.0  8.54441E-02  *U-235
1043012   4.22952E-04 3.87344E-04  600.0 1400.0  825.0 0.0 0.0
1043021   293.0  3.0 1.60748E-04 2.50  0.2634 -1.0  8.54441E-02  *U-238
```

```
1043022   4.22952E-04 3.87344E-04  600.0 1400.0  825.0 0.0 0.0
.
=HTR-10 6-Group Cross Sections 17% enriched, thermal<0.876eV, fast>0.10eV
=Reflector Spectral Zone
=Updated with moist air coolant
=1010101   0 0 1 1 8 6 1 1 1 0 0 0 0 54 1 100
1010101   0 0 1 1 9 6 1 -1 1 0 0 0 0 54 1 100
1010201   166 144 133 111 101 54
1030101   4 0 0 0 0 0 0
1030201   2 13     *Reflector Graphite at 296 K
1030202   2 14     *Reflector Boron-10
1030203   2 15     *Reflector Boron-11
1030204   2 16     *Nitrogen in reflector
1030205   2 17     *O-16 in dry air in reflector at 296 K
1030206   2 18     *Argon in reflector
1030207   2 19     *H in H2O vapor in reflector at 296 K
1030208   2 20     *O-16 in H2O vapor in reflector at 296 k
1030209   0 21     *U-235 for spectrum
1041001   4.965E-4 4.965E-4  288.15          *SPECT AT 15 deg C
1042001   600.0  6.01201   7.04227E-02 0.0 *Reflector Graphite at 296 K
1042002   525.0  5.01001   7.52415E-08 0.0 *Reflector Boron-10
1042003   528.0  5.01101   3.02857E-07 0.0 *Reflector Boron-11
1042004   725.0  7.01401   7.86E-06    0.0 *Nitrogen in reflector
1042005   825.0  8.01601   2.10E-06    0.0 *O-16 in dry air in reflector at 296 K
1042006   1837.0 18.04001  4.70E-08    0.0 *Argon in reflector
1042007   125.0  1.01801   1.73E-07    0.0 *H in H2O vapor in reflector at 296 K
1042008   825.0  8.01601   8.64E-08    0.0 *O-16 in H2O vapor in reflector at 296 K
1042009   9228.0 92.23501  1.0E-15     0.0 *U-235 to generate spectrum
.
```

A.1.8.2 PEBDAN Input Listing

The input listing presented below is the PEBDAN input.

```
MODULE Constants
  IMPLICIT NONE
  !==============================
  ! Input on fuel and core design
  !==============================
  ! HTR-10
  INTEGER, PARAMETER::npart   = 8335      ! number of particles per standard pebble
  REAL, PARAMETER::radgrn1    = 0.025     ! fuel kernel radis (cm)
  REAL, PARAMETER::radpeb1    = 2.5       ! inner zone radius (cm)
  REAL, PARAMETER::radpeb2    = 3.0       ! outer pebble radius (cm)
  REAL, PARAMETER::radref     = 0.0       ! radius of cylindrical inner reflector (cm)
  REAL, PARAMETER::radcore    = 90.0                  ! radius of the core (cm)
  REAL, PARAMETER::hgtcore    = 180.118               ! height of the core (cm)
  !=========================================
  ! Input for generation pebble coordinates
  !=========================================
  REAL, PARAMETER::randpf     = 0.61      ! theoretical packing fraction of a randomly packed bed
  INTEGER, PARAMETER::nranpeb = 200000                ! number of random points per pebble generated
```

```
!=========================================
! Input for calculation of Dancoff Factors
!=========================================
REAL, PARAMETER::sigmod     = 0.4097    ! macroscopic cross section moderator (1/cm)
REAL, PARAMETER::fuelfrac   = 0.57      ! fraction of fuel pebbles, remainder are graphite pebbles
REAL, PARAMETER::threshold  = 0.001     ! threshold for russian roulette in Dancoff calculation
INTEGER, PARAMETER::nrad    = 10        ! number of equi-volume core shells in Dancoff calculation
INTEGER, PARAMETER::nhgt    = 10        ! number of equi-volume core layers in Dancoff calculation
INTEGER, PARAMETER::nbat    = 10        ! number of batches during ray tracing in Dancoff calculation
INTEGER, PARAMETER::nray    = 100       ! number of rays per batch during ray tracing
INTEGER, PARAMETER::nipf    = 200       ! number of intervals in the packing fraction calculation

!=========================================
! Some remaining general input parameters
!=========================================
INTEGER, PARAMETER::lunout  = 6         ! unit for formatted output
INTEGER, PARAMETER::lunpeb  = 10        ! unit for input/output of pebble coordinates
INTEGER, PARAMETER::lunpak  = 11        ! unit for output packing fraction
INTEGER, PARAMETER::lundan  = 12        ! unit for output Dancoff factors
INTEGER, PARAMETER::lunplt  = 13        ! unit for plot output

!==============================================
! Parameters derived from the input parameters
!==============================================
REAL, PARAMETER::diampeb1   = 2*radpeb1
REAL, PARAMETER::diampeb2   = 2*radpeb2
REAL, PARAMETER::diampeb12  = diampeb1**2
REAL, PARAMETER::diampeb22  = diampeb2**2
REAL, PARAMETER::diamcore   = 2*radcore
REAL, PARAMETER::radgrn12   = radgrn1**2
REAL, PARAMETER::radpeb12   = radpeb1**2
REAL, PARAMETER::radpeb13   = radpeb1**3
REAL, PARAMETER::radpeb22   = radpeb2**2
REAL, PARAMETER::radpeb23   = radpeb2**3
REAL, PARAMETER::radcore2   = radcore**2
REAL, PARAMETER::radref2    = radref**2
REAL, PARAMETER::radinn     = radref+radpeb2
REAL, PARAMETER::radinn2    = radinn**2
REAL, PARAMETER::radout     = radcore-radpeb2
REAL, PARAMETER::radout2    = radout**2
REAL, PARAMETER::sigfuel    = 0.75*npart*radgrn12/radpeb13
REAL, PARAMETER::pi         = 3.14159265359
REAL, PARAMETER::halfpi     = 0.5*pi
REAL, PARAMETER::twopi      = 2*pi
REAL, PARAMETER::fourpi     = 4*pi
REAL, PARAMETER::big        = 1.0E30
REAL, PARAMETER::eps        = 1.0E-30
REAL, PARAMETER::twoeps     = 2*eps
REAL, PARAMETER::small      = 2.0E-2            ! criterion for squared overlap of pebbles
! npeb is the number of pebbles that fit theoretically in the core volume
! npeb can be less than the number of pebbles in the file,
!     then more pebble coordinates need to be generated (a kind of restart)
! npeb can be larger then the number of pebbles in the file,
```

```
 !     then only a part of the file need to be read
 ! The actual number of pebbles read always becomes "np"
 INTEGER, PARAMETER::npeb    = INT(randpf*(radcore2-radref2)*hgtcore/radpeb23)
END MODULE Constants
```

A.1.8.3 PEBBED Input Listing

The following listing is the PEBBED input for the configuration that was measured as critical by the HTR-10 group.

```
00001  HTR-10 R-Z 6-Group Critical As Run - Final corrected compositions, 17 wt %
=     ptyp ndim geo sdim NR NQ NZ
00002  1  2  1  2  40  1  99
=      R   Q   Z
00003  1 0 1 1 0 0
00004  5 2 100 1000 20 12 10
00005  1.E-4 1.0-8 1.0E-4 1.0E-4 0.2 0.1 1.0E-4
00006  1 0 0
=      ngr  ntg  infuel  inpres
00007  6     2     2      0
00008  0.95051 0.047997 1.4854E-03 5.0481E-06 0.0 0.0
00009  1.6905E7 1.1109E5 7102. 29.0232 2.38237 0.532
=
00010  21 99 3 0
00011  1.6 1.0
00015  4 0 0 0 0 0
=
00040  0
00060  0.000001  0.0
=      No pebble flow
00070  0.0  0.0
=
=            Radial mesh
00101  5 5 5.0 4 4.1875 8 3.625 4 4.8125 2 2.8
00102  5 4 3.25 8 4.0 2 4.0 2 9.5965 1 22.207
=
=      Azimuthal mesh
00201  1 1 360.
=
=      Axial mesh
00301  4 2 20.0 5 11.0 1 10.0 2 4.85
00302  4 2 7.65 18 5.48656 30 4.102 4 2.7355
00303  4 4 4.12075 2 4.7605 4 3.309 7 4.0
00304  4 4 5.0 2 7.5 4 7.5 2 7.5
00305  2 2 15.0 4 17.5
=
00500  1  1  21  61
00501  22
=
= Pebble Specifications
00700  2 1
00701  100.0 100.0
00702  FUEL  DUMMY
```

```
00703  90.8  0.0
00704  1 2
00705  0 0
=
= alphapo: each row must add to 1
00708  1.0 0.0
=
00710  0.0 0.0
00712  8335.0  0.0
=
= Composition Map
=          R    Q   Z
01201  1  1   1 21  1 1  1  2
01202  1  2   1 21  1 1  3  7
01203  1  3   1 21  1 1  8  8
01204  1  4   1 21  1 1  9 12
01205  1  5   1 21  1 1 13 30
01206  1  6   1  5  1 1 71 91
01207  1  7   1  5  1 1 92 95
01208  1  8   6 21  1 1 71 74
01209  1  9   6 21  1 1 75 81
01210  1 10   6  9  1 1 82 85
01211  1 11  10 21  1 1 82 85
01212  1 12   6  9  1 1 86 93
01213  1 13  10 21  1 1 86 87
01214  1 14  10 17  1 1 88 91
01215  1 15  18 21  1 1 88 91
01216  1 16  10 21  1 1 92 93
01217  1 17   6 23  1 1 94 95
01218  1 18   6 23  1 1 96 99
01219  1 19  22 23  1 1  1  2
01220  1 20  22 23  1 1  3  7
01221  1 21  22 23  1 1  8  8
01222  1 22  22 23  1 1  9 70
01223  1 23  22 23  1 1 71 81
01224  1 24  22 23  1 1 82 85
01225  1 25  22 23  1 1 86 87
01226  1 26  22 23  1 1 88 91
01227  1 27  24 27  1 1  1  2
01228  1 28  24 27  1 1  3  7
01229  1 29  24 27  1 1  8  8
01230  1 30  24 27  1 1 11 12
01231  1 31  24 27  1 1 13 70
01241  1 41  24 27  1 1 71 81
01242  1 42  24 27  1 1 82 85
01243  1 43  24 27  1 1 86 87
01244  1 44  24 27  1 1 88 91
01245  1 45  24 27  1 1 92 93
01246  1 46  24 27  1 1 94 95
01247  1 47  24 27  1 1 96 99
01248  1 48  28 39  1 1  3 70
01249  1 49  28 35  1 1  9 70
01250  1 50  28 35  1 1 71 81
```

```
01251  1 51  28 35  1 1 82 85
01252  1 52  28 35  1 1 86 87
01253  1 53  28 35  1 1 88 91
01254  1 54  28 35  1 1 92 93
01255  1 55  28 35  1 1 94 95
01256  1 56  28 35  1 1 96 99
01257  1 57  36 37  1 1  8  8
01258  1 58  36 37  1 1  9 70
01259  1 59  36 37  1 1 71 81
01260  1 60  36 37  1 1 82 85
01261  1 61  36 37  1 1 86 87
01262  1 62  36 37  1 1 88 91
01263  1 63  36 37  1 1 92 93
01264  1 64  36 37  1 1 94 95
01265  1 65  36 37  1 1 96 99
01266  1 66  28 35  1 1  8  8
01267  1 67  38 39  1 1 71 81
01268  1 68  38 39  1 1 82 85
01269  1 69  38 39  1 1 86 87
01270  1 70  38 39  1 1 88 91
01271  1 71  38 39  1 1 92 93
01272  1 72  38 39  1 1 94 95
01273  1 73  38 39  1 1 96 99
01274  1 74  28 39  1 1  1  2
01275  1 75  40 40  1 1  1  2
01276  1 76  40 40  1 1  3 87
01277  1 77  40 40  1 1 88 91
01278  1 78  40 40  1 1 92 95
01279  1 79  40 40  1 1 96 99
01280  1 80  22 23  1 1 92 93
01281  1 81   1  5  1 1 96 99
01282  1 82  24 27  1 1  9 10
01283  1 83  21 21  1 1 61 62
01284  1 84  19 21  1 1 63 64
01285  1 85  17 21  1 1 65 65
01286  1 86  15 21  1 1 66 66
01287  1 87  13 21  1 1 67 67
01288  1 88  11 21  1 1 68 68
01289  1 89   9 21  1 1 69 69
01290  1 90   7 21  1 1 70 70
01291  1 91   1 20  1 1 61 62
01292  1 92   1 18  1 1 63 64
01293  1 93   1 16  1 1 65 65
01294  1 94   1 14  1 1 66 66
01295  1 95   1 12  1 1 67 67
01296  1 96   1 10  1 1 68 68
01297  1 97   1  8  1 1 69 69
01298  1 98   1  6  1 1 70 70
01299  1 99   1 21  1 1 31 60
=
= Spectral Zone Assignment
01401  1  2   1 40  1 1  1 99
01402  1  3   1 21  1 1 21 60
```

```
=
= Zone Temperatures (deg. C)
01500  20.0
01501  2  2  20.0  3  20.0
=
= Combine Cross-Sections for HTR-10 6-Group
=
=    Generated on 09/09/2005
=
21100   H in H
21110     1.01 0.0000E+00 0.0000E+00 0.0000E+00 0.0000E+00
21101  2.6165E+00 4.2799E-05 0.0000E+00 0.0000E+00
21102  5.6099E+00 2.7738E-04 0.0000E+00 0.0000E+00
21103  6.7492E+00 3.2373E-03 0.0000E+00 0.0000E+00
21104  6.8306E+00 1.9218E-02 0.0000E+00 0.0000E+00
21105  9.3640E+00 5.1221E-02 0.0000E+00 0.0000E+00
21106  2.9322E+01 2.1686E-01 0.0000E+00 0.0000E+00
21111  3.6327E+00 2.0689E+00 1.4079E-01 5.3227E-04 3.5440E-05 9.0480E-06
21121  0.0000E+00 1.0715E+01 6.0162E+00 2.2662E-02 1.5747E-03 4.4902E-04
21131  0.0000E+00 0.0000E+00 1.6754E+01 3.2268E+00 2.2411E-01 6.4455E-02
21141  0.0000E+00 0.0000E+00 0.0000E+00 1.3179E+01 5.6608E+00 1.6281E+00
21151  0.0000E+00 0.0000E+00 0.0000E+00 0.0000E+00 1.1938E+01 9.4635E+00
21161  0.0000E+00 0.0000E+00 0.0000E+00 0.0000E+00 1.2365E-02 3.9377E+01
=
20600   B-10 i
20610    10.01 0.0000E+00 0.0000E+00 0.0000E+00 0.0000E+00
20601  3.1081E+00 7.3837E-01 0.0000E+00 0.0000E+00
20602  5.9186E+00 3.7928E+00 0.0000E+00 0.0000E+00
20603  3.9147E+01 3.7166E+01 0.0000E+00 0.0000E+00
20604  2.2395E+02 2.2196E+02 0.0000E+00 0.0000E+00
20605  5.9336E+02 5.9136E+02 0.0000E+00 0.0000E+00
20606  2.5054E+03 2.5034E+03 0.0000E+00 0.0000E+00
20611  2.5682E+00 1.3320E-01 5.9149E-07 4.2445E-10 0.0000E+00 0.0000E+00
20621  0.0000E+00 2.1323E+00 1.3877E-01 0.0000E+00 0.0000E+00 0.0000E+00
20631  0.0000E+00 0.0000E+00 2.0567E+00 6.7179E-02 0.0000E+00 0.0000E+00
20641  0.0000E+00 0.0000E+00 0.0000E+00 1.9877E+00 1.5216E-01 0.0000E+00
20651  0.0000E+00 0.0000E+00 0.0000E+00 0.0000E+00 2.1420E+00 0.0000E+00
20661  0.0000E+00 0.0000E+00 0.0000E+00 0.0000E+00 0.0000E+00 2.1435E+00
=
20700   B-11 i
20710    11.01 0.0000E+00 0.0000E+00 0.0000E+00 0.0000E+00
20701  2.6964E+00 2.2159E-05 0.0000E+00 0.0000E+00
20702  4.5932E+00 1.0174E-04 0.0000E+00 0.0000E+00
20703  4.5444E+00 5.2749E-05 0.0000E+00 0.0000E+00
20704  4.5447E+00 3.1871E-04 0.0000E+00 0.0000E+00
20705  4.5452E+00 8.4838E-04 0.0000E+00 0.0000E+00
20706  4.5480E+00 3.5894E-03 0.0000E+00 0.0000E+00
20711  2.8370E+00 1.8161E-01 6.0275E-07 9.5296E-11 0.0000E+00 0.0000E+00
20721  0.0000E+00 4.5839E+00 2.9026E-01 0.0000E+00 0.0000E+00 0.0000E+00
20731  0.0000E+00 0.0000E+00 4.7010E+00 1.3901E-01 0.0000E+00 0.0000E+00
20741  0.0000E+00 0.0000E+00 0.0000E+00 4.5254E+00 3.1456E-01 0.0000E+00
20751  0.0000E+00 0.0000E+00 0.0000E+00 0.0000E+00 4.8400E+00 0.0000E+00
20761  0.0000E+00 0.0000E+00 0.0000E+00 0.0000E+00 0.0000E+00 4.8400E+00
```

```
=
20500   Graphi
20510    12.00 0.0000E+00 0.0000E+00 0.0000E+00 0.0000E+00
20501  2.7220E+00 2.9868E-04 0.0000E+00 0.0000E+00
20502  4.3239E+00 1.9843E-06 0.0000E+00 0.0000E+00
20503  4.4674E+00 3.4623E-05 0.0000E+00 0.0000E+00
20504  4.4738E+00 1.9630E-04 0.0000E+00 0.0000E+00
20505  4.4861E+00 5.2440E-04 0.0000E+00 0.0000E+00
20506  4.8054E+00 2.2057E-03 0.0000E+00 0.0000E+00
20511  2.8240E+00 1.6487E-01 4.1034E-07 4.3954E-10 0.0000E+00 0.0000E+00
20521  0.0000E+00 4.3450E+00 2.5981E-01 0.0000E+00 0.0000E+00 0.0000E+00
20531  0.0000E+00 0.0000E+00 4.6081E+00 1.2538E-01 0.0000E+00 0.0000E+00
20541  0.0000E+00 0.0000E+00 0.0000E+00 4.4552E+00 2.8390E-01 0.0000E+00
20551  0.0000E+00 0.0000E+00 0.0000E+00 0.0000E+00 4.2776E+00 4.6085E-01
20561  0.0000E+00 0.0000E+00 0.0000E+00 0.0000E+00 5.1482E-03 4.8199E+00
=
20800   Nitrog
20810    14.00 0.0000E+00 0.0000E+00 0.0000E+00 0.0000E+00
20801  2.2369E+00 6.2977E-02 0.0000E+00 0.0000E+00
20802  6.0554E+00 1.9237E-03 0.0000E+00 0.0000E+00
20803  9.1713E+00 1.8428E-02 0.0000E+00 0.0000E+00
20804  9.5425E+00 1.1009E-01 0.0000E+00 0.0000E+00
20805  9.7369E+00 2.9322E-01 0.0000E+00 0.0000E+00
20806  1.0863E+01 1.2406E+00 0.0000E+00 0.0000E+00
20811  2.2659E+00 1.3331E-01 6.4639E-08 1.4682E-11 0.0000E+00 0.0000E+00
20821  0.0000E+00 6.0358E+00 4.0103E-01 0.0000E+00 0.0000E+00 0.0000E+00
20831  0.0000E+00 0.0000E+00 9.3932E+00 2.2605E-01 0.0000E+00 0.0000E+00
20841  0.0000E+00 0.0000E+00 0.0000E+00 9.3955E+00 5.1269E-01 0.0000E+00
20851  0.0000E+00 0.0000E+00 0.0000E+00 0.0000E+00 9.9201E+00 0.0000E+00
20861  0.0000E+00 0.0000E+00 0.0000E+00 0.0000E+00 0.0000E+00 1.0109E+01
=
20300   O-16 i
20310    15.99 0.0000E+00 0.0000E+00 0.0000E+00 0.0000E+00
20301  3.1852E+00 3.8153E-03 0.0000E+00 0.0000E+00
20302  3.6967E+00 1.9010E-06 0.0000E+00 0.0000E+00
20303  3.7237E+00 3.2161E-06 0.0000E+00 0.0000E+00
20304  3.7248E+00 1.1422E-05 0.0000E+00 0.0000E+00
20305  2.1938E+00 2.9528E-05 0.0000E+00 0.0000E+00
20306  3.7890E+00 1.2418E-04 0.0000E+00 0.0000E+00
20311  3.4212E+00 1.1220E-01 9.6106E-08 1.3497E-11 0.0000E+00 0.0000E+00
20321  0.0000E+00 3.6391E+00 1.6315E-01 0.0000E+00 0.0000E+00 0.0000E+00
20331  0.0000E+00 0.0000E+00 3.8070E+00 7.8163E-02 0.0000E+00 0.0000E+00
20341  0.0000E+00 0.0000E+00 0.0000E+00 3.7111E+00 1.7717E-01 0.0000E+00
20351  0.0000E+00 0.0000E+00 0.0000E+00 0.0000E+00 1.8844E+00 3.3018E-01
20361  0.0000E+00 0.0000E+00 0.0000E+00 0.0000E+00 4.6017E-03 3.9510E+00
=
20900   O-16 i
20910    15.99 0.0000E+00 0.0000E+00 0.0000E+00 0.0000E+00
20901  3.1881E+00 3.8153E-03 0.0000E+00 0.0000E+00
20902  3.6967E+00 1.9010E-06 0.0000E+00 0.0000E+00
20903  3.7237E+00 3.2161E-06 0.0000E+00 0.0000E+00
20904  3.7248E+00 1.1422E-05 0.0000E+00 0.0000E+00
20905  2.1938E+00 2.9528E-05 0.0000E+00 0.0000E+00
```

```
20906  3.7890E+00 1.2418E-04 0.0000E+00 0.0000E+00
20911  3.4256E+00 1.1220E-01 9.6106E-08 1.3497E-11 0.0000E+00 0.0000E+00
20921  0.0000E+00 3.6391E+00 1.6315E-01 0.0000E+00 0.0000E+00 0.0000E+00
20931  0.0000E+00 0.0000E+00 3.8070E+00 7.8163E-02 0.0000E+00 0.0000E+00
20941  0.0000E+00 0.0000E+00 0.0000E+00 3.7111E+00 1.7717E-01 0.0000E+00
20951  0.0000E+00 0.0000E+00 0.0000E+00 0.0000E+00 1.8844E+00 3.3018E-01
20961  0.0000E+00 0.0000E+00 0.0000E+00 0.0000E+00 4.6017E-03 3.9510E+00
=
21200   O-16 i
21210    15.99 0.0000E+00 0.0000E+00 0.0000E+00 0.0000E+00
21201  3.1881E+00 3.8153E-03 0.0000E+00 0.0000E+00
21202  3.6967E+00 1.9010E-06 0.0000E+00 0.0000E+00
21203  3.7237E+00 3.2161E-06 0.0000E+00 0.0000E+00
21204  3.7248E+00 1.1422E-05 0.0000E+00 0.0000E+00
21205  2.1938E+00 2.9528E-05 0.0000E+00 0.0000E+00
21206  3.7890E+00 1.2418E-04 0.0000E+00 0.0000E+00
21211  3.4256E+00 1.1220E-01 9.6106E-08 1.3497E-11 0.0000E+00 0.0000E+00
21221  0.0000E+00 3.6391E+00 1.6315E-01 0.0000E+00 0.0000E+00 0.0000E+00
21231  0.0000E+00 0.0000E+00 3.8070E+00 7.8163E-02 0.0000E+00 0.0000E+00
21241  0.0000E+00 0.0000E+00 0.0000E+00 3.7111E+00 1.7717E-01 0.0000E+00
21251  0.0000E+00 0.0000E+00 0.0000E+00 0.0000E+00 1.8844E+00 3.3018E-01
21261  0.0000E+00 0.0000E+00 0.0000E+00 0.0000E+00 4.6017E-03 3.9510E+00
=
20400   Si-28
20410    27.98 0.0000E+00 0.0000E+00 0.0000E+00 0.0000E+00
20401  2.8985E+00 4.6662E-03 0.0000E+00 0.0000E+00
20402  1.9813E+00 3.0649E-03 0.0000E+00 0.0000E+00
20403  2.0349E+00 2.1954E-03 0.0000E+00 0.0000E+00
20404  2.0176E+00 9.3001E-03 0.0000E+00 0.0000E+00
20405  2.0179E+00 2.4785E-02 0.0000E+00 0.0000E+00
20406  2.0978E+00 1.0468E-01 0.0000E+00 0.0000E+00
20411  3.6411E+00 1.6969E-02 2.4295E-04 8.7372E-08 0.0000E+00 0.0000E+00
20421  0.0000E+00 2.0192E+00 4.9657E-02 0.0000E+00 0.0000E+00 0.0000E+00
20431  0.0000E+00 0.0000E+00 2.0605E+00 2.4211E-02 0.0000E+00 0.0000E+00
20441  0.0000E+00 0.0000E+00 0.0000E+00 2.0037E+00 5.3928E-02 0.0000E+00
20451  0.0000E+00 0.0000E+00 0.0000E+00 0.0000E+00 2.0420E+00 0.0000E+00
20461  0.0000E+00 0.0000E+00 0.0000E+00 0.0000E+00 0.0000E+00 2.0420E+00
=
21000   Argon
21010    39.95 0.0000E+00 0.0000E+00 0.0000E+00 0.0000E+00
21001  0.0000E+00 0.0000E+00 0.0000E+00 0.0000E+00
21002  0.0000E+00 0.0000E+00 0.0000E+00 0.0000E+00
21003  0.0000E+00 0.0000E+00 0.0000E+00 0.0000E+00
21004  0.0000E+00 0.0000E+00 0.0000E+00 0.0000E+00
21005  1.0181E-01 1.0181E-01 0.0000E+00 0.0000E+00
21006  4.3086E-01 4.3086E-01 0.0000E+00 0.0000E+00
21011  0.0000E+00 0.0000E+00 0.0000E+00 0.0000E+00 0.0000E+00 0.0000E+00
21021  0.0000E+00 0.0000E+00 0.0000E+00 0.0000E+00 0.0000E+00 0.0000E+00
21031  0.0000E+00 0.0000E+00 0.0000E+00 0.0000E+00 0.0000E+00 0.0000E+00
21041  0.0000E+00 0.0000E+00 0.0000E+00 0.0000E+00 0.0000E+00 0.0000E+00
21051  0.0000E+00 0.0000E+00 0.0000E+00 0.0000E+00 0.0000E+00 0.0000E+00
21061  0.0000E+00 0.0000E+00 0.0000E+00 0.0000E+00 0.0000E+00 0.0000E+00
=
```

```
20100   U-235
20110   235.04 3.1000E-17 0.0000E+00 0.0000E+00 1.9290E+02
20101  6.0607E+00 1.3910E+00 3.1496E+00 1.2355E+00
20102  1.3493E+01 2.9359E+00 5.3492E+00 2.2024E+00
20103  3.7485E+01 2.4670E+01 4.0773E+01 1.6753E+01
20104  8.0454E+01 6.8163E+01 9.6498E+01 3.9649E+01
20105  6.8804E+01 5.5305E+01 1.0974E+02 4.5089E+01
20106  4.3674E+02 4.2200E+02 8.7811E+02 3.6080E+02
20111  6.8027E+00 1.5930E-01 1.5906E-03 1.1697E-06 0.0000E+00 0.0000E+00
20121  0.0000E+00 1.1080E+01 3.7459E-02 7.6640E-08 0.0000E+00 0.0000E+00
20131  0.0000E+00 0.0000E+00 1.2855E+01 1.5603E-02 0.0000E+00 0.0000E+00
20141  0.0000E+00 0.0000E+00 0.0000E+00 1.2291E+01 3.5879E-02 0.0000E+00
20151  0.0000E+00 0.0000E+00 0.0000E+00 0.0000E+00 1.3538E+01 0.0000E+00
20161  0.0000E+00 0.0000E+00 0.0000E+00 0.0000E+00 0.0000E+00 1.4784E+01
=
20200   U-238
20210   238.05 4.9000E-17 0.0000E+00 0.0000E+00 1.9390E+02
20201  6.1320E+00 2.3528E-01 3.8763E-01 1.4144E-01
20202  1.3160E+01 4.4233E-01 4.3791E-04 1.7562E-04
20203  3.5334E+01 8.0616E+00 6.8038E-04 2.7301E-04
20204  5.9006E+01 4.2350E+01 1.1417E-04 4.5814E-05
20205  9.6559E+00 5.2035E-01 5.0755E-06 2.0366E-06
20206  1.1115E+01 1.7866E+00 1.9225E-05 7.7145E-06
20211  8.1526E+00 1.1641E-01 2.0523E-04 3.2338E-08 0.0000E+00 0.0000E+00
20221  0.0000E+00 1.3208E+01 3.8851E-02 1.8712E-08 0.0000E+00 0.0000E+00
20231  0.0000E+00 0.0000E+00 2.7338E+01 1.0862E-02 0.0000E+00 0.0000E+00
20241  0.0000E+00 0.0000E+00 0.0000E+00 1.6681E+01 2.1347E-02 0.0000E+00
20251  0.0000E+00 0.0000E+00 0.0000E+00 0.0000E+00 9.1615E+00 0.0000E+00
20261  0.0000E+00 0.0000E+00 0.0000E+00 0.0000E+00 0.0000E+00 9.3552E+00
=
21900   H in H
21910     1.01 0.0000E+00 0.0000E+00 0.0000E+00 0.0000E+00
21901  2.6279E+00 4.2847E-05 0.0000E+00 0.0000E+00
21902  5.6138E+00 2.7828E-04 0.0000E+00 0.0000E+00
21903  6.7504E+00 3.3008E-03 0.0000E+00 0.0000E+00
21904  6.8308E+00 1.9491E-02 0.0000E+00 0.0000E+00
21905  9.3749E+00 5.1339E-02 0.0000E+00 0.0000E+00
21906  3.5919E+01 2.7204E-01 0.0000E+00 0.0000E+00
21911  3.6350E+00 2.0805E+00 1.4158E-01 5.3523E-04 3.5653E-05 9.1040E-06
21921  0.0000E+00 1.0699E+01 6.0448E+00 2.2770E-02 1.5822E-03 4.5117E-04
21931  0.0000E+00 0.0000E+00 1.6641E+01 3.3346E+00 2.3160E-01 6.6608E-02
21941  0.0000E+00 0.0000E+00 0.0000E+00 1.2990E+01 5.8081E+00 1.6705E+00
21951  0.0000E+00 0.0000E+00 0.0000E+00 0.0000E+00 1.1901E+01 9.5076E+00
21961  0.0000E+00 0.0000E+00 0.0000E+00 0.0000E+00 2.6123E-03 4.5132E+01
=
21400   B-10 i
21410    10.01 0.0000E+00 0.0000E+00 0.0000E+00 0.0000E+00
21401  3.1139E+00 7.4047E-01 0.0000E+00 0.0000E+00
21402  5.9263E+00 3.8014E+00 0.0000E+00 0.0000E+00
21403  3.9879E+01 3.7897E+01 0.0000E+00 0.0000E+00
21404  2.2711E+02 2.2512E+02 0.0000E+00 0.0000E+00
21405  5.9472E+02 5.9272E+02 0.0000E+00 0.0000E+00
21406  3.1425E+03 3.1405E+03 0.0000E+00 0.0000E+00
```

```
21411  2.5707E+00 1.3429E-01 5.8876E-07 4.2298E-10 0.0000E+00 0.0000E+00
21421  0.0000E+00 2.1300E+00 1.4011E-01 0.0000E+00 0.0000E+00 0.0000E+00
21431  0.0000E+00 0.0000E+00 2.0528E+00 7.1324E-02 0.0000E+00 0.0000E+00
21441  0.0000E+00 0.0000E+00 0.0000E+00 1.9803E+00 1.5967E-01 0.0000E+00
21451  0.0000E+00 0.0000E+00 0.0000E+00 0.0000E+00 2.1420E+00 0.0000E+00
21461  0.0000E+00 0.0000E+00 0.0000E+00 0.0000E+00 0.0000E+00 2.1447E+00
=
21500   B-11 i
21510    11.01 0.0000E+00 0.0000E+00 0.0000E+00 0.0000E+00
21501  2.7006E+00 2.1983E-05 0.0000E+00 0.0000E+00
21502  4.5939E+00 1.0195E-04 0.0000E+00 0.0000E+00
21503  4.5444E+00 5.3833E-05 0.0000E+00 0.0000E+00
21504  4.5447E+00 3.2315E-04 0.0000E+00 0.0000E+00
21505  4.5452E+00 8.5033E-04 0.0000E+00 0.0000E+00
21506  4.5489E+00 4.5026E-03 0.0000E+00 0.0000E+00
21511  2.8398E+00 1.8311E-01 6.0399E-07 9.5369E-11 0.0000E+00 0.0000E+00
21521  0.0000E+00 4.5820E+00 2.9308E-01 0.0000E+00 0.0000E+00 0.0000E+00
21531  0.0000E+00 0.0000E+00 4.6923E+00 1.4771E-01 0.0000E+00 0.0000E+00
21541  0.0000E+00 0.0000E+00 0.0000E+00 4.5099E+00 3.3012E-01 0.0000E+00
21551  0.0000E+00 0.0000E+00 0.0000E+00 0.0000E+00 4.8400E+00 0.0000E+00
21561  0.0000E+00 0.0000E+00 0.0000E+00 0.0000E+00 0.0000E+00 4.8400E+00
=
21300   Graphi
21310    12.00 0.0000E+00 0.0000E+00 0.0000E+00 0.0000E+00
21301  2.7262E+00 2.9526E-04 0.0000E+00 0.0000E+00
21302  4.3245E+00 1.9895E-06 0.0000E+00 0.0000E+00
21303  4.4676E+00 3.5257E-05 0.0000E+00 0.0000E+00
21304  4.4738E+00 1.9912E-04 0.0000E+00 0.0000E+00
21305  4.4862E+00 5.2560E-04 0.0000E+00 0.0000E+00
21306  4.8971E+00 2.7628E-03 0.0000E+00 0.0000E+00
21311  2.8272E+00 1.6624E-01 4.1165E-07 4.4114E-10 0.0000E+00 0.0000E+00
21321  0.0000E+00 4.3430E+00 2.6235E-01 0.0000E+00 0.0000E+00 0.0000E+00
21331  0.0000E+00 0.0000E+00 4.6003E+00 1.3331E-01 0.0000E+00 0.0000E+00
21341  0.0000E+00 0.0000E+00 0.0000E+00 4.4412E+00 2.9797E-01 0.0000E+00
21351  0.0000E+00 0.0000E+00 0.0000E+00 0.0000E+00 4.2713E+00 4.6719E-01
21361  0.0000E+00 0.0000E+00 0.0000E+00 0.0000E+00 1.0870E-03 4.8227E+00
=
21600   Nitrog
21610    14.00 0.0000E+00 0.0000E+00 0.0000E+00 0.0000E+00
21601  2.2405E+00 6.2591E-02 0.0000E+00 0.0000E+00
21602  6.0629E+00 1.9272E-03 0.0000E+00 0.0000E+00
21603  9.1781E+00 1.8792E-02 0.0000E+00 0.0000E+00
21604  9.5441E+00 1.1165E-01 0.0000E+00 0.0000E+00
21605  9.7376E+00 2.9390E-01 0.0000E+00 0.0000E+00
21606  1.1280E+01 1.5562E+00 0.0000E+00 0.0000E+00
21611  2.2691E+00 1.3443E-01 6.4465E-08 1.4511E-11 0.0000E+00 0.0000E+00
21621  0.0000E+00 6.0396E+00 4.0499E-01 0.0000E+00 0.0000E+00 0.0000E+00
21631  0.0000E+00 0.0000E+00 9.3853E+00 2.4057E-01 0.0000E+00 0.0000E+00
21641  0.0000E+00 0.0000E+00 0.0000E+00 9.3702E+00 5.3816E-01 0.0000E+00
21651  0.0000E+00 0.0000E+00 0.0000E+00 0.0000E+00 9.9201E+00 0.0000E+00
21661  0.0000E+00 0.0000E+00 0.0000E+00 0.0000E+00 0.0000E+00 1.0219E+01
=
21700   O-16 i
```

```
21710    15.99 0.0000E+00 0.0000E+00 0.0000E+00 0.0000E+00
21701  3.1936E+00 3.7994E-03 0.0000E+00 0.0000E+00
21702  3.6968E+00 1.8951E-06 0.0000E+00 0.0000E+00
21703  3.7237E+00 3.2499E-06 0.0000E+00 0.0000E+00
21704  3.7248E+00 1.1499E-05 0.0000E+00 0.0000E+00
21705  2.2125E+00 2.9595E-05 0.0000E+00 0.0000E+00
21706  3.8293E+00 1.5574E-04 0.0000E+00 0.0000E+00
21711  3.4298E+00 1.1314E-01 9.5813E-08 1.3458E-11 0.0000E+00 0.0000E+00
21721  0.0000E+00 3.6379E+00 1.6476E-01 0.0000E+00 0.0000E+00 0.0000E+00
21731  0.0000E+00 0.0000E+00 3.8021E+00 8.3211E-02 0.0000E+00 0.0000E+00
21741  0.0000E+00 0.0000E+00 0.0000E+00 3.7023E+00 1.8598E-01 0.0000E+00
21751  0.0000E+00 0.0000E+00 0.0000E+00 0.0000E+00 1.8966E+00 3.3528E-01
21761  0.0000E+00 0.0000E+00 0.0000E+00 0.0000E+00 9.7212E-04 3.9922E+00
=
22000   O-16 i
22010    15.99 0.0000E+00 0.0000E+00 0.0000E+00 0.0000E+00
22001  3.1936E+00 3.7994E-03 0.0000E+00 0.0000E+00
22002  3.6968E+00 1.8951E-06 0.0000E+00 0.0000E+00
22003  3.7237E+00 3.2499E-06 0.0000E+00 0.0000E+00
22004  3.7248E+00 1.1499E-05 0.0000E+00 0.0000E+00
22005  2.2125E+00 2.9595E-05 0.0000E+00 0.0000E+00
22006  3.8293E+00 1.5574E-04 0.0000E+00 0.0000E+00
22011  3.4298E+00 1.1314E-01 9.5813E-08 1.3458E-11 0.0000E+00 0.0000E+00
22021  0.0000E+00 3.6379E+00 1.6476E-01 0.0000E+00 0.0000E+00 0.0000E+00
22031  0.0000E+00 0.0000E+00 3.8021E+00 8.3211E-02 0.0000E+00 0.0000E+00
22041  0.0000E+00 0.0000E+00 0.0000E+00 3.7023E+00 1.8598E-01 0.0000E+00
22051  0.0000E+00 0.0000E+00 0.0000E+00 0.0000E+00 1.8966E+00 3.3528E-01
22061  0.0000E+00 0.0000E+00 0.0000E+00 0.0000E+00 9.7212E-04 3.9922E+00
=
21800   Argon
21810    39.95 0.0000E+00 0.0000E+00 0.0000E+00 0.0000E+00
21801  0.0000E+00 0.0000E+00 0.0000E+00 0.0000E+00
21802  0.0000E+00 0.0000E+00 0.0000E+00 0.0000E+00
21803  0.0000E+00 0.0000E+00 0.0000E+00 0.0000E+00
21804  0.0000E+00 0.0000E+00 0.0000E+00 0.0000E+00
21805  1.0204E-01 1.0204E-01 0.0000E+00 0.0000E+00
21806  5.4048E-01 5.4048E-01 0.0000E+00 0.0000E+00
21811  0.0000E+00 0.0000E+00 0.0000E+00 0.0000E+00 0.0000E+00 0.0000E+00
21821  0.0000E+00 0.0000E+00 0.0000E+00 0.0000E+00 0.0000E+00 0.0000E+00
21831  0.0000E+00 0.0000E+00 0.0000E+00 0.0000E+00 0.0000E+00 0.0000E+00
21841  0.0000E+00 0.0000E+00 0.0000E+00 0.0000E+00 0.0000E+00 0.0000E+00
21851  0.0000E+00 0.0000E+00 0.0000E+00 0.0000E+00 0.0000E+00 0.0000E+00
21861  0.0000E+00 0.0000E+00 0.0000E+00 0.0000E+00 0.0000E+00 0.0000E+00
=
22100  Void
22110  0.0000E+00 0.0000E+00 0.0000E+00 0.0000E+00 0.0000E+00
22101  7.1579E-03 0.0000E+00 0.0000E+00 0.0000E+00
22102  7.1579E-03 0.0000E+00 0.0000E+00 0.0000E+00
22103  7.1579E-03 0.0000E+00 0.0000E+00 0.0000E+00
22104  7.1579E-03 0.0000E+00 0.0000E+00 0.0000E+00
22105  7.1579E-03 0.0000E+00 0.0000E+00 0.0000E+00
22106  7.1579E-03 0.0000E+00 0.0000E+00 0.0000E+00
22111  0.0000E+00 0.0000E+00 0.0000E+00 0.0000E+00 0.0000E+00 0.0000E+00
```

```
22121  0.0000E+00 0.0000E+00 0.0000E+00 0.0000E+00 0.0000E+00 0.0000E+00
22131  0.0000E+00 0.0000E+00 0.0000E+00 0.0000E+00 0.0000E+00 0.0000E+00
22141  0.0000E+00 0.0000E+00 0.0000E+00 0.0000E+00 0.0000E+00 0.0000E+00
22151  0.0000E+00 0.0000E+00 0.0000E+00 0.0000E+00 0.0000E+00 0.0000E+00
22161  0.0000E+00 0.0000E+00 0.0000E+00 0.0000E+00 0.0000E+00 0.0000E+00
=
=      Compositions
=
30100   Boronated carbon bricks (1)
30101   3
30111   13 14 15
30121   7.29410E-2  6.56324E-4  2.64179E-3
=
30200   Top graphite reflector
30201   8
30211   13 14 15 16 17 18 19 20
30221   8.51462E-2 9.09725E-8 3.66176E-7 1.36389E-6
30222   3.65893E-7 8.15710E-9 3.00997E-8 1.50498E-8
=
30300   Cold helium chamber
30301   8
30311   13 14 15 16 17 18 19 20
30321   1.45350E-2 1.55296E-8 6.25088E-8 3.24753E-5
30322   8.71219E-6 1.94227E-7 7.16697E-7 3.58349E-7
=
30400   Top reflector
30401   8
30411   13 14 15 16 17 18 19 20
30421   8.02916E-2 8.59362E-8 3.45298E-7 3.50289E-6
30422   9.39723E-7 2.09498E-8 7.73051E-8 3.86526E-8
=
30500   Top core cavity
30501   6
30511   16 17 18 19 20 21
30521   3.88795E-5 1.04303E-5 2.32528E-7 8.58030E-7
30522   4.29015E-7 1.0 ! Moist air at 15 C
=
30600   Dummy balls simplified (1)
30601   8
30611   13 14 15 16 17 18 19 20
30621   5.72501E-2 6.14369E-9 2.47292E-8 1.51630E-5
30622   4.06779E-6 9.06859E-8 3.34631E-7 1.67316E-7
=
30700   Dummy balls simplified (2)
30701   8
30711   13 14 15 16 17 18 19 20
30721   5.72501E-2 6.14369E-9 2.47292E-8 1.51630E-5
30722   4.06779E-6 9.06859E-8 3.34631E-7 1.67316E-7
=
30800   Bottom reflector structures (1)
30801   8
30811   13 14 15 16 17 18 19 20
30821   7.81408E-2 8.34879E-8 3.36049E-7 4.45053E-6
```

```
30822   1.19395E-6 2.66175E-8 9.82187E-8 4.91093E-8
=
30900   Bottom reflector structures (2)
30901   8
30911   13 14 15 16 17 18 19 20
30921   8.23751E-2 8.80119E-8 3.54259E-7 2.58488E-6
30922   6.93448E-7 1.54595E-8 5.70456E-8 2.85228E-8
=
31000   Bottom reflector structures (3)
31001   8
31011   13 14 15 16 17 18 19 20
31021   8.43647E-2 5.94023E-5 2.39102E-4 1.57694E-6
31022   4.23047E-7 9.43126E-9 3.48014E-8 1.74007E-8
=
31100   Bottom reflector structures (4)
31101   8
31111   13 14 15 16 17 18 19 20
31121   8.17101E-2 3.11268E-5 1.25289E-4 2.80916E-6
31122   7.53616E-7 1.68008E-8 6.19952E-8 3.09976E-8
=
31200   Bottom reflector structures (5)
31201   8
31211   13 14 15 16 17 18 19 20
31221   8.50790E-2 4.16093E-5 1.67483E-4 1.30161E-6
31222   3.49184E-7 7.78458E-9 2.87252E-8 1.43626E-8
=
31300   Bottom reflector structures (6)
31301   8
31311   13 14 15 16 17 18 19 20
31321   8.19167E-2 7.13473E-6 2.87182E-5 2.77125E-6
31322   7.43445E-7 1.65741E-8 6.11585E-8 3.05793E-8
=
31400   Bottom reflector structures (7)
31401   8
31411   13 14 15 16 17 18 19 20
31421   5.41118E-2 1.14914E-5 4.62542E-5 1.50124E-5
31422   4.02740E-6 8.97853E-8 3.31308E-7 1.65654E-7
=
31500   Bottom reflector structures (8)
31501   8
31511   13 14 15 16 17 18 19 20
31521   3.32110E-2 3.54835E-8 1.42826E-7 2.42467E-5
31522   6.50468E-6 1.45013E-7 5.35099E-7 2.67549E-7
=
31600   Bottom reflector structures (9)
31601   3
31611   13  14  15
31621   8.81811E-2  7.14143E-6  2.87452E-5
=
31700   Boronated carbon bricks (2)
31701   3
31711   13  14  15
31721   7.65984E-2  6.89235E-4  2.77426E-3
```

```
=
31800   Carbon bricks (1)
31801   1
31811   13
31821   7.97184E-2
=
31900   Boronated carbon bricks (3)
31901   3
31911   13  14  15
31921   7.61157E-2  6.84890E-4  2.75677E-3
=
32000   Graphite reflector structure (1)
32001   8
32011   13 14 15 16 17 18 19 20
32021   8.78374E-2 9.38478E-8 3.77749E-7 1.78179E-7
32022   4.78003E-8 1.06564E-9 3.93223E-9 1.96612E-9
=
32100   Graphite reflector structure (2)
32101   8
32111   13 14 15 16 17 18 19 20
32121   5.79696E-2 6.19364E-8 2.49302E-7 1.33380E-5
32122   3.57820E-6 7.97711E-8 2.94359E-7 1.47180E-7
=
32200   Graphite reflector structure (3)
32201   3
32211   13  14  15
32221   8.82418E-2  9.42800E-8  3.79489E-7
=
32300   Graphite reflector structure (4)
32301   3
32311   13  14  15
32321   8.82418E-2  9.42800E-8  3.79489E-7
=
32400   Graphite reflector structure (5)
32401   8
32411   13 14 15 16 17 18 19 20
32421   8.79541E-2 3.35054E-5 1.34864E-4 5.27856E-8
32422   1.41609E-8 3.15697E-10 1.16492E-9 5.82462E-10
=
32500   Graphite reflector structure (6)
32501   3
32511   13  14  15
32521   8.82418E-2  9.42800E-8  3.79489E-7
=
32600   Graphite reflector structure (7)
32601   8
32611   13 14 15 16 17 18 19 20
32621   8.46754E-2 9.04696E-8 3.64151E-7 1.57136E-6
32622   4.21552E-7 9.39792E-9 3.46784E-8 1.73392E-8
=
32700   Boronated carbon bricks (4)
32701   3
32711   13  14  15
```

```
32721   5.89319E-2  5.30271E-4  2.13441E-3
=
32800   Graphite reflector structure (8)
32801   8
32811   13 14 15 16 17 18 19 20
32821   6.78899E-2 2.78600E-6 1.12140E-5 8.96110E-6
32822   2.40400E-6 5.35940E-8 1.97762E-7 9.88811E-8
=
32900   Graphite reflector structure (9)
32901   8
32911   13 14 15 16 17 18 19 20
32921   4.03794E-2 2.78600E-6 1.12140E-5 2.10822E-5
32922   5.65574E-6 1.26087E-7 4.65262E-7 2.32631E-7
=
33000   Graphite reflector structure (10)
33001   8
33011   13 14 15 16 17 18 19 20
33021   6.78899E-2 7.25335E-8 2.91965E-7 8.52248E-6
33022   2.28634E-6 5.09708E-8 1.88082E-7 9.40412E-8
=
33100   Graphite reflector, control rod borings region
33101   8
33111   13 14 15 16 17 18 19 20
33121   6.34459E-2 6.76727E-8 2.72853E-7 1.09251E-5
33122   2.93090E-6 6.53404E-8 2.41106E-7 1.20553E-7
=
34100   Graphite reflector structure (11)
34101   8
34111   13 14 15 16 17 18 19 20
34121   6.78899E-2 7.25335E-8 2.91965E-7 8.52248E-6
34122   2.28634E-6 5.09708E-8 1.88082E-7 9.40412E-8
=
34200   Graphite reflector structure (12)
34201   8
34211   13 14 15 16 17 18 19 20
34221   6.76758E-2 2.49409E-5 1.00390E-4 9.00634E-6
34222   2.41614E-6 5.38646E-8 1.98761E-7 9.93804E-8
=
34300   Graphite reflector structure (13)
34301   8
34311   13 14 15 16 17 18 19 20
34321   8.61476E-2 6.77874E-8 2.72853E-7 9.22759E-7
34322   2.47550E-7 5.51879E-9 2.03643E-8 1.01822E-8
=
34400   Graphite reflector structure (14)
34401   8
34411   13 14 15 16 17 18 19 20
34421   8.29066E-2 8.85797E-8 3.56544E-7 2.35070E-6
34422   6.30625E-7 1.40589E-8 5.18775E-8 2.59388E-8
=
34500   Graphite reflector structure (15)
34501   8
34511   13 14 15 16 17 18 19 20
```

```
34521   8.61476E-2 6.77874E-8 2.72853E-7 9.22759E-7
34522   2.47550E-7 5.51879E-9 2.03643E-8 1.01822E-8
=
34600   Boronated carbon bricks (5)
34601   3
34611   13  14  15
34621   7.47805E-2  6.72877E-4  2.70841E-3
=
34700   Carbon bricks (2)
34701   1
34711   13
34721   7.78265E-2
=
34800   Graphite reflector structure (16)
34801   3
34811   13  14  15
34821   8.82418E-2  9.42800E-8  3.79489E-7
=
34900   Graphite reflector structure (17)
34901   3
34911   13  14  15
34921   8.82418E-2  9.42800E-8  3.79489E-7
=
35000   Graphite reflector structure (18)
35001   3
35011   13  14  15
35021   8.82418E-2  9.42800E-8  3.79489E-7
=
35100   Graphite reflector structure (19)
35101   8
35111   13 14 15 16 17 18 19 20
35121   8.79541E-2 3.35054E-5 1.34864E-4 5.27856E-8
35122   1.41609E-8 3.15697E-10 1.16492E-9 5.82462E-10
=
35200   Graphite reflector structure (20)
35201   3
35211   13  14  15
35221   8.82418E-2  9.42800E-8  3.79489E-7
=
35300   Graphite reflector structure (21)
35301   8
35311   13 14 15 16 17 18 19 20
35321   8.55860E-2 9.14425E-8 3.68068E-7 1.17015E-6
35322   3.13917E-7 6.99836E-9 2.58240E-8 1.29120E-8
=
35400   Graphite reflector structure (22)
35401   3
35411   13  14  15
35421   8.82418E-2  9.42800E-8  3.79489E-7
=
35500   Boronated carbon bricks (6)
35501   3
35511   13  14  15
```

```
35521   7.65984E-2  6.89235E-4  2.77426E-3
=
35600   Carbon bricks (3)
35601   1
35611   13
35621   7.97184E-2
=
35700   Graphite reflector structure (23)
35701   8
35711   13 14 15 16 17 18 19 20
35721   7.28262E-2 7.78096E-8 3.13193E-7 6.79213E-6
35722   1.82213E-6 4.06220E-8 1.49895E-7 7.49476E-8
=
35800   Graphite reflector, cold He flow region (1)
35801   8
35811   13 14 15 16 17 18 19 20
35821   7.60368E-2 8.12398E-8 3.27000E-7 5.37755E-6
35822   1.44264E-6 3.21617E-8 1.18677E-7 5.93385E-8
=
35900   Graphite reflector, cold He flow region (2)
35901   8
35911   13 14 15 16 17 18 19 20
35921   7.60368E-2 8.12398E-8 3.27000E-7 5.37755E-6
35922   1.44264E-6 3.21617E-8 1.18677E-7 5.93385E-8
=
36000   Graphite reflector, cold He flow region (3)
36001   8
36011   13 14 15 16 17 18 19 20
36021   7.57889E-2 2.88713E-5 1.16211E-4 5.42301E-6
36022   1.45484E-6 3.24336E-8 1.19680E-7 5.98401E-8
=
36100   Graphite reflector, cold He flow region (4)
36101   8
36111   13 14 15 16 17 18 19 20
36121   7.60368E-2 8.12398E-8 3.27000E-7 5.37755E-6
36122   1.44264E-6 3.21617E-8 1.18677E-7 5.93385E-8
=
36200   Graphite reflector, cold He flow region (5)
36201   8
36211   13 14 15 16 17 18 19 20
36221   7.37484E-2 7.87948E-8 3.17159E-7 6.38580E-6
36222   1.71313E-6 3.81919E-8 1.40928E-7 7.04641E-8
=
36300   Graphite reflector, cold He flow region (6)
36301   8
36311   13 14 15 16 17 18 19 20
36321   7.60368E-2 8.12398E-8 3.27000E-7 5.37755E-6
36322   1.44264E-6 3.21617E-8 1.18677E-7 5.93385E-8
=
36400   Boronated carbon bricks (7)
36401   3
36411   13  14  15
36421   6.60039E-2  5.93904E-4  2.39054E-3
```

```
=
36500   Carbon bricks (4)
36501   1
36511   13
36521   6.86924E-2
=
36600   Graphite reflector structure (24)
36601   8
36611   13 14 15 16 17 18 19 20
36621   5.82699E-2 6.22572E-8 2.50593E-7 1.32057E-5
36622   3.54270E-6 7.89797E-8 2.91435E-7 1.45718E-7
=
36700   Graphite reflector structure (25)
36701   3
36711   13  14  15
36721   8.82418E-2  9.42800E-8  3.79489E-7
=
36800   Graphite reflector structure (26)
36801   8
36811   13 14 15 16 17 18 19 20
36821   8.79541E-2 3.35054E-5 1.34864E-4 5.27856E-8
36822   1.41609E-8 3.15697E-10 1.16492E-9 5.82462E-10
=
36900   Graphite reflector structure (27)
36901   3
36911   13  14  15
36921   8.82418E-2  9.42800E-8  3.79489E-7
=
37000   Graphite reflector structure (28)
37001   8
37011   13 14 15 16 17 18 19 20
37021   8.61500E-2 9.20451E-8 3.70493E-7 9.21653E-7
37022   2.47253E-7 5.51217E-9 2.03399E-8 1.01700E-8
=
37100   Graphite reflector structure (29)
37101   3
37111   13  14  15
37121   8.82418E-2  9.42800E-8  3.79489E-7
=
37200   Boronated carbon bricks (8)
37201   3
37211   13  14  15
37221   7.65984E-2  6.89235E-4  2.77426E-3
=
37300   Carbon bricks (5)
37301   1
37311   13
37321   7.97184E-2
=
37400   Boronated carbon bricks (9)
37401   3
37411   13  14  15
37421   7.65984E-2  6.89235E-4  2.77426E-3
```

```
=
37500   Boronated carbon bricks (10)
37501   3
37511   13  14  15
37521   7.65984E-2  6.89235E-4  2.77426E-3
=
37600   Boronated carbon bricks (11)
37601   3
37611   13  14  15
37621   7.65984E-2  6.89235E-4  2.77426E-3
=
37700   Boronated carbon bricks (12)
37701   3
37711   13  14  15
37721   7.49927E-2  6.74785E-4  2.71609E-3
=
37800   Boronated carbon bricks (13)
37801   3
37811   13  14  15
37821   7.65984E-2  6.89235E-4  2.77426E-3
=
37900   Boronated carbon bricks (14)
37901   3
37911   13  14  15
37921   7.65984E-2  6.89235E-4  2.77426E-3
=
38000   Graphite reflector structure (30)
38001   3
38011   13  14  15
38021   8.82418E-2  9.42800E-8  3.79489E-7
=
38100   Dummy balls taken as carbon bricks
38101   6
38111   13 16 17 18 19 20
38121   8.47872E-2 3.75543E-6 1.00747E-6 2.24603E-8
38122   8.28784E-8 4.14392E-8
=
38200   Graphite reflector structure (31)
38201   8
38211   13 14 15 16 17 18 19 20
38221   6.78899E-2 2.78600E-6 1.12140E-5 8.96110E-6
38222   2.40400E-6 5.35940E-8 1.97762E-7 9.88811E-8
=
38300   Bottom reflector with hot He flow borings (1)
38301   8
38311   13 14 15 16 17 18 19 20
38321   8.51047E-2 9.09283E-8 3.65998E-7 1.38221E-6
38322   3.70808E-7 8.26665E-9 3.05040E-8 1.52520E-8
=
38400   Bottom reflector with hot He flow borings (2)
38401   8
38411   13 14 15 16 17 18 19 20
38421   8.51047E-2 9.09283E-8 3.65998E-7 1.38221E-6
```

```
38422   3.70808E-7 8.26665E-9 3.05040E-8 1.52520E-8
=
38500   Bottom reflector with hot He flow borings (3)
38501   8
38511   13 14 15 16 17 18 19 20
38521   8.51047E-2 9.09283E-8 3.65998E-7 1.38221E-6
38522   3.70808E-7 8.26665E-9 3.05040E-8 1.52520E-8
=
38600   Bottom reflector with hot He flow borings (4)
38601   8
38611   13 14 15 16 17 18 19 20
38621   8.51047E-2 9.09283E-8 3.65998E-7 1.38221E-6
38622   3.70808E-7 8.26665E-9 3.05040E-8 1.52520E-8
=
38700   Bottom reflector with hot He flow borings (5)
38701   8
38711   13 14 15 16 17 18 19 20
38721   8.51047E-2 9.09283E-8 3.65998E-7 1.38221E-6
38722   3.70808E-7 8.26665E-9 3.05040E-8 1.52520E-8
=
38800   Bottom reflector with hot He flow borings (6)
38801   8
38811   13 14 15 16 17 18 19 20
38821   8.51047E-2 9.09283E-8 3.65998E-7 1.38221E-6
38822   3.70808E-7 8.26665E-9 3.05040E-8 1.52520E-8
=
38900   Bottom reflector with hot He flow borings (7)
38901   8
38911   13 14 15 16 17 18 19 20
38921   8.51047E-2 9.09283E-8 3.65998E-7 1.38221E-6
38922   3.70808E-7 8.26665E-9 3.05040E-8 1.52520E-8
=
39000   Bottom reflector with hot He flow borings (8)
39001   8
39011   13 14 15 16 17 18 19 20
39021   8.51047E-2 9.09283E-8 3.65998E-7 1.38221E-6
39022   3.70808E-7 8.26665E-9 3.05040E-8 1.52520E-8
=
39100   Dummy balls simplified (3)
39101   8
39111   13 14 15 16 17 18 19 20
39121   5.72501E-2 6.14369E-9 2.47292E-8 1.51630E-5
39122   4.06779E-6 9.06859E-8 3.34631E-7 1.67316E-7
=
39200   Dummy balls simplified (4)
39201   8
39211   13 14 15 16 17 18 19 20
39221   5.72501E-2 6.14369E-9 2.47292E-8 1.51630E-5
39222   4.06779E-6 9.06859E-8 3.34631E-7 1.67316E-7
=
39300   Dummy balls simplified (5)
39301   8
39311   13 14 15 16 17 18 19 20
```

```
39321   5.72501E-2 6.14369E-9 2.47292E-8 1.51630E-5
39322   4.06779E-6 9.06859E-8 3.34631E-7 1.67316E-7
=
39400   Dummy balls simplified (6)
39401   8
39411   13 14 15 16 17 18 19 20
39421   5.72501E-2 6.14369E-9 2.47292E-8 1.51630E-5
39422   4.06779E-6 9.06859E-8 3.34631E-7 1.67316E-7
=
39500   Dummy balls simplified (7)
39501   8
39511   13 14 15 16 17 18 19 20
39521   5.72501E-2 6.14369E-9 2.47292E-8 1.51630E-5
39522   4.06779E-6 9.06859E-8 3.34631E-7 1.67316E-7
=
39600   Dummy balls simplified (8)
39601   8
39611   13 14 15 16 17 18 19 20
39621   5.72501E-2 6.14369E-9 2.47292E-8 1.51630E-5
39622   4.06779E-6 9.06859E-8 3.34631E-7 1.67316E-7
=
39700   Dummy balls simplified (9)
39701   8
39711   13 14 15 16 17 18 19 20
39721   5.72501E-2 6.14369E-9 2.47292E-8 1.51630E-5
39722   4.06779E-6 9.06859E-8 3.34631E-7 1.67316E-7
=
39800   Dummy balls simplified (10)
39801   8
39811   13 14 15 16 17 18 19 20
39821   5.72501E-2 6.14369E-9 2.47292E-8 1.51630E-5
39822   4.06779E-6 9.06859E-8 3.34631E-7 1.67316E-7
=
39900   Mixture balls
39901   12
39911   1  2  3  4  5  6  7  8
39912   9 10 11 12
39921   6.69520E-6 3.22755E-5 7.79414E-5 8.51054E-5
39922   5.40964E-2 9.92089E-9 3.99328E-8 1.55875E-5
39923   4.09021E-6 9.11929E-8 3.34631E-7 1.67316E-7
.
```

APPENDIX B
CALCULATION OF BASE-CASE ATOMIC NUMBER DENSITIES IN THE CORE REGION

This appendix presents the calculation of the atomic number densities for Region 99 in the PEBBED model, which is the core region, where the mixture of fuel and dummy balls is located.

First, some data from Table 3 are repeated:

Fuel enrichment = 17% by weight
Core unit cell volume = 185.405 cm^3
Kernel density = 10.4 g/cm^3
Buffer layer density = 1.1 g/cm^3
IPyC density = 1.9 g/cm^3
SiC density = 3.18 g/cm^3
OPyC density = 1.9 g/cm^3
Fuel matrix density = 1.73 g/cm^3
Dummy matrix density = 1.84 g/cm^3
Pebble packing fraction = 61%
Fuel loading per fuel pebble = 5 g U
Number of kernels in a fuel pebble = 8335
Ratio of fuel pebbles to dummy pebbles: 57:43
Boron concentration in kernel (by weight) = 4 ppm
Boron concentration in fuel matrix (by weight) = 1.3 ppm
Boron concentration in dummy-ball matrix (by weight) = 0.125 ppm
Kernel radius = 0.025 cm
Buffer layer thickness = 0.009 cm
IPyC layer thickness = 0.004 cm
SiC layer thickness = 0.0035 cm
OPyC layer thickness = 0.004 cm

The weights of one gram-mole of the nuclides and elements used in the calculations are taken from the Chart of the Nuclides.[B1]

B.1 Nuclides in kernel

The uranium is 17% U-235 by weight. Ignore all isotopes except U-235 and U-238. Let $\tilde{N}_{235}$ and $\tilde{N}_{238}$ be the atom fractions of U-235 and U-238, respectively, A_{235} and A_{238} be the

molecular weights of U-235 and U-238, respectively, and $\bar{A}$ be the average molecular weight of the mixture of the two isotopes. Then

$$0.17\bar{A} = \tilde{N}_{235}A_{235}$$

and $0.83\bar{A} = \tilde{N}_{238}A_{238}$,

so that $\dfrac{0.17\bar{A}}{0.83\bar{A}} = \dfrac{\tilde{N}_{235}A_{235}}{\tilde{N}_{238}A_{238}} = \dfrac{\tilde{N}_{235}x235.043928}{\tilde{N}_{238}x238.050788}$,

or $\dfrac{\tilde{N}_{235}}{\tilde{N}_{238}} = 0.207439$.

But $\tilde{N}_{235} + \tilde{N}_{238} = 1$. This and the previous equation are solved simultaneously to yield

$$\tilde{N}_{235} = 0.171801$$

and $\tilde{N}_{238} = 0.828199$.

The mass of uranium in an average UO_2 molecule is

(0.171801x235.043928 + 0.828199x238.050788)(g/mole)x 1 mole/6.022x10^{23} molecules = 3.94444x10^{-22} g.

The ratio of fuel balls to dummy balls is 57:43. Thus, the computational cell is defined to contain 57% of a fuel ball and 43% of a dummy ball, plus the volume of coolant associated with one ball in the core. The number of U atoms, or UO_2 molecules, in a computational cell is thus

$(N_U)_{cell}$ = 0.57x5 g/3.94444x10^{-22} g/molecule = 7.22536x10^{21} molecules.

Then the atomic number densities are

$(n_{U\text{-}235})_{cell}$ = 0.171801 x 7.22536x10^{21} x 10^{-24}/185.405 a/b-cm = 6.69520x10^{-6}a/b-cm

and, analogously, $(n_{U\text{-}238})_{cell}$ = 3.22755x10^{-5} a/b-cm

and $(\bar{n}_O)_{cell}^{kernels} = 7.79414x10^{-5}$ a/b-cm.

The oxygen in the kernel is given a different material label from the oxygen in the water vapor in the PEBBED and COMBINE inputs because the cross sections are different in different

materials. Similarly, identical nuclides in the core and reflector are given different labels because their cross sections will be different in the two spectral zones.

The boron concentration in the kernel is 4 ppm by weight of uranium. The mass of the average boron atom is (10.811g/mole)/6.022x10^{23} atoms/mole) = 1.79525x10^{-23} g/atom. Then the ratio of the number of boron atoms to the number of UO_2 molecules is

$$\frac{4x10^{-6}\,x\,3.94444x10^{-22}}{1.79525x10^{-23}} = 8.78861x10^{-5}$$

and the number of atoms of boron in the computational cell from kernels is

$$(N_B)_{cell}^{kernels} = 8.78861x10^{-5}(N_U)_{cell} = 6.35009x10^{17}\,\text{atoms}.$$

B.2 Nuclides in fuel particle layers

The number of TRISO particles in the cell is 0.57x8335=4751. The volume of the buffer layer is $4\pi[(0.025 + 0.009)^3 - 0.025^3]/3$ cm^3 = 9.91864x10^{-5} cm^3, so the total volume of buffer zone in the cell is 4751 x 9.91864x10^{-5} cm^3 = 0.471235 cm^3. The density of the buffer zone is 1.1 g/cm^3, and the boron content is 1.3 ppm (by weight).

The masses of the average carbon and boron atoms are 12.011/6.022x10^{23} g = 1.99452x10^{-23} g and 10.811/6.022x10^{23} g = 1.79525x10^{-23} g, respectively; by number, a boron content of 1.3 ppm by mass is

1.3x10^{-6} x 12.011/10.811 = 1.44430x10^{-6}.

Then $(n_C)_{buffer}$ = 1.1 g/cm^3 / (1.99452x10^{-23} + 1.4443x10^{-6} x 1.79525x10^{-23}) g = 5.51510x10^{22} atoms/cm^3

and the total number of C atoms in the cell from buffer zones is

$$(N_C)_{cell}^{buffer} = 5.51510x10^{22}\,\text{atoms}/cm^3\,x\,0.471235\,cm^3 = 2.59891x10^{22}\,\text{atoms}.$$

It is assumed that the graphite in the carbon layers of the TRISO particle have the same boron concentration as the graphite fuel matrix. This assumption can only affect the boron content of the computational cell slightly. The number of boron atoms in the cell from buffer zones is

$$(N_B)_{cell}^{buffer} = 1.4443x10^{-6}\,x\,2.59891x10^{22}\,\text{atoms}=3.75361x10^{16}\text{atoms}\ .$$

In similar fashion, the carbon, silicon, and boron contents of the remaining zones are found. The

silicon carbide layer is assumed to contain no boron.

$$(N_C)_{cell}^{IPyC} = 2.95135x10^{22} \text{ atoms}$$

$$(N_B)_{cell}^{IPyC} = 4.26264x10^{16} \text{ atoms}$$

$$(N_C)_{cell}^{SiC} = 1.57790x10^{22} \text{ atoms}$$

$$(N_{Si})_{cell}^{SiC} = 1.57790x10^{22} \text{ atoms}$$

$$(N_C)_{cell}^{OPyC} = 4.30778x10^{22} \text{ atoms}$$

$$(N_B)_{cell}^{OPyC} = 6.22173x10^{16} \text{ atoms}$$

B.3 Nuclides in fuel matrix and dummy-ball matrix

The total volume of TRISO particles in the cell is 4751x4π(0.0455 cm)^3/3 = 1.87460 cm^3. The volume of one pebble is 4π(3 cm)^3/3 = 113.097 cm^3, of which in the computational cell 57% is fuel pebble and 43% is dummy pebble. Then the volume of fuel matrix in the cell is 0.57x113.097 cm^3 -1.87460 cm^3 = 62.5907 cm^3, and the volume of dummy matrix in the cell is 0.43x113.097 cm^3 = 48.6317 cm^3. From the given densities of the graphite matrix in the fuel and dummy balls, 1.73 g/cm^3 and 1.84 g/cm^3, respectively, and the mass of the average carbon atom, it is found that the atomic number densities of carbon in the fuel and dummy matrix materials are 8.67377x10^{22} atoms/cm^3 and 9.22528x10^{22} atoms/cm^3, respectively. Then the carbon atomic number densities are

$$(N_C)_{cell}^{fuel\,matrix} = 5.42897x10^{24} \text{ atoms}$$

and

$$(N_C)_{cell}^{dummy\,matrix} = 4.48641x10^{24} \text{ atoms}.$$

In the fuel matrix the boron concentration is 1.3 ppm, but in the dummy matrix it is 0.125 ppm by weight, which is equivalent to 0.138875 ppm by number. These proportions give the boron content of the matrix materials:

$$(N_B)_{cell}^{fuel\,matrix} = 7.84269x10^{18} \text{ atoms}$$

and

$(N_B)_{cell}^{dummy\,matrix} = 6.23050x10^{17}$ atoms .

B.4 Total carbon and boron number densities

When all the contributions to the carbon and boron contents of the cell are summed and divided by the cell volume, and the result is converted to a/b-cm, the resulting densities are

$(\overline{n}_C)_{cell} = 5.40964x10^{-2}$ a/b-cm

$(\overline{n}_{B-10})_{cell} = 9.92089x10^{-9}$ a/b-cm

and

$(\overline{n}_{B-11})_{cell} = 3.99328x10^{-8}$ a/b-cm .

B.5 Nuclides in air

The densities of the gaseous constituents are found from the specified conditions and the assumption that the air is saturated with water vapor. At 15 °C (288.15 K), at a relative humidity of 100% the water vapor density is[B2] 1.28343x10^{-5} g/cm^3 and the vapor pressure is 1.70507x10^{-3} MPa. (Reference B2 gives data in British units; 15 °C = 59 °F, at which the saturation pressure is 0.2473 lbf/in^2 (psi) and the saturated vapor specific volume is 1248.1 ft^3/lbm. The conversion factors used to obtain metric units are[B3] 6894.7572 N/m^2-psi and 16.018463 kg-ft^3/lbm-m^3) At this mass density, the number density of water vapor molecules is found to be 4.29014x10^{17} molecules/cm^3, and the average number densities of hydrogen and oxygen from vapor in the cell are

$(\overline{n}_H)_{cell} = 3.34631x10^{-7}$ a/b-cm

and

$(\overline{n}_O)_{cell}^{vapor} = 1.67316x10^{-7}$ a/b-cm .

The pressure of the dry air is then 0.1013 MPa – 1.70507x10^{-3} MPa = 9.95949x10^{-2} MPa. The ideal gas law (with R = 8.314 Pa-m^3/mole-K)[B4] then gives a molecular density of 2.50351x10^{19} molecules/cm^3. The proportions given in subsection 3.1.3 lead to the following atomic densities:

$(\overline{n}_N)_{cell} = 1.55875x10^{-5}$ a/b-cm

$(\overline{n}_O)_{cell}^{air} = 4.09021x10^{-6}$ a/b-cm

$(\overline{n}_{Ar})_{cell} = 9.11929x10^{-8}$ a/b-cm

REFERENCES FOR APPENDIX B

B1. *Chart of the Nuclides*, Thirteenth Edition, General Electric Company, 1984.

B2. Joseph H. Keenan and Frederick G. Keyes, *Thermodynamic Properties of Steam*, Wiley, New York, Thirty-fifth Printing, 1963.

B3. Donald R. Pitts and Leighton E. Sissom, *Heat Transfer*, Schaum's Outline Series in Engineering, McGraw-Hill, New York, 1977.

B4. Samuel Glasstone and Alexander Sesonske, *Nuclear Reactor Engineering,* Third Edition, Van Nostrand Reinhold, New York, 1981.

APPENDIX C

NUCLEAR CONSTANTS

Avogadro's Number $6.022 \times 10^{23} \frac{\text{atoms}}{\text{gram} - \text{mole}}$

TABLE C1. Atomic Weights.

Nuclide or Isotope	Atomic Weight
H	1.00794
Li	6.941
B	10.811
^{10}B	10.0129
^{11}B	11.0093
C	12.011
O	15.9994
Si	28.0855
^{235}U	235.043928
^{238}U	238.050788

[2] "Chart of the Nuclides," Thirteenth Edition, General Electric Company, 1984.